Table 11.1
 Pore structure parameters of MCM-48 and Pd-MCM-48

Sample	surface area (m²/g)	pore size (nm)	pore volume (cc/g)
Pure MCM-48	1593	2.445	0.9736
1%Pd-MCM-48	1535	2.167	0.8317
2%Pd-MCM-48	1617	2.225	0.8991
3%Pd-MCM-48	1579	2.326	0.9181
4%Pd-MCM-48	1436	2.254	0.8497
5%Pd-MCM-48	1401	2.431	0.7893

 Table 11.2
 XRF analysis of Pd-MCM-48

Sample	Si (%)	O (%)	Pd (%)
1%Pd-MCM-48	38.759	61.233	0.008
2%Pd-MCM-48	33.005	66.983	0.012
3%Pd-MCM-48	39.873	60.104	0.023
4%Pd-MCM-48	37.819	62.155	0.026
5%Pd-MCM-48	36.785	63.187	0.028

Table 11.3 Microwave-assisted Suzuki reaction using various Pd-MCM-48 catalysts at 120 °C for different reaction times

Time	Conversion (%)					
(min)	MCM-48	1% PdMCM-48	3% PdMCM-48	5% PdMCM-48		
10	0	0	2.1 ± 0.5	1.9 ± 1.6		
20	0	0	39.4 ± 2.9	42.3 ± 4.9		
30	0	0	17.0 ± 0.8	27.0 ± 1.7		

CHAPTER XII CONCLUSIONS

Conclusions

MCM-48, M-MCM-48, and M,M'-MCM-48 were successfully synthesized by a novel silica source known as silatrane and CTAB as a template under basic condition, with high surface area (up to 1,711 m²/g) and narrow pore-size distribution (2.02-2.86 nm). In this research, the amount of CTAB needed was lower than conventional requirement. The synthesized MCM-48, M-MCM-48, and M,M'-MCM-48 indicated a well-ordered structure of MCM-48 with a truncated octahedral shape. The maximum ratios of M/Si incorporated into the MCM-48 without destroying the long-range ordered of parent structure were obtained. DR-UV results provided the upper limit of the metals incorporated into MCM-48 framework. The oxidation of styrene catalyzed by Ti- and Cr-MCM-48 provided %conversion higher than Ce-MCM-48. From their optimal conditions, the %conversion of styrene reached the maximum of 61.9, 96.6, and 5.1% for Ti-MCM-48-0.01, Cr-MCM-48-0.005, and Ce-MCM-48-0.03, respectively. The kinetic study of Cr-MCM-48 catalysts toward the oxidation of styrene showed the temperature, the amounts of oxidant and styrene greatly affected to the reaction rate. The rate equation from the two-stage mechanism, under a steady state assumption, was proposed to be the representative of this reaction. The optimal conditions for the synthesized Pd-MCM-48 catalysts applied for microwave-assisted Suzuki reaction of phenylboronic acid with 1-bromo-4-fluorobenzene in presence of K₂CO₃ base using DMF solvent were performed at 120 °C for 20 min reaction time, giving the highest conversion of 39.4 and 42.3% when using 3 and 5%Pd-MCM-48, respectively.

REFERENCES

- Adam, F., Thankappan, R. (2010) Chem. Eng. 160, 249-258.
- Alfredsson, V., Anderson, M.W., Ohsuna, T., Terasaki, O., Jacob, M., and Bojrup M. (1997) Cubosome description of the inorganic mesoporous structure MCM-48. Chem. Mater., 9, 2066–2070.
- Asefa, T. and Tao, Z. (2012) Mesoporous silica and organosilica materials—
 Review of their synthesis and organic functionalization. <u>Can. J. Chem.</u>,
 90(12), 1015-1031.
- Beck, J.S., Vartuli, J.C., Roth, W.J., Leonowicz, M.E., Kresge, C.T., Schmitt, K.D., Chu, C.T.W., Olson, D.H., Sheppard, E.W., McCullen, S.B., Higgins, J.B. and Schlenker, J.L. (1992) A new family of mesoporous molecular sieves prepared with liquid crystal templates. <u>J. Am. Chem. Soc.</u>, 114, 10834-10843.
- Charoenpinijkarn, W., Suwankruhasn, M., Kesapabutr, B., Wongkasemjit, S., and Jamieson A.M. (2001) Sol–gel processing of silatranes. <u>Eur. Polym. J.</u>, 37, 1441–1448.
- Corma, A., Kan, Q., and Rey, F. (1998) Synthesis of Si and Ti-Si-MCM-48 mesoporous materials with controlled pore sizes in the absence of polar organic additives and alkali metal ions. Chem. Commun., 579–580.
- Díaz, I., Pérez-Pariente, J., and Terasaki O. (2004) Structural study by transmission and scanning electron microscopy of the time-dependent structural change in M41S mesoporous silica (MCM-41 to MCM-48, and MCM-50). <u>J. Mater.</u> Chem., 14, 48–53.
- Gallis, K.W. and Landry, C.C. (1997) Synthesis of MCM-48 by a Phase Transformation Process. <u>Chem. Mater.</u>, 9, 2035-2038.
- Huo, Q., Margolese, D.I., and Stucky, G.D. (1996) Surfactant control of phases in the synthesis of mesoporous Silica-Based materials. <u>Chem. Mater.</u>, 8, 1147-1160.
- Huo, Q., Margolese, D.I., Ciesla, U., Feng, P., Gier, T.E., Sieger, P., Leon, R., Petroff, P.M., Schüth, F., and Stucky, G.D. (1994) Generalized synthesis of periodic surfactant/inorganic composite materials. <u>Nature</u>, 368, 317–321.

- Huo, Q.S., Margolese, D.I., Ciesla, U., Demuth, D.G., Feng, P.Y., Gier, T.E.,
 Sieger, P., Firouzi, A., Chmelka, B.F., Schuth, F., and Stucky, G.D. (1994)
 Organization of Organic Molecules with Inorganic Molecular Species into
 Nanocomposite Biphase Arrays. <u>Chem. Mater.</u>, 6, 1176–1191.
- Israelachivili, J.N., Mitchell, D.J., and Ninham B.W. (1976) Theory of Self-Assembly of Hydrocarbon Amphiphiles into Micelles and Bilayers. <u>J.</u>

 <u>Chem. Soc. Faraday. Trans.</u>, 72 (2), 1525-1568.
- Kim, T.W., Chun, P.W., and Lin V.S.Y. (2010) Facile Synthesis of Monodisperse Spherical MCM-48 Mesoporous Silica Nanoparticles with Controlled Particle Size. <u>Chem. Mater.</u>, 22, 5093–5104.
- Kresge, C.T., Leonowicz, M.E., Roth, W.J., Vartuli, J.C., and Beck J.S. (1992) Ordered mesoporous molecular sieves synthesized by a liquid-crystal template mechanism. <u>Nature</u>, 359, 710-712.
- Kruk, M., Jaroniec, M., Ryoo, R., and Kim, J.M. (1999) Characterization of high-quality MCM-48 and SBA-1 mesoporous silicas. Chem. Mater., 11, 2568-2572.
- Kumar, D., Schumarcher, K., Hohenesche, C., Grün, M., and Unger K.K. (2001) MCM-41, MCM-48 and related mesoporous adsorbents: their synthesis and characterization. <u>Colloids. Surf. A</u>, 187–188, 109–116.
- Lysenko, N.D., Shvets, A.V., and Il'in, V.G. (2008) Field of concentrations and conditions of template structure formation of a silica mesoporous molecular sieves of MCM-48 type. <u>Theor. Exp. Chem.</u>, 44, 195–199.
- Mathieu, M., Van Der Voort, P., Weckhuysen, B.M., Rao, R.R., Catana, G., Schoonheydt, R.A., and Van-sant, E.F. (2001) Vanadium-Incorporated MCM-48 Materials: Optimization of the Synthesis Procedure and an in Situ Spectroscopic Study of the Vanadium Species. <u>J. Phys. Chem. B</u>, 105, 3393-3399.
- Meynen, V., Cool, P., and Vansant E.F. (2009) Verified syntheses of mesoporous materials. Micropor. Mesopor. Mater., 125, 170–223.
- Mintova, S. and Čejka J. (2007) Chapter 9 Micro/mesoporous composites. <u>Stud. Surf. Sci. Catal.</u>, 168, 301–326.
- Monnier, A., Schüth, F., Huo, Q., Kumar, D., Margolese, D., Maxwell, R.S., Stucky, M., Krishnamurty, G.D., Petroff, P., Firouzi, A., and Janicke M. (1993)

- Cooperative Formation of Inorganic-Organic Interfaces in the Synthesis of Silicate Mesostructures. <u>Science</u>, 261, 1299-1303.
- Perez-Ramírez, J., Christensen, C.H., Egeblad, K., Christensen, C.H., and Groen, J.C. (2008) Hierarchical zeolites: enhanced utilisation of microporous crystals in catalysis by advances in materials design. <u>Chem. Soc. Rev.</u>, 37, 2530–2542.
- Phiriyawirut, P., Jamieson, A.M., and Wongkasemjit S. (2005) VS-1 zeolite synthesized directly from silatrane. <u>Micropor. Mesopor. Mater.</u>, 77, 203–213.
- Phiriyawirut, P., Magaraphan, R., Jamieson, A.M., and Wongkasemjit S. (2003) Morphology study of MFI zeolite synthesized directly from silatrane and alumatrane via the sol–gel process and microwave heating. <u>Micropor. Mesopor. Mater.</u>, 64(1–3), 83–93.
- Phonthammachai, N., Chairassameewong, T., Gulari, E., Jameison, A.M., and Wongkasemjit S. (2003) Oxide one pot synthesis of a novel titanium glycolate and its pyrolysis. J. Met. Mater. Min., 12, 23.
- Rath, D., Parida, K.M. (2011) Ind. Eng. Chem. Res. 50, 2839-2849.
- Ryoo, R., Joo, S.H., and Kim, J.M. (1999) Energetically Favored Formation of MCM-48 from Cationic-Neutral Surfactant Mixtures. <u>J. Phys. Chem. B</u>, 103, 7435-7440.
- Sakthivel, A., Dapurkar, S.E., and Selvam, P. (2001) Mesoporous (Cr)MCM-41and (Cr)MCM-48 Molecular Sieves: Promising Heterogeneous Catalysts for Liquid Phase Oxidation Reactions. Catal. Lett., 7, 155-158.
- Sathupanya, M., Gulari, E., and Wongkasemjit S. (2003) Na-A (LTA) Zeolite Synthesis Directly from Alumatrane and Silatrane by Sol–Gel Microwave Techniques. J. Eur. Ceram. Soc., 23, 2305–2314.
- Sathupanya, M., Gulari, E., and Wongkasemjit, S. (2002) ANA and GIS Zeolite Synthesis Directly from Alumatrane and Silatrane by Sol–Gel Process and Microwave Techniques. J. Eur. Ceram. Soc., 22, 1293–1303.
- Sayari, A. (1996) Catalysis by Crystalline Mesoporous Molecular Sieves. <u>Chem.</u> <u>Mater.</u>, 8(8), 1840-1852.
- Sayari, A. (2000) Novel Synthesis of High-Quality MCM-48 Silica. <u>J. Am. Chem.</u> Soc., 122, 6504-6505.

- Shao, Y., Wang, L., Zhang, J., and Anpo, M. (2005) Novel synthesis of high hydrothermal stability and long-range order MCM-48 with a convenient method. Micropor. Mesopor. Mater., 86, 314.
- Shao, Y., Wang, L., Zhang, J., and Anpo, M. (2008) Synthesis and characterization of high hydrothermally stable Cr-MCM-48. <u>Micropor. Mesopor. Mater.</u>, 109, 271-277.
- Stucky, G.D., Monnier, A., Schüth, F., Huo, Q., Margolese, D., Kumar, D., Krishnamurty, M., Petroff, P., Firouzi, A., Janicke, M., and Chmelka, B.F. (1994) Molecular and Atomic Arrays in Nano- and Mesoporous Materials Synthesis. Mol. Cryst. Liq. Cryst., 240, 187.
- Thanabodeekij, N., Sadthayanon, S., Gulari, E., and Wongkasemjit, S. (2006) Extremely high surface area of ordered mesoporous MCM-41 by atrane route. Mater. Chem. Phys., 98, 131–137.
- Thanabodeekij, N., Tanglumlert, W., Gulari, E., and Wongkasemjit S. (2005) Synthesis of Ti-MCM-41 directly from silatrane and titanium glycolate and its catalytic activity. Appl. Organomet. Chem., 19, 1047–1054.
- Vartuli, J.C., Schmitt, K.D., Kresge, C.T., Roth, W.J., Leonowicz, M.E., McCullen, S.B., Hellring, S.D., Beck, J.S., Schlenker, J.L., Olson, D.H., and Sheppard E.W. (1994) Effect of Surfactant/Silica Molar Ratios on the Formation of Mesoporous Molecular Sieves: Inorganic Mimicry of Surfactant Liquid-Crystal Phases and Mechanistic Implications. Chem. Mater., 6, 2317-2326.
- Wang, C.Y., Bai, H. (2001) Catal. Today.
- Wang, L., Shao, Y., Zhang, J., and Anpo, M. (2006) Synthesis of MCM-48 mesoporous molecular sieve with thermal and hydrothermal stability with the aid of promoter anions. <u>Micropor. Mesopor. Mater.</u>, 95, 17–25.
- Wang, L., Zhang, J., and Chen, F. (2009) Synthesis of hydrothermally stable MCM-48 mesoporous molecular sieve at low cost of CTAB surfactant. Micropor. Mesopor. Mater., 122, 229–233.
- Wangcheng, Z., Guanxhong, L., Yanglong, F., Yun, G., Yanqin, W., Yunsong, W., Zhigang, Z., and Xiaohui, L. (2008) Synthesis of cerium-doped MCM-48 molecular sieves and its catalytic performance for selective oxidation of cyclohexane. J. Rare Earths, 26, 515-522.

- Xia Y.D. and Mokaya R. (2003) Facile and high yield synthesis of mesostructured MCM-48 silica crystals. <u>J. Mater. Chem.</u>, 13, 657-659.
- Xu, J., Luan, Z., Hartmann, M., and Kevan, L. (1999) Synthesis and Characterization of Mn-Containing Cubic Mesoporous MCM-48 and AlMCM-48 Molecular Sieves. <u>Chem. Mater.</u>, 11, 2928-2936.
- Yuan, S., Shi, L., Mori, K., and Yamashita, H. (2008) Synthesis of Ti-containing MCM-48 by using TiF₄ as titanium source. <u>Mater. Lett.</u>, 62, 3028–3030.
- Zhang, Y., Gao, F., Wan, H., Wu, C., Kong, Y., Wu, X., Zhao, B., Dong, L., Chen, Y. (2008) Microporous Mesoporous Mater. 113, 393-401.
- Zheng, Y., Li, Z., Zheng, Y., Shen, X., Lin, L. (2006) Mater. Lett. 60, 3221-3223.

PROJECT OUTPUTS

International publications

- Rujirat Longloilert, Thanyalak Chaisuwan, Apanee Luengnaruemitchai, and Sujitra Wongkasemjit*, "Novel silica source for synthesis of MCM-48 via sol-gel process", Journal of Sol-Gel Science and Technology, 58 (2011), 427–435.
- Chaiyaporn Witpathomwong, Rujirat Longloilert, Sujitra Wongkasemjit and Sirirat Jitkarnka, "Improving Light Olefins and Light Oil Production Using Ru/MCM-48 in Catalytic Pyrolysis of Waste Tire", Energy Procedia, 9 (2011), 245-251.
- 3. Rujirat Longloilert, Thanyalak Chaisuwan, Apanee Luengnaruemitchai, and Sujitra Wongkasemjit, "Synthesis and characterization of M-MCM-48 (M = Cr, Ce) from silatrane via sol-gel process", Journal of Sol-Gel Science and Technology, (2012) 61:133–143.
- 4. Hussaya Maneesuwan, Rujirat Longloilert, Thanyalak Chaisuwan, Sujitra Wongkasemjit, "Synthesis and characterization of Fe-Ce-MCM-48 from silatrane precursor via sol-gel process", Materials Letters, 94 (2013) 65-68.
- Chonnikarn Deeprasertkul, Rujirat Longloilert, Thanyalak Chaisuwan, and S. Wongkasemjit, "IMPRESSIVE LOW REDUCTION TEMPERATURE OF SYNTHESIZED MESOPOROUS CERIA VIA NANOCASTING", Catalysis Communications, Submitted.
- 6. Hussaya Maneesuwan, Thanyalak Chaisuwan, and Sujitra Wongkasemjit, "Important role of anionic counterion on Ce-MCM-48 synthesis using silatrane precursor via sol-gel process", Applied Surface Science, Submitted.
- 7. Hussaya Maneesuwan, Thanyalak Chaisuwan, and Sujitra Wongkasemjit, "Synthesis of Fe-Ti-MCM-48 from silatrane precursor via sol-gel process and its hydrothermal stability", Colloids and Surfaces A: Physicochemical and Engineering Aspects, Submitted.

International Presentations

- Longloilert, R., Luengnaruemitchai, A., Chaisuwan, T., Wongkasemjit, S. (20-24 March, 2011) "Novel silica source for synthesis of MCM-48 via solgel process", POLYCHAR 19 – World Forum on Advanced Materials, Kathmandu, Nepal.
- Nuttheewan Kittisarunlerd, Thanyalak Chaisuwan, Apanee Luengnaruemitr, and Sujitra Wongkasemjit*, "MCM-48-Polybenzoxazine mixed matrix membranes for CO₂/CH₄ separation", the 243rd ACS National Meeting & Exposition, San Diego, California, USA, March 24-29, 2012.
- 3. Longloilert, R., Luengnaruemitchai, A., Chaisuwan, T., Wongkasemjit, S., "Synthesis and characterization of Ce-MCM-48 from silatrane via sol-gel process", the 3rd Research Symposium on Petrochemical and Materials Technology and the 18th PPC Symposium on Petroleum, Petrochemicals, and Polymers, Queen Sirikit National Convention Center, Bangkok, Thailand, April 24, 2012.
- 4. Deeprasertkul, C., Chaisuwan, T., and Wongkasemjit, S., (2013, March 3-7) Synthesis of ordered mesoporous ceria using MCM-48 as template, Third International Conference on Multifunctional, Hybrid and Nanomaterials, The Hilton Sorrento Palace Hotel in Sorrento, Italy.
- Budmuang, K., Chaisuwan, T., Luengnaruemitchai, A., and Wongkasemjit, S., (2013, March 3-7) Catalytic Activity of Pd Loaded MCM-48. Third International Conference on Multifunctional, Hybrid and Nanomaterials, The Hilton Sorrento Palace Hotel in Sorrento, Italy.
- 6. Sujitra Wongkasemjit, Rujirat Longloilert, Thanyalak Chaisuwan, Apanee Luengnaruemitchai, "SYNTHESIS AND CHARACTERIZATION OF METAL-MCM-48 (M = Ti, Cr AND Ce) VIA HYDROTHERMAL TREATMENT AND SOL-GEL TECHNIQUE", POLYCHAR 21 World Forum on Advanced Materials, 11-15 March 2013 Gwangju, Republic of KOREA.

APPENDICES INTERNATIONAL PUBLICATIONS

ORIGINAL PAPER

Synthesis of MCM-48 from silatrane via sol–gel process

Rujirat Longloilert · Thanyalak Chaisuwan · Apanee Luengnaruemitchai · Sujitra Wongkasemjit

Received: 11 October 2010/ Accepted: 17 January 2011 / Published online: 27 January 2011 © Springer Science+Business Media, LLC 2011

Abstract High-quality cubic MCM-48 is successfully synthesized using a new silica source known as silatrane and cetyltrimethylammonium bromide (CTAB) as the structure-directing agent via sol-gel process. The effects of synthesis parameters, viz. crystallization temperature, crystallization time, surfactant concentration, quantity of NaOH, and silica source, on the product structure are investigated. The synthesized samples are characterized using X-ray diffractometer (XRD), N2 adsorption-desorption isotherms, and electron microscopy. Optimally, this product is synthesized from samples crystallized at 140°C for 16 h with a CTAB/SiO2 ratio of 0.3 and NaOH/SiO2 ratio of 0.5. The XRD result exhibits a well-resolved pattern, corresponding to the Ia3d space group of MCM-48. The BET surface area of this product is as high as 1,300 m²/g with a narrow pore-size distribution of 2.86 nm. The scanning electron microscopic (SEM) images also show the truncated octahedral shape and well-ordered pore system of MCM-48 particles.

Keywords MCM-48 · Silatrane · Sol-gel process · Truncated octahedral shape

1 Introduction

MCM-48 is one of the members of ordered mesoporous

molecular sieves known as the M41S family, reported by

activity because it has a three-dimensional pore structure which reduces the diffusion limitations and avoids the pore-blocking of the catalysts [6]. Although MCM-48 is a more attractive candidate as a catalyst support or adsorbent than MCM-41, its success is curtailed by the lengthy reaction times and rigorous conditions required for its synthesis. The cubic MCM-48 is an intermediate during the transformation from hexagonal to lamellar phases; thus, the synthesis conditions must be carefully controlled. Silica sources are also found to affect the MCM-48 formation, as studied by Xu et al. [7], resulting in different silica structures. Therefore, most researchers have mainly focused on MCM-41 rather than MCM-48 [8-13]. Furthermore, a high surfactant amount and additives are required to obtain the cubic Ia3d MCM-

researchers from Mobil Oil Co [1, 2]. The characteristic

properties of materials in this group are high surface area

and a narrow pore-size distribution [3]. There are three

categories of M41S divided by the different arrays, viz.

hexagonal (MCM-41), cubic (MCM-48), and lamellar

(MCM-50) [4, 5]. The cubic MCM-48 indexed in the space

group of Ia3d is the most interesting in terms of catalytic

48 mesoporous structure. To date, many researchers have tried to minimize the surfactant amount in many ways, using such means as organic additives [14, 15] or salts (i.e. NaF and Na2SO4) [16, 17]. Generally, to obtain MCM-48, the most widely used raw materials are CTAB as a surfactant, NaOH as a catalyst, and tetraethylorthosilicate (TEOS) as a silica source, using conventional autoclave heating for several days. According to the materials safety data sheets (MSDS), however, TEOS presents significant handling problems due to such factors as high toxicity and moisture sensitivity. In this research, we introduce another source of silica known as silatrane. Silatrane can be easily synthesized from inexpensive and commercially available

R. Longloilert · T. Chaisuwan · A. Luengnaruemitchai S. Wongkasemjit (⊠)

The Petroleum and Petrochemical College and the Center for Petroleum, Petrochemicals and Advanced Materials, Chulalongkorn University, Bangkok 10330, Thailand e-mail: dsujitra@chula.ac.th



starting materials, namely, silicon dioxide and triethanolamine, in ethylene glycol solvent [18, 19]. One unique characteristic of silatrane is a moisture stability lasting up to several weeks, thus allowing for control of the hydrolysis rate during sol–gel processing.

In previous works, we successfully synthesized many microporous [20–23] and mesoporous [24–28] zeolites via sol–gel process, using silatrane as the silica precursor. In the present paper, we systematically studied the effects of crystallization temperature, crystallization time, surfactant concentration, amount of NaOH, and silica source on the product structure to obtain the optimum synthesis conditions of MCM-48.

2 Experimental

2.1 Synthesis of silatrane

Following Wongkasemjit's synthetic method [29], silatrane was synthesized by mixing 0.1 mol fumed silica (99.8%, Sigma-Aldrich, St. Louis, MO), 0.125 mol triethanolamine (TEA; QREC, New Zealand), and 100 ml ethylene glycol (EG; J.T. Baker, Philipsburg, NJ). The reaction was refluxed at 200°C under nitrogen atmosphere for 10 h in oil bath. The excess of EG was removed under vacuum at 110°C to obtain a crude brown solid. The obtained product was purified by using acetronitrile (Labscan, Bangkok, Thailand) to remove any TEA and EG residues. The white silatrane product was vacuum-dried overnight before characterization by Fourier transform infrared absorption spectrometry (FT-IR, Bruker Optics EQUINOX55) at a resolution of 2 cm⁻¹, and by thermogravimatric analysis (TGA, Perkin-Elmer instruments) using a heating rate of 10°C/min from room temperature to 650°C in a nitrogen atmosphere. The FT-IR bands observed were $3,000-3,700 \text{ cm}^{-1}$ (w, vO-H), $2,860-2,986 \text{ cm}^{-1}$ (s, vC-H), $1,244-1,275 \text{ cm}^{-1}$ (m, $\nu\text{C-N}$), $1,170-1,117 \text{ cm}^{-1}$ vSi-O), 1,093 cm⁻¹ (s, vSi-O-C), 1,073 cm⁻¹ (s, vC-O), 1,049 cm⁻¹ (s, vSi-O), 1,021 cm⁻¹ (s, vC-O), 785 and 729 cm⁻¹ (s, ν Si–O–C), and 579 cm⁻¹ (w, ν N \rightarrow Si). TGA exhibited one sharp mass loss at 390°C and gave a 19% ceramic yield, corresponding to N(CH2CH2O)3 Si-OCH2CH2-N(CH2CH2OH)2.

2.2 Synthesis of MCM-48

To synthesize this material, CTAB (Sigma–Aldrich) was dissolved in a solution containing water and 2 M NaOH. The mixtures were vigorously stirred with slight heating to dissolve surfactant. Then, silatrane precursor was added, followed by stirring for 1 h. The molar composition of the gel was 1.0 SiO₂:xCTAB:0.50NaOH:62.0 H₂O, where

 $0.15 \le x \le 0.65$. The resulting mixture was transferred to a Teflon-lined stainless steel autoclave and treated at 130–150°C for a certain time in a range of 12–24 h. The resulting solid product was collected by filtration and dried overnight at ambient conditions. The removal of the surfactant was performed by calcination at 550°C for 6 h (Carbolite, CFS 1200, Hope Valley, UK) at a heating rate of 0.5°C/min to obtain mesoporous MCM-48. In this study, crystallization time and temperature, surfactant concentration, alkalinity, and silica source were varied.

2.3 Characterization

The mesoporous products were characterized using a Rigaku X-ray diffractometer (XRD, Tokyo, Japan) and CuK α radiation in the range of $2\theta=2$ –8° at a scanning speed of 1°C/min, 40 kV, and 30 mA. MCM-48 morphology was carried out by a field emission scanning electron microscope (FE-SEM, Hitachi/S-4800) and the samples shadowed with platinum. The order of mesopores was investigated using a transmission electron microscope (TEM, JEOL 2010F). The surface area and average pore size were estimated by the Brunauer-Emmett-Teller (BET) method on a Quantasorb JR instrument (Mount Holly, NJ).

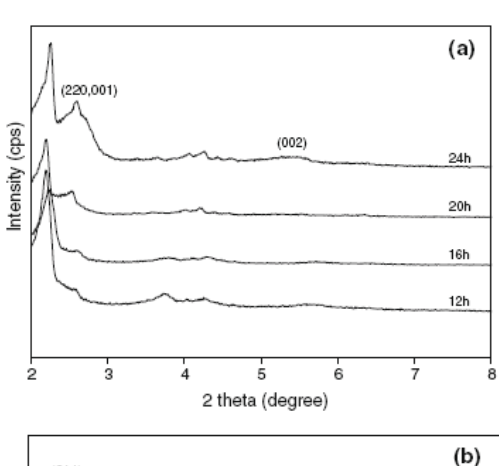
3 Results and discussion

3.1 Effects of crystallization time and temperature

The crystallization time and temperature are the important key factors in synthesizing MCM-48, due to a consecutive transformation of MCM-48 via hexagonal to cubic and lamellar phases. Thus, these studies were attempted at 130, 140, and 150°C for various times using a gel molar composition of SiO₂:0.65CTAB:0.5NaOH:62H₂O and silatrane as silica source.

The results of the as-synthesized samples obtained at 17, 19, and 24 h showed that MCM-48 started to form at 130°C for 24 h (not shown). However, upon calcination, poor-resolved diffraction peaks were obtained probably due to either a too-low crystallization temperature or a tooshort crystallization time to form MCM-48 since all three samples showed the dominance of the hexagonal phase (MCM-41). When the crystallization temperature increased to 140°C, the samples that were heated for 16 h and above showed the diffraction (220) characteristic peak of MCM-48 (Fig. 1). However, the occurrence of mixed phase of the cubic and the lamellar phases was observed from the sample heated for 24 h, as shown in Fig. 1a. The results are in good agreement with those described by Kruk et al. [30], who also showed a significant difference of XRD patterns between a pure cubic MCM-48 and a mixed phase when

they synthesized MCM-48 at 150°C for 1 day. They found that the (220) peak of MCM-48 overlapped with the (001) peak of the lamellar phase, resulting in a broad peak of (220), along with (211), (420), and (332) peaks of MCM-48, and a broad (002) peak of the lamellar phase. In addition, as crystallization time increased, the first dominant peak of (211) started to lose its intensity while the peaks of (001) and (002) increased, indicating that the lamellar phase of MCM-50 had begun to develop, as found by Roth [31]. In contrast to the sample crystallized for 12 h at 140°C, it showed a mixed phase between the hexagonal and the cubic phases, hinting at a relationship to the cubic phase (see Fig. 1a, 12 h). Furthermore, the structure was not strongly established, and it deteriorated considerably upon calicination, as shown by a poor-quality XRD pattern (Fig. 1b, 12 h). The results demonstrated that the samples synthesized at 140°C for 16 and 20 h were crystallized completely. The XRD patterns of the calcined samples synthesized for 16-24 h exhibited a significant increase in



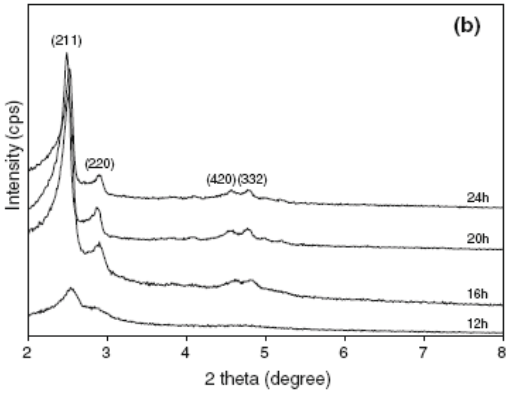


Fig. 1 XRD-patterns of a the as-synthesized samples and b the calcined samples prepared at 140° C for 12, 16, 20 and 24 h

the intensity of peaks, indicating that an atomic reorganization occurred during the removal of the surfactant molecules in the calcination process, and the degree of ordering was enhanced [32, 33]. Another attempt was performed at 150°C of the crystallization temperature for the desired length of time (17–24 h) and failed to obtain pure MCM-48. Instead, a mixed phase between the lamellar and the cubic phases was obtained (not shown).

The XRD patterns of the calcined samples, compared to the as-synthesized samples, were shifted to the higher value of 2-theta, meaning that the contraction of the lattice occurred during the process of removing surfactant because of the condensation of silanol groups on the wall [34].

The samples synthesized for different periods of time were characterized further by N2-adsorption and desorption isotherms, as illustrated in Fig. 2. According to IUPAC classification, all samples showed a typical type IV isotherm, consisting of three stages. At low relative pressure of $P/P_0 < 0.2$, the lines can be extrapolated to the origin due to monolayer adsorption of nitrogen on the walls of the mesopores. This confirms the absence of any detectable micropore filling at low partial pressure [33]. In the region of $P/P_0 = 0.2-0.3$, a steep in isotherms was observed, as a result of the capillary condensation in the mesopores, indicating a uniform pore-size distribution and a highly ordered pore structure. This can also be confirmed by calculating pore-size distribution with BJH method by using the desorption branch of isotherms, as given in Fig. 2 inset. The peak showing a very narrow pore-size distribution with a peak maximum of about 2.3 nm was observed. After the relative pressure P/P₀ ~ 0.3, the isotherm was almost flat owing to multilayer adsorption on the outer surface of the particles, as can be

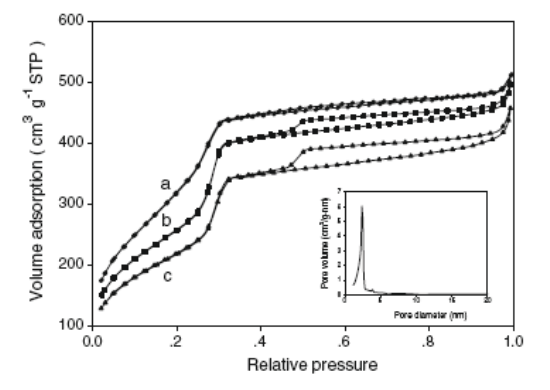


Fig. 2 N₂-adsorption and desorption isotherms of the calcined samples prepared using molar gel composition of SiO₂:0.65C-TAB:0.5NaOH:62H₂O at 140°C for a 16, b 20, and c 24 h. The *inset* shows the BJH pore-size distribution of the calcined sample (a) calculated from the desorption branch of isotherm

 $\textbf{Table 1} \ \ \text{The characteristics of the calcined samples prepared at } 140^{\circ}\text{C for different crystallization times (16, 20, 24 h) using the molar gel composition of $SiO_2:0.65CTAB:0.5NaOH:62H_2O$ and $O_2:0.65CTAB:0.5NaOH:62H_2O$ are the samples prepared at $O_2:0.65CTAB:0.5CTAB$

Crystallization time (h)	S_{BET} (m ² /g)	Pore size (nm)	Pore volume (cm ³ /g)	Unit cell a ₀ (nm)	Wall thickness (nm)
16	1,365	2.3	0.78	8.62	1.65
20	1,148	2.6	0.75	8.69	1.51
24	921	2.9	0.68	8.59	1.31

seen in Fig. 2a [35, 36]. Additionally, the absence of hysteresis loop in Fig. 2a was observed, which can be attributed to the small size of the particles [33]. On the contrary, in Fig. 2b, c, the presence of a triangular hysteresis loop at relative pressure of 0.5-1 on the isotherms indicates the contamination with the lamellar phase after calcinations, leading to the lower surface area [30], as shown in Table 1. In agreement with the study of Kruk et al. [30], they showed a decrease of surface area from 1,240 m²/g for a pure MCM-48-840 m²/g for a mixed lamellar phase. These results also agree with Sing et al. [37], who suggested that this type of hysteresis loop represented a slit-shaped pore or plate-like particle. In addition to the surface area, the pore volume also decreased with increased time, contributing to a collapsed lamellar phase upon calcinations [38]. From these studies. it can be concluded that the crystallization temperature of 140°C for 16 h is suitable for synthesizing MCM-48, and an increase in crystallization temperature accelerated the rate for crystallite formation while shortening the time.

3.2 Effect of surfactant concentration

The effect of CTAB concentration was investigated by preparing samples with different molar gel compositions of SiO₂:xCTAB:0.5NaOH:62H₂O, where $0.15 \le x \le 0.65$. The study was carried out at 140° C for 16 h. Due to the environmental concerns, the surfactant amount should be minimized. In addition, when compared to higher ratios, the low surfactant/silicon ratio provides several advantages, such as increased wall thickness, improved stability of the entire mesostructure, and prevention of structural collapse during calcinations [15].

When the ratio of CTAB/SiO₂ was kept at 0.65, the cubic MCM-48 was obtained. Similar results were reported for the system using the formula TEOS-0.5NaOH-0.65CTACI-62H₂O at 100°C for 3 days [6]. The XRD patterns in Fig. 3 show that the cubic MCM-48 can be obtained in the CTAB/SiO₂ ratio range of 0.2–0.65, whereas the hexagonal MCM-41-type mesoporous silica material was formed at the CTAB/SiO₂ ratio equal to 0.15. The formation of MCM-48 even at a low CTAB-to-SiO₂ ratio can be explained using the surfactant packing

parameter [15, 36], g, determined by the following equation:

$$g = V/(a_0L)$$

where V is the total volume of surfactant chains plus any co-solvent (organic molecules), a_0 is the effective head-group area at the organic-inorganic interface, and L is the length of motional surfactant tail.

Small values of g stabilize more curved surfaces, such as MCM-41, which has a g value between 1/3 and 1/2, while g = 1 stabilizes layers and larger values stabilize structures with less curvature, such as MCM-48, having a g value between 1/2 and 2/3.

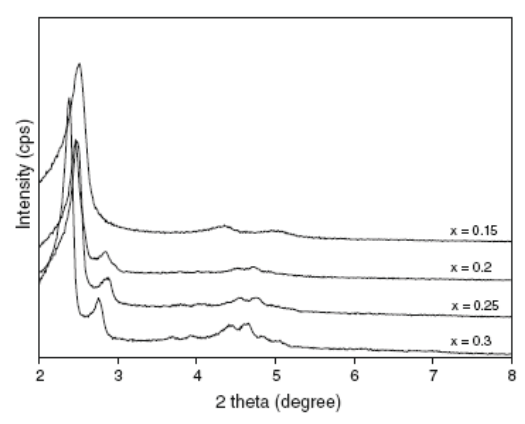
When considering the sol–gel processing of the silatrane precursor, TEA molecules are generated in the mixture as a by-product via the hydrolysis reaction. The TEA molecules stay in the hydrophilic region of the surfactant molecules [39] due to the hydroxyl groups of the molecule, causing more effective polar head-group area of the CTA⁺ micelle, resulting in a decrease of a_0 . From the equation for calculating the parameter g, g is inversely proportional to a_0 , thus, a decrease of a_0 increases g, which is favorable for the cubic MCM-48 formation. This suggests that MCM-48 can be successfully synthesized with use of the silatrane precursor even if the concentration of CTAB is low, and there is no need to include other additives in the system.

From Fig. 3, the XRD pattern of using 0.3 mol CTAB exhibits a well-resolved secondary diffraction at above 3.5 degrees of 2-theta, indicating a highly long range order of this material, as compared to other ratios. Lysenko and coworkers [40] also synthesized MCM-48 with a CTAB/TEOS ratio of 0.3; but the reaction was performed at 100° C for 3 days. In our work, at the same ratio, a much shorter reaction time is required at a higher temperature. The N_2 -adsorption and desorption result also shows nice isotherms and pore-size distribution (see Fig. 4).

In our study, the pore volume and d spacing decreased as the surfactant/silicon ratio increased, whereas the surface area increased (Table 2). The trend was similar to the results obtained from Yu et al. [41] who varied a surfactant/silicon ratio from 0.1 to 0.25 at 110°C for 72 h. When surfactant/silicon ratio increased, there was no slit-shaped pores or plate-like particles of the solid, as observed from

J Sol-Gel Sci Technol (2011) 58:427-435

198



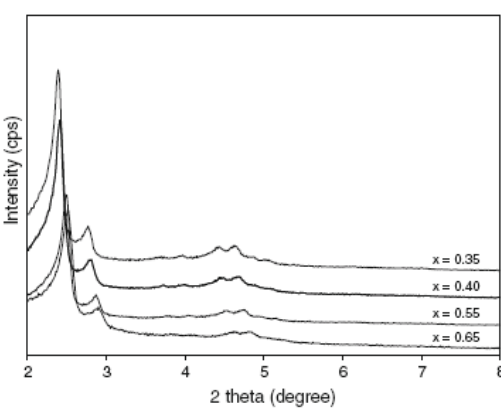


Fig. 3 XRD-patterns of the calcined samples prepared at 140°C for 16 h with molar gel composition of SiO₂:xCTAB:0.5NaOH:62H₂O, where $0.15 \le x \le 0.65$

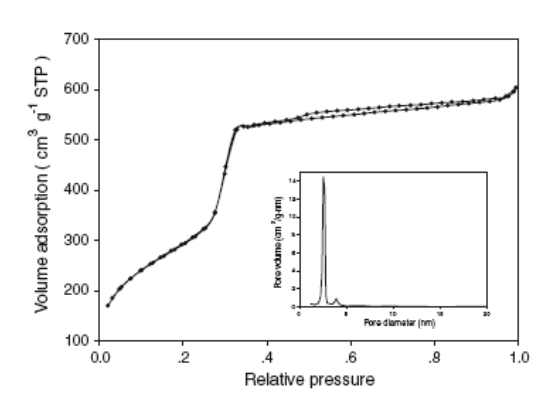


Fig. 4 N₂-adsorption and desorption isotherms and pore-size distribution (*inset*) of the calcined samples prepared at 140°C for 16 h with molar gel composition of SiO₂:0.3CTAB:0.5NaOH:62H₂O

the disappearance of a hysteresis loop between $P/P_0 = 0.4$ and 1 in the adsorption-desorption isotherms (Fig. 2a) whereas the lower surfactant/silicon ratio provided a hysteresis loop, implying that the complementary inter-particles appeared in a mesoporous structure, leading to an increase of pore volume. Moreover, the decrease of the d spacing with an increase in surfactant/silicon ratio was resulted from a thinner wall and a decreasing of pore size obtained when increasing the surfactant concentration to form liquid crystals [41]. However, conversely, the increase of the surface area with an increase in surfactant/ silicon ratio can be described in terms of the smaller size of particles. According to the Scherrer equation, particle sizes of MCM-48 synthesized by using 0.3 and 0.65 mol of CTAB were found to be 110.8 and 92.3 nm, respectively. In addition, as the surfactant concentration increased, the redundant surfactant could be adsorbed on the surface of particles of MCM-48 which reduced the surface tension and prevented the aggregation of particles evidenced indirectly by the disappearance of hysteresis loop. Therefore, the external surface area increased, resulting in the increase of the total surface area. In the range of $0.3 \le x \le 0.65$, the surface areas of our samples were slightly different; however, we observed that when x was less than 0.3, the surface area significantly decreased (not

3.3 Effect of the alkalinity

Another important parameter examined was the alkalinity in the synthesis gel ascertained by NaOH concentration. To study this effect, the synthetic gel was prepared, using the formula of SiO2:0.3 CTAB:y NaOH:62 H2O, where $0.45 \le y \le 0.55$. The OH⁻/Si ratio was varied as 0.45, 0.5, and 0.55. Figure 5a shows XRD patterns of MCM-48 with various amounts of NaOH. All these samples revealed a well-resolved pattern of the Ia3d cubic MCM-48. However, as shown in Fig. 5b, although all samples illustrate the capillary condensation step at P/Po of 0.2-0.3 belonging to MCM-48, the samples prepared from using the NaOH concentration above 0.45 seem to have the lamellar phase mixing with MCM-48, as indicated by the presence of the hysteresis loop, which is consistent with the study of Kruk et al. [30]. This suggests that a high concentration of alkali probably drives the reaction to go further to the lamellar phase, as also suggested by Behrens et al. [42]. Moreover, the pore size and the pore volume decreased with an increase in the OH-/Si ratio (see Table 3), consistent with the results obtained by Collart et al. [43] who synthesized MCM-48 using a molar gel composition of $Si:xOH^-:100H_2O:0.1GEM$ 16-12-16, where x = 0.2 and 0.26 at 130°C for 3 days, and found that a reduction of the OH-/Si ratio increased the pore diameter of the calcined

Table 2 The characteristics of the calcined samples synthesized at 140°C for 16 h using the molar gel composition of SiO₂:xCTAB:0.5-NaOH:62H₂O ratios

Amount of CTAB x mol	$S_{\rm BET}~({\rm m}^2/{\rm g})$	Pore size (nm)	Pore volume (cm³/g)	d spacing (nm)
x = 0.65	1,365	2,28	0.78	3.52
x = 0.55	1,168	2.85	0.83	3.55
x = 0.40	1,291	2.76	0.89	3.67
x = 0.35	1.258	2.99	0.94	3.70
x = 0.30	1.288	2.86	0.92	3.71

MCM-48 samples. As a conclusion and in agreement with Behrens et al. [42], the formation of the lamellar phase of MCM-50 was encouraged by using higher synthesis temperatures, higher basicities of the synthesis solutions, and longer reaction times.

3.4 Effect of silica source

We also performed the same reaction conditions with a traditional silica source such as TEOS instead of the

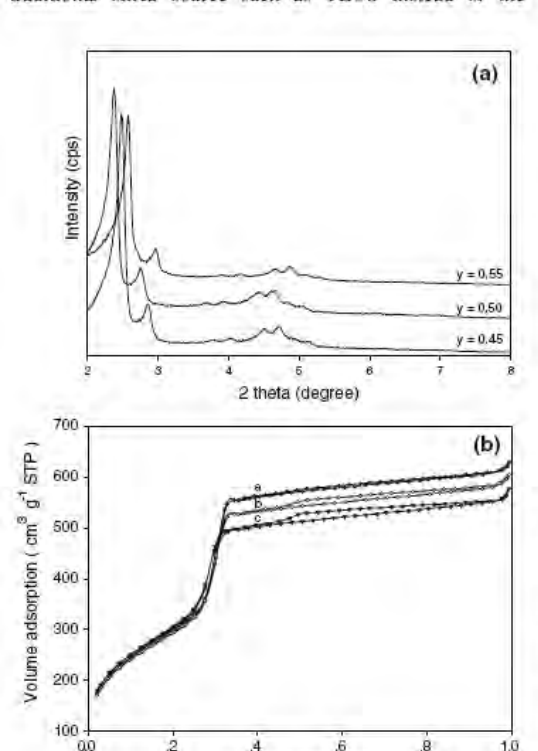


Fig. 5 a XRD-patterns and b N₂-adsorption and desorption isotherms of the calcined samples prepared at 140°C for 16 h with molar gel composition of SiO₂:0,3CTAB:yNaOH:62H₂O, where y is a 0.45, b 0.5, and c 0.55

Relative pressure

Table 3. The effect of the alkalinity on the physical characteristics of the calcined MCM-48 synthesized at 140°C for 16 h using the molar gel composition of SiO₂:0.3CTAB:yNaOH:62H₂O

Property	Y (mol)				
	0.45	0.50	0.55		
Pore diameter Pore volume	29.8 Å 0.96 cm ³ /g	28,6 Å 0.92 cm ³ /g	25.6 Å 0.87 cm ³ /g		
Wall thickness	13,3 Å	15.1 Å	14.3 Å		

silatrane precursor, and found that the crystalline phase of MCM-48 could not be obtained. This result can be explained in terms of the property of the material itself. TEOS is very sensitive to the reaction so it can be hydrolyzed very quickly, as compared to the moisture-stable silatrane. Consequently, the addition of ethanol is usually required for the synthesis of MCM-48 in the TEOS system to retard the hydrolysis reaction and also to increase a surfactant packing parameter, as described elsewhere [44, 46]. Moreover, the longer crystallization time is needed for the phase transformation from hexagonal to cubic phases; thus, the MCM-48 could not be obtained within 16 h. In contrast to the synthesis of MCM-48 using the silatrane precursor, the TEA molecules, the by-product after the hydrolysis process, can improve a surfactant packing parameter, as discussed earlier. Moreover, there is no need to add ethanol into the system since the hydrolysis rate of the silatrane is not as fast as the TEOS. It could be inferred that the silatrane is a good candidate as a silica source for the synthesis of high quality MCM-48 with a lower surfactant/silica ratio for a shorter crystallization time.

3.5 Electron microscopic results of MCM-48 samples

3,5.1 Field emission scanning electron microscopy

The samples synthesized in this work were examined by FE-SEM to investigate their morphology. The images in Fig. 6 are the sample synthesized with a molar gel composition of SiO₂:0.3CTAB:0.5NaOH:62H₂O at 140°C for 16 h, and exhibit the truncated octahedral shape of aggregated MCM-48 particles, consistent with the results

433

Fig. 6 a-c FE-SEM images of MCM-48 synthesized with a molar gel composition of SiO₂:0.3CTAB:0.5NaOH:62H₂O at 140°C for 16 h. d Schematic representation of the gyroid surface according to space

group Ia3d divides a regular truncated octahedron in two, cutting six of the eight hexagonal faces [44]

observed by Diaz et al. [44] and Alfredsson et al. [45]. Diaz et al. obtained this shape when they synthesized with SiO₂:0.65CTAB:0.5NaOH:120H₂O:4.7EtOH at 140°C for 20 h, and after prolonging the reaction time to 48 h, the lettuce-like morphology, corresponding to lamellar phase of MCM-50, was obtained; whereas, Alfredsson et al. synthesized the truncated octahedral shape of MCM-48 using TEOS:0.65CTACl:0.5NaOH:62H₂O at 95°C for 3 days.

In our case, as CTAB concentration increased from 0.3 (Fig. 6) to 0.65 (Fig. 7) mol, FE-SEM images of the synthesized MCM-48 did not show only the truncated octahedral shape, as did those prepared from 0.3 mol CTAB. The image obtained from the mixture heated for 24 h crystallization time (Fig. 7a) shows an especially mixed morphology of the truncated octahedral shape and the lettuce-like morphology. It can be inferred that the molar ratio of CTAB to SiO2 indeed affects the MCM-48 formation. These results are consistent with the N2-adsorption and desorption isotherms of the calcined samples prepared at 140°C for various times (see Fig. 2b, c). On the contrary, the lettuce-like morphology disappeared in the sample prepared with the CTAB/SiO2 ratio equal to 0.3, suggesting that a lamellar phase (MCM-50) required a higher surfactant-to-silica ratio and a longer synthesis time.

3.5.2 Transmission electron microscopy

Figure 8 shows the TEM images of the MCM-48 sample synthesized with a molar gel composition of SiO₂:0.3C-TAB:0.5NaOH:62H₂O at 140°C for 16 h. Figure 8a shows the pore structure along the cubic [100] direction with a uniform channel system, consistent with the reports from Xu et al. [33] and Schumacher et al. [46]. Nonetheless, the [111] direction, see Fig. 8b, exhibits a well-defined hexagonal arrangement [33] and continuous channels running through the structure [47].

4 Conclusions

A novel silica source known as silatrane has been successfully used for synthesis of MCM-48 with high surface area and narrow pore-size distribution. XRD, SEM, and TEM indicate a well-ordered structure of MCM-48 with a truncated octahedral shape. The results also show that all synthesis parameters studied have a considerable effect on the synthesis of MCM-48. The optimum synthesis condition for synthesizing MCM-48 is as follows; SiO₂:0.3C-TAB:0.5NaOH:62H₂O at 140°C for 16 h. The lower amount of CTAB is needed due to the TEA molecules

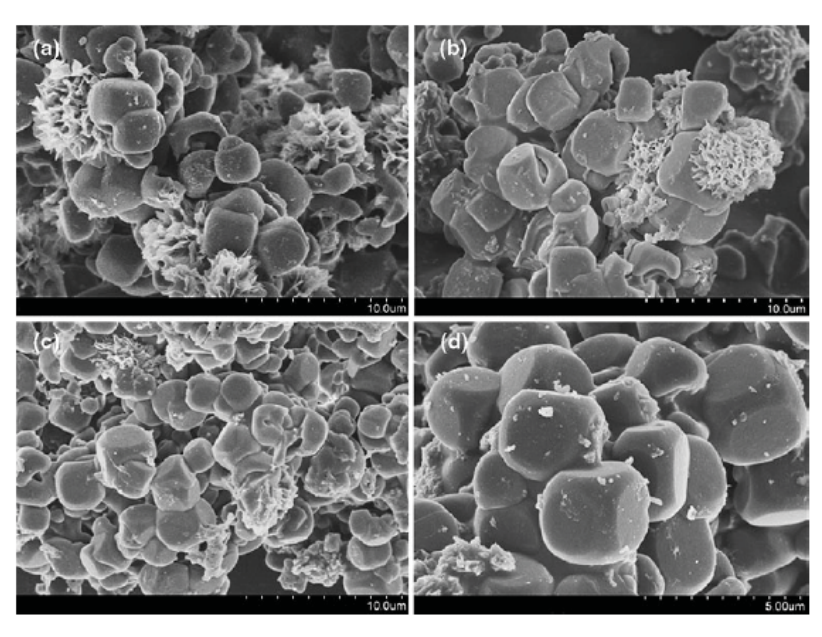
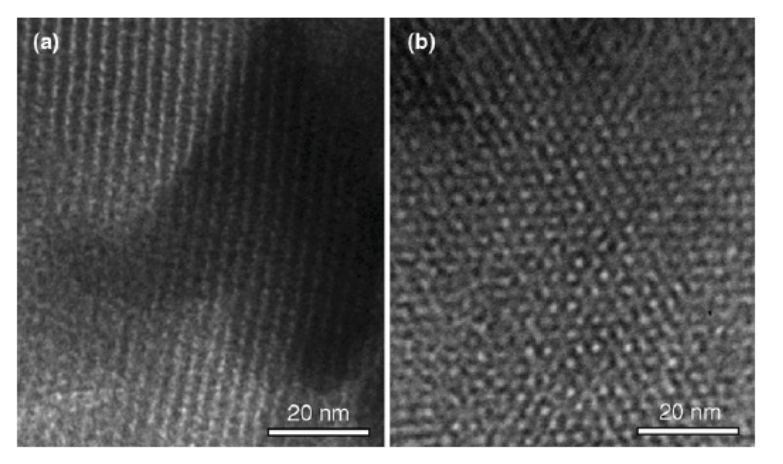


Fig. 7 FE-SEM images of MCM-48 synthesized with a molar gel composition of $SiO_2:0.65CTAB:0.5NaOH:62H_2O$ at $140^{\circ}C$ for a 24, b 20, c 16 ($\times 5000$), and d 16 h ($\times 10000$)



 $\textbf{Fig. 8} \ \ \text{TEM images of MCM-48 synthesized with a molar gel composition of SiO}_2:0.3CTAB:0.5NaOH:62H_2O \ at \ 140^{\circ}C \ for \ 16 \ h \ with incident direction along \ a \ [100] \ and \ b \ [111]$

generated from the silatrane precursor, causing higher surfactant packing parameter of micelle which is preferable for the cubic phase.

Acknowledgments This research is financially supported by the Thailand Research Fund and the Center for Petroleum, Petrochemicals, and Advanced Materials, Chulalongkorn University, Thailand.

The authors would like to thank Mr. John M. Jackson for English proofreading.

References

 Kresge CT, Leonowicz ME, Roth WJ, Vartuli JC, Beck JS (1992) Nature 359:710



- Beck JS, Vartuli JC, Roth WJ, Leonowicz ME, Kresge CT, Schmitt KD, Chu CTW, Olson DH, Sheppard EW, McCullen SB, Higgins JB, Schlenker JL (1992) J Am Chem Soc 114:10834
- Shao Y, Wang L, Zhang J, Anpo M (2005) Microporous Mesoporous Mater 86:314
- Sayari A (1996) Chem Mater 8:1840–1852
- Vinu A, Murugesan V, Hartmann M (2003) Chem Mater 15: 1385–1393
- Monnier A, Schüth F, Huo Q, Kumar D, Margolese D, Maxwell RS, Stucky M, Krishnamurty GD, Petroff P, Firouzi A, Janicke M (1993) Science 261:1299
- Xu J, Luan Z, He H, Zhou W, Kevan L (1998) Chem Mater 10:3690
- 8. Huo Q, Margolese DI, Stucky GD (1996) Chem Mater 8:1147
- 9. Gallis KW, Landry CC (1997) Chem Mater 9:2035
- 10. Corma A, Kan Q, Rey F (1998) Chem Commun 579-580
- 11. Ryoo R, Joo SH, Kim JM (1999) J Phys Chem B 103:7435
- 12. Sayari A (2000) J Am Chem Soc 122:6504
- 13. Xia YD, Mokaya R (2003) J Mater Chem 13:657
- Kumar D, Schumarcher K, Hohenesche C, Grün M, Unger KK (2001) Colloids Surf A 187–188:109–116
- 15. Kim TW, Chun PW, Lin VSY (2010) Chem Mater 22:5093–5104
- Wang L, Shao Y, Zhang J, Anpo M (2006) Microporous Mesoporous Mater 95:17–25
- Wang L, Zhang J, Chen F (2009) Microporous Mesoporous Mater 122:229–233
- Phiriyawirut P, Magaraphan R, Jamieson AM, Wongkasemjit S (2003) Mater Sci Eng A 361:147–154
- Charoenpinijkarn W, Suwankruhasn M, Kesapabutr B, Wongkasemjit S, Jamieson AM (2001) Eur Polym J 37:1441–1448
- Sathupanya M, Gulari E, Wongkasemjit S (2002) J Eur Ceram Soc 22:1293–1303
- Sathupanya M, Gulari E, Wongkasemjit S (2003) J Eur Ceram Soc 23:2305–2314
- Phonthammachai N, Chairassameewong T, Gulari E, Jameison AM, Wongkasemjit S (2003) J Met Mater Min 12:23
- Phiriyawirut P, Jamieson AM, Wongkasemjit S (2005) Microporous Mesoporous Mater 77:203–213
- Thanabodeekij N, Tanglumlert W, Gulari E, Wongkasemjit S (2005) Appl Organomet Chem 19:1047–1054
- Thanabodeekij N, Sadthayanon S, Gulari E, Wongkasemjit S (2006) Mater Chem Phys 98:131–137

- 26. Mintova S, Cejka J (2007) Stud Surf Sci Catal 168:301-326
- 27. Cejka J, Mintova S (2007) Catal Rev 49:457-509
- Perez-Ramirez J, Christensen CH, Egeblad K, Christensen CH, Groen JC (2008) Chem Soc Rev 37:2530–2542
- Phiriyawirut P, Magaraphan R, Jamieson AM, Wongkasemjit S (2003) Microporous Mesoporous Mater 64(1–3):83–93
- Kruk M, Jaroniec M, Peña ML, Rey F (2002) Chem Mater 14: 4434–4442
- 31. Roth WJ (2009) Adsorption 15:221-226
- 32. Chang Z, Zhu L, Kevan L (1999) J Phys Chem B 103:9442
- Xu J, Luan Z, He H, Zhou W, Kwvan L (1998) Chem Mater 10:3690–3698
- Taralkar US, Jha RK, Joshi PN (2007) J Non Cryst Solids 353: 194–199
- Taralkar US, Kasture MW, Joshi PN (2008) J Phys Chem Solids 69:2075–2081
- Wei FY, Liu ZW, Lu J, Liu ZT (2010) Microporous Mesoporous Mater 131:224–229
- Sing KSW, Everett DH, Houl RAW, Moscou L, Pierotti RA, Rouquerol J, Siemieniewska T (1985) Pure Appl Chem 57:603
- Petitto C, Galarneau A, Driole MF, Chiche B, Alonso B, Renzo FD, Fajula F (2005) Chem Mater 17:2120–2130
- Tanglumlert W, Imae T, White TJ, Wongkasemjit S (2007) J Am Ceram Soc 90(12):3992–3997
- Lysenko ND, Shvets AV, Il'in VG (2008) Theor Exp Chem 44:195–199
- Yu J, Shi JL, Wang LZ, Gao JH, Yan DS (2000) J Mater Sci Lett 19:1461–1464
- Behrens P, Glaue A, Haggenmüller C, Schechner G (1997) Solid state Ionics 101–103:255–260
- Collart O, Van Der Voort P, Vansant EF, Desplantier D, Galarneau A, Di Renzo F, Fajula F (2001) J Phy Chem B 105: 12777–112771
- Díaz I, Pérez-Pariente J, Terasaki O (2004) J Mater Chem 14:48–53
- Alfredsson V, Anderson MW, Ohsuna T, Terasaki O, Jacob M, Bojrup M (1997) Chem Mater 9:2066–2070
- Schumacher K, Ravikovitch PI, Chensne AD, Neimark AV, Unger KK (2000) Langmuir 16:4648–4654
- Zhao W, Li Q, Wang L, Chu J, Qu J, Li S, Qi T (2010) Langmuir 26(10):6982–6988



Available online at www.sciencedirect.com

SciVerse ScienceDirect

Procedia

Energy Procedia 9 (2011) 245 - 251

9th Eco-Energy and Materials Science and Engineering Symposium

Improving Light Olefins and Light Oil Production Using Ru/MCM-48 in Catalytic Pyrolysis of Waste Tire

Chaiyaporn Witpathomwong^a, Rujirat Longloilert^a, Sujitra Wongkasemjit^{a,b} and Sirirat Jitkarnka^{a,*}

^aThe Petroleum and Petrochemical College, Chulalongkorn University, Soi Chulalongkorn 12, Phayathai Road, Phathumwan, Bangkok 10330, Thailand
^bCenter for Petroleum, Petrochemicals, and Advanced Materials, Chulalongkorn University, Soi Chulalongkorn 12, Phayathai Road, Phathumwan, Bangkok 10330, Thailand

Abstract

Mobil Composition of Matter (MCM) is the name given for a series of mesoporous materials. The MCM-48 is one of three phases of the mesoporous materials, which is cubic crystalline structure. The MCM-48 in this work was synthesized from silatrane route, and Ru metal was loaded by incipient wetness impregnation. This work investigated the activity and selectivity of MCM-48 and Ru/MCM-48 used as the catalysts for waste tire pyrolysis. The results showed that Ru/MCM-48 improved the gas yield. In addition, the use of Ru/MCM-48 catalyst produced light olefins twice as much as the non-catalytic pyrolysis. On the other hand, the catalyst helped to improve the oil quality by increasing light oil portion. Furthermore, it also reduced poly- and polar-aromatic compounds and sulfur content in the derived oil. Surface area analysis, XRD, and CHNS analysis were performed to explain the experimental results.

© 2011 Published by Elsevier Ltd. Selection and/or peer-review under responsibility of CEO of Sustainable Energy System, Rajamangala University of Technology Thanyaburi (RMUTT).

Keywords: Pyrolysis; Waste tires; Light olefins; Ruthenium; Silica MCM-48; Aromatics;

1. Introduction

Tires are non-biodegradable materials resulting in many problems such as landfill, hazardous, and environmental problems. Pyrolysis is an effective choice to manage the waste tire problem. It is a thermal decomposition of large molecular weight molecules to lower molecular weight products in the absence of

^{*} Corresponding author. Sirirat Jitkarnka, Tel.:+662-218-4148; fax: +662-215-4459. E-mail address: sirirat.j@chula.ac.th

oxygen. In general, the products of tire pyrolysis can be separated into liquid, gas and solid char. The light olefins are one of the fractions in the gas product from the pyrolysis of waste tire. They can be used as petrochemical feedstock and raw material of plastic industry. The use of catalyst can improve the quality of the product from pyrolysis. Ru/MCM-41 has been found to increase the gas yield (light olefins) due to its high cracking and dehydrogenating activity [1]. In 2008, Basagiannis and Verykios [2] studied the influence of the carrier on the steam reforming of acetic acid over Ru-based catalysts. They found that Ru can help increase the catalytic activity toward lower temperatures and higher hydrogen production rates. Moreover, Ru/HMOR can produce the high amount of light olefins and gas yield as studied by Dũng *et al.*, [1]. Later, it was found that 0.7% Ru supported HMOR can provide the highest light olefins yield [3]. Furthermore, the use of Ru/MCM-41 in the catalytic pyrolysis can produce 4 times higher light olefins yield than the non-catalytic case [1].

In particular, Mobil Composition of Matter (MCM) is the name given for a series of mesoporous materials that were first synthesized in 1992. The MCM-48 is a one of three phases of mesoporous MCMs which are MCM-41(hexagonal), MCM-48 (cubic), and MCM-50 (lamellar). The MCM-48 used in this work is the cubic mesoporous hydroxylated silicate, which consists of sub-micron-sized crystallites [4]. Since it is a mesoporous material that is in the same series of MCM-41, whose pore size has been proven appropriate to crack large moleculs of HCs and preserve light olefins formation, MCM-48 might have high potential to be used as a support for light olefins production as well. Consequently, 0.7%wt ruthenium metal supported on MCM-48 was used as a catalyst for potentially producing light olefins from waste tire pyrolysis.

2. Experimental Setup

2.1. Catalyst preparation

The silica MCM-48 was synthesized by silatrane route. Silatrane was first synthesized using the method of Wongkasenjit's group [5]. Silatrane precursor was added to hexadecyltrimethyl ammonium bromide (CTAB, purchased from Sigma Chemical Co.), and sodium hydroxide (NaOH, sigma Chemical Co.). After that, water was added with vigorous stirring, and gel was kept in an autoclave 16 hr at 140°C. The obtained crude product was filtered and washed with water to keep a white solid. The ratio of chemicals: Si/CTAB/NaOH/H₂O was 1:0.3:0.5:62. Next, the white solid was dried at room temperature and calcined at 550 °C for 6 hours with the ramping rate of 0.5°C/min to obtain mesoporous MCM-48. For the Ru metal loading, the precursor solution of ruthenium (III) chloride hydrate was dropped on the support using the impregnation technique. The 0.7%Ru was loaded to 5 g. of the support, which needed 0.0719 g of RuCl₃. After that, the wet support was dried in an oven at 110°C for 3 hours and calcined in a furnace at 500°C for 3 hours with the heating rate of 10°C/min to obtain the catalysts in an oxide form. Then, the catalyst was reduced with H₂ at 400°C for 1-2 hours in order to convert the metal oxide form to metal element.

$$RuO_2 + H_2 \longrightarrow Ru + H_2O \tag{1}$$

2.2. Catalyst Characterization

The crystalline phase of the catalysts was examined using the X-ray diffraction pattern. X-ray diffraction (XRD) patterns were taken by using a Rigaku, Rint X-Ray diffractometer system (RINT 2200)

with Cu tube for generating CuK α radiation (1.5406 Å) and nickel filter. In this experiment, XRD determines the structure of catalysts and crystal size on the supports. A catalyst sample was ground to be fine and homogeneous particles, and then packed in a glass specimen holder. The data from XRD were analyzed and recorded by an on-line computer at the scanning speed of 0.5° min-1 and 20 from 2° to 90°. The surface area, pore volume, and pore size of the studied catalysts were determined by N_2 physical adsorption with the Sorptomatic 2900 instrument. The percentage composition of sulfur in oil products and sulfur deposition on the spent catalysts were performed by using a LECO® Elemental Analyzer (TruSpec®S). The oil product of 0.1–1 g was absorbed on an aid support, which was put in a ceramic boat. The analyzed temperature of sulfur furnace was 1,350 °C.

2.3. Pyrolysis of Waste Tire

10 gram of waste tire sample was loaded, and was pyrolyzed at 500°C in the lower zone of the pyrolysis reactor as in [6]. 2.5 gram of catalyst was packed and heated at 350 °C in the upper zone. The pyrolysis product was carried by a nitrogen flow, and was swept to the condensers. The non-condensable product was passed through the condensers and collected in the gas sampling bag. The solid and liquid products were weighed to determine the gas quantity by mass balance. The gas product was analyzed by a Gas Chromatography; Agilent Technologies 6890 Network GC system. The oil product was separated into maltene and asphaltene by adding n-pentane into the pyrolytic oil at the ratio of 40:1. Then, the maltenes were fractionated into saturated hydrocarbons, mono-, di-, poly-, and polar-aromatics by liquid adsorption chromatography [4].

3. Results and Discussion

MCM-48 is a mesoporous material, which has the 3D pore structure. The XRD patterns of synthesized MCM-48 and Ru-supported MCM-48 are presented in Fig.1. Only one peak of the both samples is detected at $2\theta = 2.2^{\circ}$, which is the unique peak. The peaks corresponding of Ru metal are generally obtained at 38° , 42° , 44° , and 58° [7]. However, they are rarely detected because of low amount of Ru loading (0.7%wt). The loaded ruthenium metal does not affect the crystal structure.

The physical properties of fresh catalysts are shown in Table 1. The BET surface area and B.J.H. pore volume of the synthesized MCM-48 are $1,405 \text{ m}^2/\text{g}$ and $0.87 \text{ cm}^3/\text{g}$, respectively. Moreover, the average pore diameter of synthesized MCM-48 is 35.9 Å. The covering of Ru metal causes the dramatic reduction in the surface area. In addition, the reduction of pore volume and pore diameter is caused by Ru metal, which covers the pore of synthesized MCM-48.

Table 1. Physical properties of studied catalysts.

	Surface area	Pore volume	Pore diameter		
	$(m^2/g)*$	(cm ³ /g)**	(Å)**		
MCM-48	1,405	0.87	35.87		
0.7% Ru/MCM-48	915.7	0.63	32.94		
*BET method, **B.J.H. method					

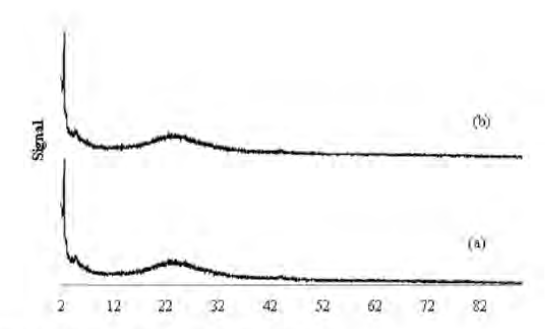


Fig. 1. XRD pattern of catalysts: (a) MCM-48; and (b) 0.7%Ru/MCM-48

3.1. Pyrolysis Products

According to Fig.2, the non-catalytic pyrolysis can produce the yield of gas, oil, and solid char of approximately 13%, 40%, and 47%, respectively. The use of MCM-48 can produce the gas yield of about 23%, and its production is higher than the non-catalytic case by 10%. Furthermore, Ru metal loading on MCM-48 also improves the gas production by 3% higher than the MCM-48 case. Moreover, the synthesized MCM-48 and Ru/MCM-48 decrease the oil production. They can produce less oil than the non-catalytic case by 7%, and 8%, respectively. MCM-48 was synthesized by silatrane route; therefore, it is not an acidic material. However, the effect on gas production of synthesized MCM-48 is through the 3D pore structure [8], which holds up the reactants inside at a long enough time that hydrocarbons have great mass transfer to undergo cracking reaction in the porous MCM-48. Moreover, the acidity of synthesized MCM-48 is less than other acidic zeolites such as HMOR, and HBeta; therefore, it has the low amount of coke deposition. The activity of catalyst is maintained because of the low amount of coke deposition [9]. Furthermore, the Ru loading on the MCM-48 increases the gas production. Ru metal, providing the metal sites, promotes the hydrogenation reaction of aromatic hydrocarbons, which are subsequently cracked and undergo ring-opening reaction in the pore of MCM-48.

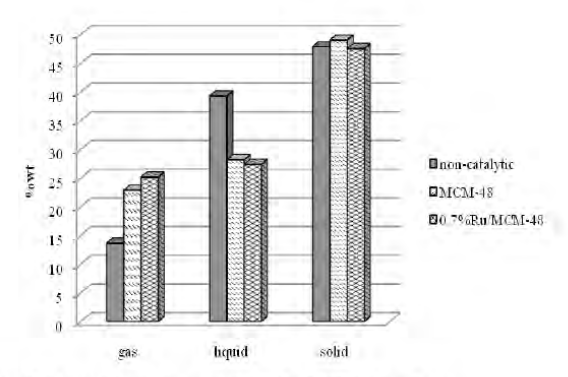


Fig. 2. Product distribution of pyrolysis products from using 0.7% Ru/MCM-48 catalysts.

3.2. Gaseous Products

The gas obtained from tire pyrolysis are, in general, composed of methane, ethylene, ethane, propylene, propane, C4-, C5-, and some traces of C6-, C7-, and C8-hydrocarbons. It was found that the gas also consisted of 0.233% H₂, and 0.423% CO_x for the non-catalytic case [10]. Fig.3. shows the composition of pyrolytic gas obtained from this work. The use of synthesized MCM-48 can drastically improve methane, ethane, and especially C4-, and C5-hydrocarbons. The C4- and C5-hydrocarbons productions are high in the gas because the tire is originally made from some butadiene and isoprene; hence, hydrocarbons chains tend to be cracked to the monomers. Moreover, the increment of C5hydrocarbon might be resulted from the 3D pore structure of MCM-48, which holds up hydrocarbon molecules, then allowing some small gas molecules combine to larger gas molecules. Ru loaded catalyst produces the same gas yields as those of the MCM-48, except that of C5-hydrocarbons. Ru/MCM-48 can produce the significantly high amount of C5-hydrocarbons as compared to that of the other gases. It was reported that Ru metal can crack heavy hydrocarbons to gas products [11]. The increment of C5-HCs shown in the result consequently occurs from Ru metal that selectively cracks heavy HCs to C5s. According to Fig.4, MCM-48 and Ru/MCM-48 can produce high light olefins, which consist of ethylene and propylene in the gas. They can convert invaluable waste tire to valuable products at a high yield of light olefins. When Ru metal is loaded on MCM-48, the Ru/MCM-48 can improve the selectivity of light olefins. Due to the non-acidity of synthesized MCM-48, light olefins molecules can be preserved, because they are not further cracked to other HCs. Additionally, the meso-pore of MCM-48 gives higher selectivity of propylene than that of ethylene. With Ru metal, the yields of ethylene and propylene are slightly improved in conjunction with the higher gas production.

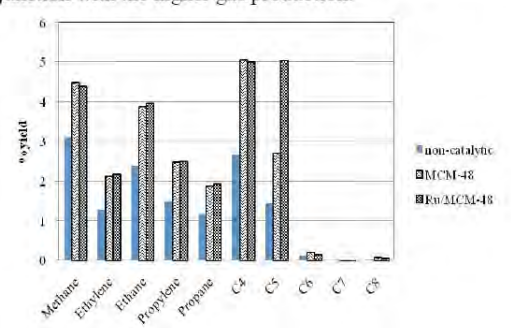


Fig. 3. Composition of pyrolytic gas

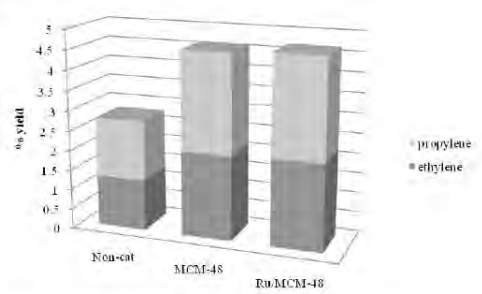


Fig. 4. Light olefins production from using synthesized MCM-48 and Ru/MCM-48 catalysts.

3.3. Pyrolytic Oil

Furthermore, the catalysts can improve the quality of pyrolytic oils. As shown in Table 2, the amount of asphaltene is significantly reduced with using the synthesized MCM-48 and Ru/MCM-48. It can be seen that the MCM-48 has cracking ability; accordingly, the large HCs such as poly- and polar-aromatic can be cracked to smaller molecules. Thus, the MCM-48 dramatically reduces asphaltene. However, the Ru-loaded MCM-48 does not further reduce the amount of asphaltene as compared to the unloaded MCM-48; instead it slightly increases asphaltene.

In Fig.5, the molecular fractions, obtained from the liquid chromatography, in the oils indicate that the synthesized MCM-48 causes the increment of mono-, and di-aromatic HCs in accordance with decreasing saturated, poly-, and polar-aromatic HCs. As previously explained, the non-acidic MCM-48 has mild cracking activity with meso pore sizes, allowing large molecules to enter; thus, the amounts of poly- and polar-aromatics slightly decrease. In addition, saturated HCs are found decreasing as well. On the other hand, Ru loading on the MCM-48 support can dramatically improve saturated HCs in accordance with decreasing all aromatic compounds, indicating that Ru metal can promote high hydrogenation reaction. Consequently, multi-ring aromatics, especially poly- and polar-aromatic HCs, can be hydrogenated on the metal sites. Therefore, saturated HCs are increased at the expense of aromatic compounds from using the Ru/MCM-48 catalyst. Table 2 also shows that MCM-48 and Ru/MCM-48 insignificantly reduce the amount of sulfur in oil, because the sulfur slightly changes as compared to the non-catalytic case. This indicates the mild cracking activity of MCM-48 and the low activity of Ru on breaking C-S bonds in the pyrolytic oil. Due to the low C-S bond cracking activity, sulfur deposition on the spent catalysts is low as well.

Table 2. Amount of asphaltene in oil, sulfur deposition on spent catalysts, and sulfur in oils

	%Asphaltene	%Sulfur deposition on spent catalysts	%Sulfur în oils
Non-catalytic	0.71	-	0.73
MCM-48	0.2	0.43	0.69
Ru/MCM-48	0.28	0.43	0.69

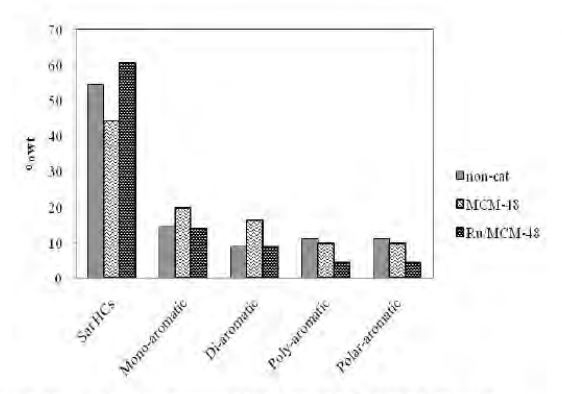


Fig. 5. Molecular compounds in oils from using synthesized MCM-48 and Ru/MCM-48 catalysts.

4. Results and Discussion

The catalytic pyrolysis of waste tire with using MCM-48 and 0.7% Ru/MCM-48 was performed in this work. The synthesized MCM-48 gave the dramatic improvement of gas production as compared to the non-catalytic case in accordance with decreasing the oil production, and Ru-supported MCM-48 also further increased the gas yield from using the pure MCM-48. Both MCM-48 and 0.7% Ru/MCM-48 enhanced the light olefins production. Furthermore, the catalysts can improve the quality of oil. Ru/MCM-48 gave the lighter oil as compared to the non-catalytic case. In particular, the maltene from using Ru/MCM-48 catalyst had the high concentration of saturated-hydrocarbons and low poly-, and polar-aromatic hydrocarbons.

The high activity and selectivity of Ru/MCM-48 is attributed to its mild cracking activity, preventing light olefins from over-cracking. The 3D pore structure of MCM-48 allowed high mass transfer, which improved overall reaction. Moreover, the Ru metal sites improved cracking and hydrogenation activities.

Acknowledgements

The authors would like to thank the Petroleum and Petrochemical College, the Wongkasemjit's group, Thailand Research Fund, the Commissions on Higher Education, and the National Center of Excellence for Petroleum, Petrochemicals, and Advanced Materials, Chulalongkorn University, Thailand.

References

- Düng NA, Raweewan K, Wongkasemjit S, and Jitkamka S. Light olefins and light oil production from catalytic pyrolysis of waste tire. J Anal Appl Pyrol 2009;86:281–286.
- [2] Basagiannis AC, Verykios XE. Influence of the carrier on steam reforming of acetic acid over Ru-based catalysts. Appl Catal B Envir 2008;82:77–88.
- [3] Kongkadee K. Effect of Metals loaded on zeolite supports on tire pyrolysis products: Ru on HMOR and HZSM5. M.S. Thesis 2008 The Petroleum and Petrochemical College, Chulalongkom University, Bangkok, Thailand.
- [4] Viveka A. Michael W, Tetsu O, Michael J, Malin B. Cubosome Description of the Inorganic Mesoporous Structure MCM-48. Chem Mater 1997;9:2,066-2,070.
- [5] Longloilert R, Chaisuwan T, Luengnaruemitchai A, Wongkasemjit S. Synthesis of MCM-48 from silatrane via sol-gel process. J Sol-Gel Sci Technol 2011; doi:10.1007/s10971-011-2409-8
- [6] D\u00fcng NA, Wongkasemjit S, Jitkamka S. Effects of pyrolysis temperature and Pt-loaded catalysts on polar-aromatic content in tire-derived oil. J Anal Appl Pyrol 2008;91:300-307.
- [7] Perring L, Bussy F, Gachon JC, Peschotte P. The Ruthenium-Silicon System. Alloy and compounds 1998;284:198-205.
- [8] Rodriguez M, Laresgoiti MF, Cabrero MA, Torres A, Chomón MJ, Caballero B. Pyrolysis of scrap tyres Fuel Proc Technol 2001;72:9–22.
- [9] Lan-Lan L, Shuangxi L. CuO-containing MCM-48 as catalysts for phenol hydroxylation. Catal Comm 2005;6:762-765.
- [10] Alsobaai AM, Zakaria R, Hameed BH. Hydrocracking of petroleum gas oil over NiW/MCM-48-USY composite catalyst. Fuel Proc Technol 2007;88:921-928.
- [11] Berrueco C, Esperanza E, Mastral FJ, Ceamanos J, Garcı a-Bacaicoa P. Pyrolysis of waste tyres in an atmospheric static-bed batch reactor: Analysis of the gases obtained. J Anal Appl Pyrol 2005;74:245–253.
- [12] Düng NA, Mhodmonthin A, Wongkasemjit S, Jitkamka S. Effects of ITQ-21 and ITQ-24 as zeolite additives on the oil products obtained from the catalytic pyrolysis of waste tire. J Anal Appl Pyrol 2008;85:338–344.

ORIGINAL PAPER

Synthesis and characterization of M-MCM-48 (M = Cr, Ce) from silatrane via sol-gel process

Rujirat Longloilert · Thanyalak Chaisuwan · Apanee Luengnaruemitchai · Sujitra Wongkasemjit

Received: 9 March 2011/Accepted: 3 October 2011/Published online: 12 October 2011 © Springer Science+Business Media, LLC 2011

Abstract Chromium and cerium incorporated into MCM-48 framework are hydrothermally synthesized via sol-gel process without any additives and characterized by X-ray diffraction, N2 adsorption/desorption, Scanning electron microscopy (SEM), Transmission electron microscopy (TEM), Diffuse reflectance UV-vis spectroscopy, and Thermogravimetric analysis. Results indicate that the materials possess a long-range ordered structure, high specific surface area, and narrow pore size distribution. SEM images illustrate the edge-truncated octahedron morphology of Cr-MCM-48 while Ce-MCM-48 preserves the truncated octahedron of the MCM-48 parent material. TEM images show the pore network of Ia3d symmetry after loading metals. Spectroscopic data confirm the existence of metals in the framework and extra-framework. At low Cr content, Cr-MCM-48 contains only Cr(VI) species while rich Cr content loading results in both the Cr(VI) and Cr(III) species. The hydrothermal stability of MCM-48 is enhanced by carefully incorporating metals into the parent material.

Keywords Sol–gel process · Cr-MCM-48 · Ce-MCM-48 · Hydrothermal stability

1 Introduction

Since the 1992 discovery of mesoporous molecular sieves in the M41S family by Mobil's group [1, 2], these materials

R. Longloilert · T. Chaisuwan · A. Luengnaruemitchai · S. Wongkasemjit (☒)

The Petroleum and Petrochemical College, and the Center for Petroleum, Petrochemicals, and Advanced Materials, Chulalongkon University, Bangkok 10330, Thailand e-mail: dsuiitra@chula.ac.th

have attracted remarkable attention due to their high specific surface area, ordered pore structure array, and narrow pore size distribution [3]. Among them, MCM-48 is a more attractive candidate as a catalyst, catalyst support, adsorbent, or template for synthesis of advanced nanostructures, probably owing to its unique three-dimensional pore network. However, these materials possess weak acidity and are deficient in necessary redox ability, thus exhibiting low activity when directly used as catalyst [4]. To obtain materials with high catalytic performance, many attempts have been made to incorporate a hetero-element, such as Cr, Ti, Ce, or V, to the silicate framework so as to enhance the acid and/or redox properties of the materials [5]. Among those hetero-atoms, Cr is attractive as a redoxactive site for many chemical reactions. Consequently, in recent years many researchers have focused on the synthesis of Cr-containing mesoporous materials, including Cr-MCM-41 [6, 7], Cr-MCM-48 [3, 8, 9], Cr-MSU-1 [10, 11], and tested for selective oxidation reaction. Cerium (Ce) is also interesting in terms of catalytic applications since incorporation of Ce in the silica framework provides the Lewis and Bronsted acid sites which affect to the catalytic properties [12]. Hence, many researches focused on the incorporation of Ce in mesoporous materials, such as Ce-KIT-6 [12], Ce-MCM-48 [13-15], Ce-SBA-15 [16], and Ce-MCM-41 [17]. Besides the catalytic properties, the incorporation of hetero-atoms can also enhance hydrothermal stability, as compared to the pure siliceous mesoporous materials found in many reports [3, 15]. However, the synthesis of chromium or cerium-containing MCM-48 with highly ordered pore structure, high specific surface area as well as the truncated octahedron morphology using silatrane as silica source has not been reported.

In this study, we have expanded our previous work [18] by incorporating Cr and Ce into the MCM-48 framework.



The synthesis of M-MCM-48 (where M=Cr and Ce) with various amounts of metals were investigated and characterized using powder XRD, N_2 adsorption/desorption, SEM, TEM, DR-UV, and TGA. In addition, the influence of metal-incorporated MCM-48 on a hydrothermal stability was studied.

2 Experimental

2.1 Materials

Cr-MCM-48 and Ce-MCM-48 mesoporous materials were synthesized hydrothermally, using fumed silica (SiO₂, 99.8%, Sigma-Aldrich, USA), triethanolamine (TEA, Carlo Erba, Italy), triethylenetetramine (TETA) (Facai, Thailand), ethylene glycol (EG, J.T. Baker, USA), acetronitrile (Labscan, Thailand), sodium hydroxide (NaOH, Labscan, Asia), cetyltrimethylammonium bromide (CTAB, Sigma-Aldish, Denmark), chromium(III)nitrate nonahydrate (Himedia, India), and cerium(IV) hydroxide (Sigma-Aldish, U.S.A.)

2.2 Synthesis of M-MCM-48 (M = Cr,Ce)

The Cr-containing MCM-48 materials were synthesized using our previously published method [18]. CTAB, used as a structure-directing agent, was dissolved in a solution containing water and 2 M NaOH. The mixture was stirred continuously with slight heating to dissolve CTAB. Our homemade silatrane, used as a silica source and prepared according to Wongkasemjit's synthetic method [19], was added into the CTAB mixture, followed by adding a required amount of 0.3 M chromium nitrate solution under continuous stirring for 1 h. The molar composition of the gel was 1.0 SiO₂:0.3CTAB:0.50NaOH:62.0H₂O:xCr, where $0.005 \le x \le 0.1$. The process of synthesizing Ce-MCM-48 was similar to that of Cr-MCM-48, except the metal precursor. In this case, we used homemade cerium glycolate synthesized according to a procedure described elsewhere [20]. After the silatrane was added to the solution, a required amount of cerium glycolate was added into the solution under continuous stirring for 1 h. The molar composition of the gel was 1.0 SiO2:0.3CTAB:0.50-NaOH:62.0H₂O:yCe, where $0.01 \le y \le 0.09$. The resulting mixture was transferred to a Teflon-lined stainless steel autoclave and treated at 140 °C for 16 h. The resulting solid product was collected by filtration and dried overnight at ambient conditions. The removal of all organics was performed by calcination at 550 °C for 6 h (Carbolite, CFS 1200, Hope Valley, UK) at a heating rate of 0.5 °C/min to obtain mesoporous M-MCM-48. All of the obtained Cr-MCM-48 samples varied in color from yellow to green, depending on the amount of Cr, while the color of the obtained Ce-MCM-48 was only yellow. The samples prepared were denoted as Cr-MCM-48-(x) and Ce-MCM-48-(y), where x and y were the ratios of Cr/Si and Ce/Si in the solution, respectively. The metal-free MCM-48 was synthesized with the same procedure to compare.

2.3 Characterization

The M-MCM-48 products were characterized using an XRD (Rigaku, Japan) and CuK α radiation in the range of $2\theta=2^{\circ}$ –60° at a scanning speed of 1 °C/min, 40 kV, and 30 mA. The morphology of products was studied by a field emission scanning electron microscope (FE-SEM, Hitachi/S-4800). The order of mesopores was investigated using a TEM (JEOL 2010F). The specific surface area and average pore size were estimated by the Brunauer-Emmett-Teller (BET) method on a Quantasorb JR instrument (Mount Holly, NJ). DRUV spectra of samples were recorded from 200 to 800 nm on a Shimadzu UV-2550 spectrophotometer using BaSO₄ as a reference. Thermogravimetric analysis of materials was carried out on Perkin-Elmer instruments using a heating rate of 10 °C/min from room temperature to 650 °C in a nitrogen atmosphere.

2.4 Hydrothermal stability test

Following the method of Jun et al. [21], 0.1 g of a calcined sample in 100 mL of distilled water was boiled in a round-bottom flask connected with a reflux condenser for 12 h. The sample was recovered by filtration and drying in air overnight for further characterization. Then, the XRD pattern was obtained and compared with the same sample before the heat treatment to determine the hydrothermal stability.

3 Results and discussion

3.1 XRD

According to Table 1, unit cell parameter and d-spacing of the as-synthesized samples slightly increased with an increase in Cr/Si ratio, indicating that Cr had slightly or no influence on the silica framework [6]. This can be explained in terms of the incorporation of a larger cation, such as Cr(III) (0.76 Å) in the tetrahedral geometry of Si (0.40 Å), as a consequence of the expansion of the unit cell. However, the small expansion in a_0 and higher d values were noticed, which could imply that the chromium species was filled in the pores, in agreement with those described by Sakthivel and Selvam [6]. Nevertheless, the structure of MCM-48 was preserved after loading of Cr, as can be noticed in the XRD patterns in Fig. 1a. Furthermore, the as-synthesized samples were pale green in color and



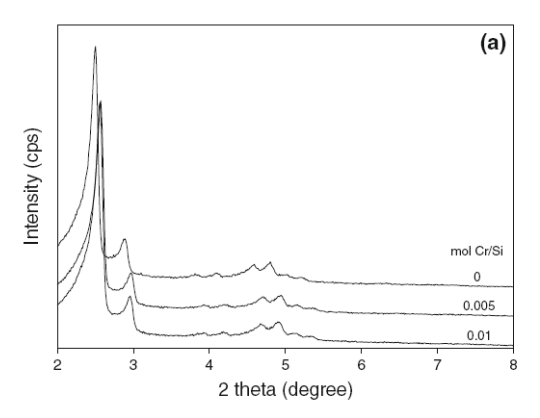
Table 1 The unit cell parameter $(a_0$, calculated by $a_0 = d_{211}(6)^{1/2}$ and the d spacing of all synthesized samples with different chromium and cerium contents

Sample	M/Si (M = Cr,Ce) (mol)	a ₀ (nm)	d-spacing (nm)
MCM-48	∞	9.45	3.86
Cr-MCM-48	0.005	9.49	3.88
Cr-MCM-48	0.01	9.66	3.94
Ce-MCM-48-(0.01)	0.01	9.53	3.89
Ce-MCM-48-(0.03)	0.03	9.58	3.91
Ce-MCM-48-(0.05)	0.05	9.79	4.00
Ce-MCM-48-(0.07)	0.07	9.71	3.96
Ce-MCM-48-(0.09)	0.09	9.75	3.98

changed to yellow after calcination. This could suggest that the trivalent chromium ions in octahedral geometry were changed to the higher valent chromium ions, viz., chromate and/or polychromate ions, in the tetrahedral environment [6]. These results were consistent with the decrease in a₀ values of calcined samples in Table 2, which may be attributed to the short double bond Cr = O in Cr_2O_3 or Cr_2O_5 . As mentioned earlier, it is also indicated that the calcined samples were composed mostly of Cr(VI) or Cr(V) species, as compared to a lower valent [22]. However, the structural alteration was obtained in increasing the Cr/Si ratio higher than 0.01 (not shown). This might be a result of the high Cr content affecting the surfactant-silicate interaction which was involved in the assembly of the surfactant and silicate species [23]. Similar to the work of Shao et al. [3] the lessordered structure at high Cr content was obtained due to the lower peak intensity and unresolved patterns, probably due to the partially collapsed structure. Interestingly, for the first time, we found in our case that the structure was changed from MCM-48 to MCM-41 as Cr content increased.

Figure 1b exhibited the XRD patterns of calcined Cr-MCM-48 samples over the range of 10° – 60° . The addition of small diffraction peaks at $2\theta=24.5^{\circ}$, 33.6° , 36.2° , and 54.8° belonging to the hexagonal phase of Cr_2O_3 was detected at a Cr/Si ratio above 0.05 [11]. It could be inferred that all Cr/Si ratios below 0.05 resulted in Cr incorporated into MCM-48 framework. Additionally, there was no Cr_2O_3 metal oxide diffraction peaks at high-angle XRD patterns of the samples having the Cr/Si ratio in the range of 0.005–0.03. Shen and coworker [24] found that Cr was well dispersed in silica when observing no diffraction peak at the high angle XRD pattern. Thus, in our case, we could imply that the Cr atoms were in the framework of MCM-48 structure since the DR-UV–Vis results, which is discussed later in more detail, was also used to confirm.

Considering the XRD patterns of calcined Ce-MCM-48, all samples provided a well-resolved XRD pattern of MCM-48 even at high Ce loadings. It could be inferred that the



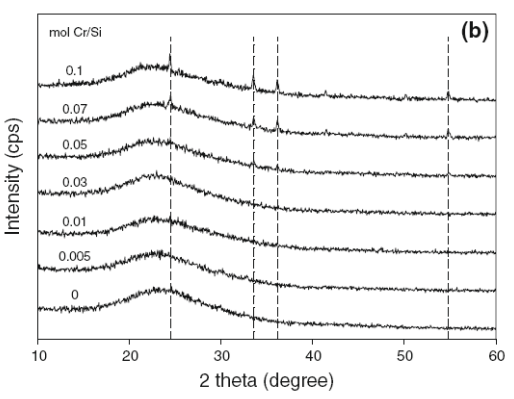


Fig. 1 The XRD patterns of the calcined Cr-MCM-48 samples with different Cr contents over the range of a 2 theta = 2° -8° and b 2 theta = 10° -60°

incorporation of cerium in the silica framework did not change the cubic Ia3d pore network. Moreover, the secondary peaks $(2\theta = 3^{\circ}-6^{\circ})$ were obviously seen in all samples, as shown in Fig. 2a. It could be pointed out that the long-range order of the MCM-48 structure was obtained [25]. As compared to the study of Shao et al. [15], who synthesized the long-range ordered Ce-MCM-48 by the aid of fluoride ions with 0.1 molar ratio, our results were obtained with no addition of any ions. The unit cell parameters and the d-spacing of both as-synthesized and calcined Ce-MCM-48 were shown in Tables 1 and 2, respectively.

The XRD patterns of the calcined Ce-MCM-48 materials, over the range of 10° – 60° , are demonstrated in Fig. 2b. The MCM-48 provided the pattern corresponding to the amorphous-like nature of silica [26]. No additional peaks appeared for all the materials prepared with the Ce/Si ratios in the range of 0.01–0.03. Even over the Ce/Si range of 0.05–0.09, only a few weak broad peaks could barely be noticed around the 2 theta of 28.55°, 47.47° and 56.33°,



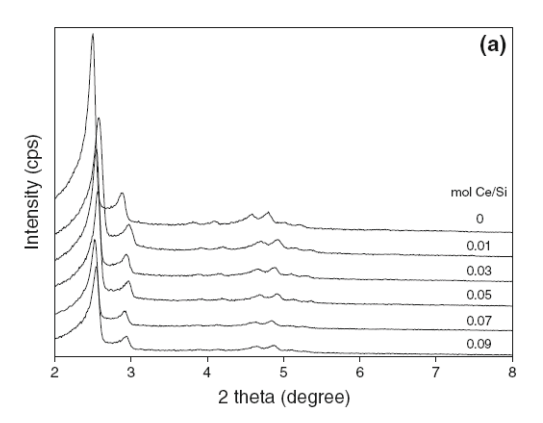
Table 2 The characteristics of the calcined samples with a molar gel composition of 1.0SiO_2 :0.3CTAB:0.50NaOH:62.0H₂O:xCr or yCe, where $0 \le x \le 0.01$ and $0 \le y \le 0.09$ (a₀ was calculated by $d_{211}(6)^{1/2}$ and wall thickness was calculated by $a_0/3.0919$ — pore diameter/2)

Sample	S_{BET} (m^2/g)	Pore volume (cm ³ /g)	Pore diameter (nm)	a ₀ (nm)	d-spacing (nm)	Wall thickness (nm)
MCM-48	1,711	1.14	2.67	8.66	3.53	1.47
Cr-MCM-48-(0.005)	1,511	0.86	2.27	8.42	3.44	1.60
Cr-MCM-48-(0.01)	1,477	0.85	2.30	8.45	3.45	1.59
Ce-MCM-48-(0.01)	1,581	0.95	2.41	8.39	3.42	1.51
Ce-MCM-48-(0.03)	1,286	0.78	2.42	8.49	3.46	1.54
Ce-MCM-48-(0.05)	1,183	0.72	2.44	8.45	3.45	1.51
Ce-MCM-48-(0.07)	1,028	0.62	2.41	8.59	3.51	1.58
Ce-MCM-48-(0.09)	1,062	0.66	2.47	8.52	3.48	1.52

corresponding to the (111), (220) and (311) planes, respectively, for the main characteristic lines of ceria (CeO2) structure. These results indicate that the fine, small particles of ceria might be formed within MCM-48, as described by Khalil [27]. He synthesized Ce-containing MCM-41 prepared via a direct and non-hydrothermal method with 5% and 10% (w/w) of CeO2/silica and found that the cerium inserted into the framework of MCM-41 and/or the formation of finely divided ceria nanoparticles on the wall of MCM-41 was obtained. The intensity of ceriacharacteristic peaks gradually increased with an increase in the Ce content, meaning that the amount of CeO2 in the channel or in the extra-framework increased, as also reported by Wangcheng et al. [13]. Additionally, they obtained low intense diffractions of the secondary peaks even at low Ce content (Ce/Si = 0.02), implying that there was no long-range ordered structure. In contrast to our work, the highly ordered structure was sustained even at high Ce loadings. This might be a result from the presence of the by-products, EG and TEA, generated from the hydrolysis of cerium glycolate and silatrane precursors, respectively. Both EG and TEA were able to enhance the ordering of MCM-48 structure, as discussed elsewhere [18].

3.2 Hydrothermal stability test

The XRD patterns (not shown) of the calcined MCM-48 after refluxing in boiling water for 12 h indeed lost its mesoporous-ordered structure, as described by Shao et al. [15]. Generally, the hydrolysis rate of Si–O–Si bonds is quite fast, resulting in the collapsed structure, if the pore walls of the materials are thin or have less polymerization [3]. However, the XRD pattern of calcined Cr-MCM-48 samples (not shown) exhibited a partly maintained mesoporous structure when compared to the complete loss of peaks in the MCM-48. This could imply that the incorporation of Cr to the structure was able to enhance the hydrothermal stability of MCM-48, as explained in terms



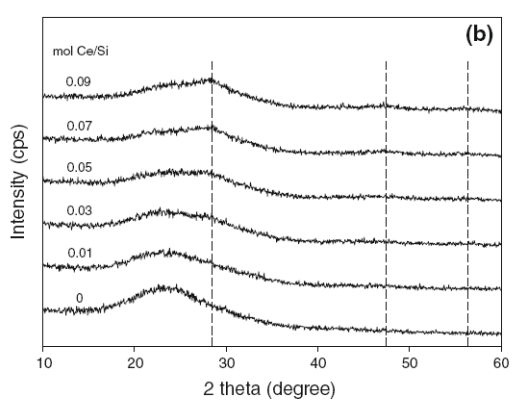


Fig. 2 The XRD patterns of the calcined Ce-MCM-48 samples with different Ce contents over the range of a 2 theta = 2° -8° and b 2 theta = 10° -60°

of the higher resistance to water attack of the Si–O-Cr bonds compared to the Si–O-Si bonds [15]. A similar effect was found by Xia et al. [28, 29] who incorporated Al into mesoporous materials.



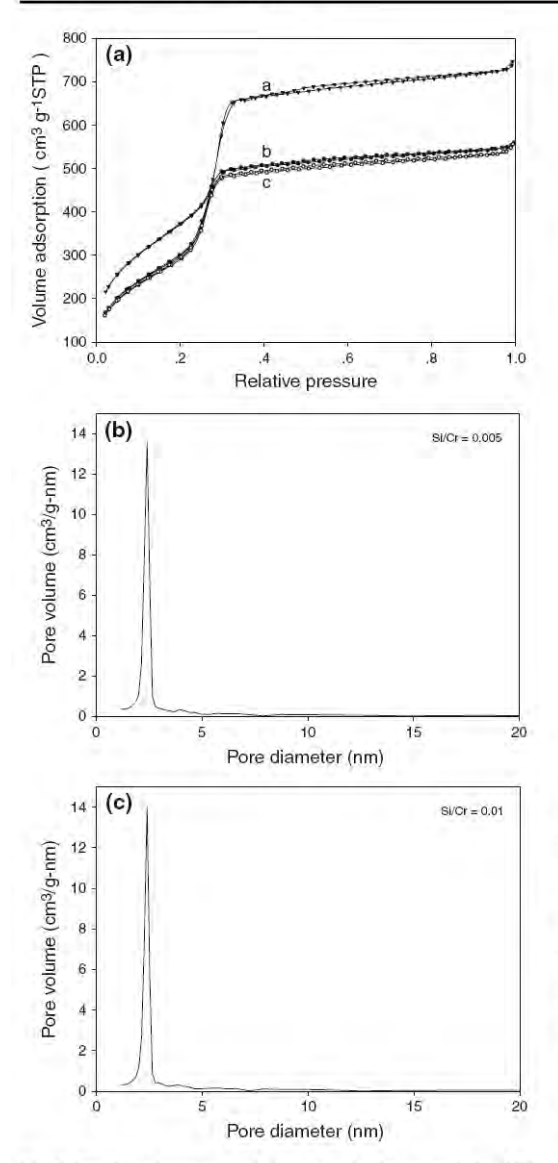
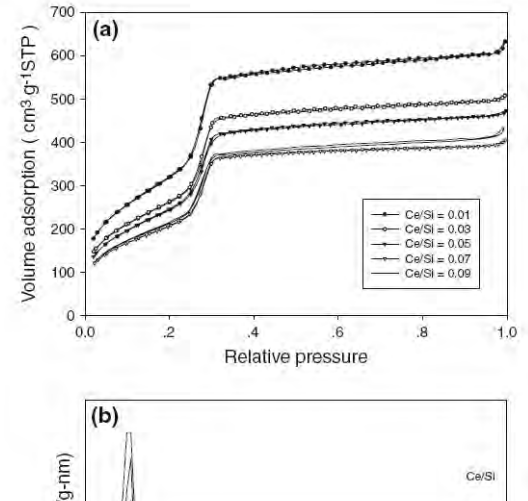


Fig. 3 The N_2 adsorption and desorption isotherms and the BJH pore-size distributions (calculated from desorption branch of isotherm) of calcined Cr-MCM-48 with different Cr/Si ratios of a 0, b 0.005 and c 0.01

In contrast to the calcined Ce-MCM-48 materials with all Ce/Si ratios, after refluxing the samples in boiling water for 12 h, the results showed that most of the samples could not preserve the structure of MCM-48 (XRD patterns not shown), excluding 0.01 Ce/Si ratio. A structure of Ce-



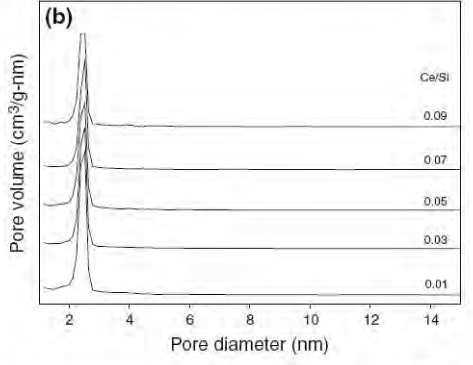


Fig. 4 a The N_2 adsorption and desorption isotherms and b the BJH pore-size distributions (calculated from desorption branch of isotherm) of calcined Ce-MCM-48 with different Ce/Si ratios

MCM-48-(0.01) was not completely lost, as compared to others. A similar observation was found in the work of Shao et al. [15], who explained in terms of the formation of Si-O-Ce bonds, which possessed more resistance to water attack than the Si-O-Si bonds, and high Ce contents could not efficiently enhance this property. They, thus, suggested that the structure ordering was considerably destroyed at the high Ce contents, leading to the decrease of hydrothermal stability.

$3.3\ N_2$ adsorption and desorption isotherms

The N_2 adsorption and desorption isotherms in Fig. 3 were typical type IV isotherms in the IUPAC classification. The isotherms exhibited a sharp curve in the region of $P/P_0 = 0.3$ –0.4, indicating a uniform pore size and highly ordered pore structure. These results were in harmony with the XRD patterns (Fig. 1a), showing a well-resolved secondary diffraction above 3.5 degrees of 2-theta, corresponding to a highly long-range order of these materials.

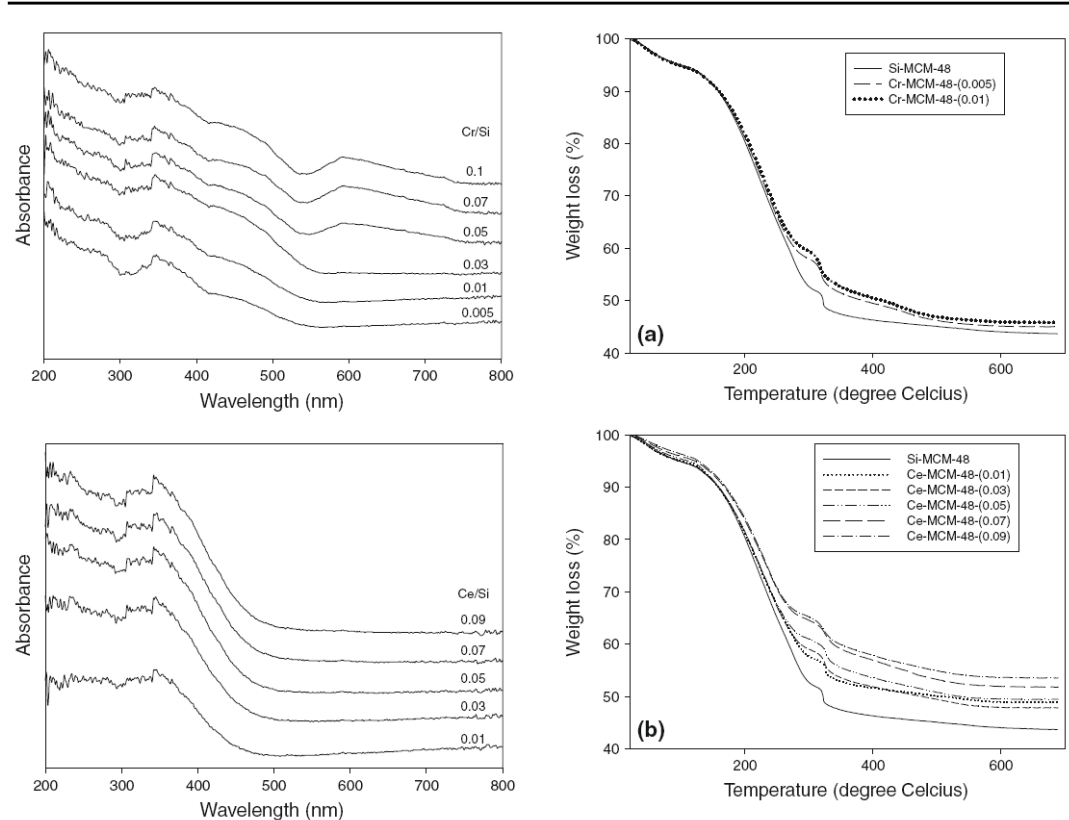


Fig. 5 DR-UV-Vis spectra of calcined Cr-MCM-48 and Ce-MCM-48 with different Cr/Si and Ce/Si ratios

Furthermore, according to Figs. 3 and 4, there is no hysteresis loop in the isotherms due to the absence of the capillary condensation in the materials with the pore diameter in the range of 2.27-2.47 nm. In addition, the inflection became less sharp with an increase in the amount of Cr in the materials, meaning that the well-ordered mesoporous structure could be destroyed by increasing the Cr content. Similar results were obtained by incorporation of Cr into MCM-41 [24]. Table 2 presents the characteristics of materials, viz., surface area, pore volume, and pore diameter. Interestingly, Cr-MCM-48-(0.005) and Cr-MCM-48-(0.01) have extremely high specific surface areas of 1,511 and 1,477 m²/g, respectively, and a very narrow pore size distribution with a pore size of 2.27 and 2.30 nm, respectively. A decrease in the specific surface area with an increase in the Cr content was similar to the Cr-MCM-48 synthesized by Shao et al. [3], using a molar composition of the final gel mixture of 1.0TEOS:

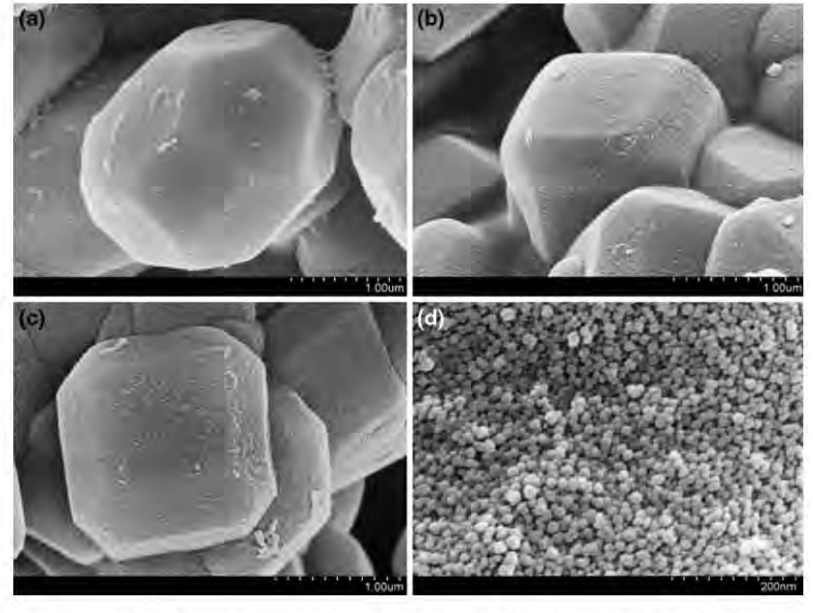
Fig. 6 TGA plots of a Cr-MCM-48 and b Ce-MCM-48

0.65CTAB:0.5NaOH:62H₂O:xCr(NO₃)₃.9H₂O where x = 0.005-0.04; or similar to Ga- or Al-containing MCM-41 [30, 31].

In the case of the calcined Ce-MCM-48 materials, the results revealed a decrease in surface area from 1,571 and 1,062 m²/g as the Si/Ce ratio was increased from 0.01 to 0.09 (see Table 2), similar to the incorporation of Cr. Generally, an increase of the pore wall thickness is known to increase hydrothermal stability [21]. In our case, both Cr- and Ce- incorporated MCM-48, providing a thicker wall thickness, should give a positive effect to the hydrothermal stability. The materials also possessed the long plateau at higher relative pressure (see Figs. 3, 4), implying that there was no pore filling after $P/P_0 = 0.3$, relating to wider mesopores [27]. Furthermore, the pore volume also decreased with an increase in the metal content, resulting in irregularity of mesopores, as described by Prabhu et al. [12]. Due to the steep of the capillary step in all samples, a narrow pore size distribution with diameters of 2.41-2.47 nm was thus achieved.



Fig. 7 SEM images of a MCM-48 (×35,000), b Cr-MCM-48 (0.005, ×40,000), c Cr-MCM-48 (0.01, ×40,000), and d Cr-MCM-48 (0.005, ×200.000)



In general, the unit cell parameter (a₀) and the d-spacing should increase with an increase in the amount of heteroatoms into the silicate framework [13, 24]. Many authors suggested that the M-O bond distance was longer than the Si-O one, leading to an increase in those parameters, as a result, knowing the presence of metal atoms in the framework of porous materials. In our case, the ao and the d-spacing decreased as metals were introduced into the materials, meaning that our results were not in agreement with those suggested elsewhere, but they were consistent with the study of Liu et al. [10]. They synthesized Cr-MSU-1, and the results showed that the d-spacing of the Cr-MSU-1 was not always larger than that of MSU-1. According to the explanation of Liu et al. [10], the higher degree of freedom of the system and the larger Cr-O bond, compared to the Si-O bond, should both contribute to the slight difference in the repeat distance in pure MSU-1 and Cr-MSU-1. This explanation could be supported by Arnold et al. [32] who synthesized V-MCM-41 and postulated that the bond distance and bond angle in mesoporous metallosilicate materials had a higher degree of freedom, as compared to the crystalline materials. They also suggested that MCM-41 was not a crystalline material and an alteration of repeat distance could not be directly compared with those crystalline materials.

3.4 DR-UV-Vis spectroscopy

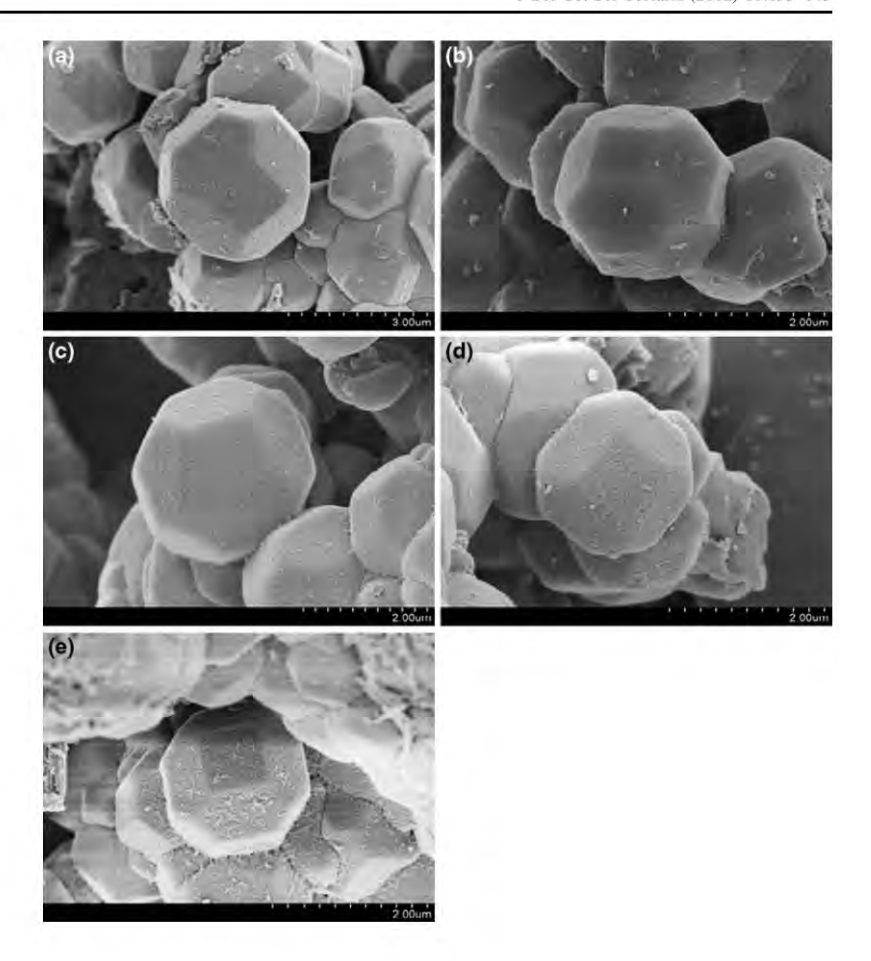
Generally, this technique is a very sensitive tool for characterizing metal ion coordination of metal containing

zeolites to provide valuable information about the presence of metal ions in the framework and/or extra-framework [27]. Figure 5 depicts the DR-UV-Vis spectra of calcined Cr-MCM-48 and Ce-MCM-48 with different Cr and Ce contents, respectively. All the spectra of the calcined Cr-MCM-48 with different Cr/Si ratios showed two bands around 260 and 350 nm. These absorption bands are generally assigned to O → Cr(VI) charge transfers of the chromate species [3]. The Cr(VI) polychromates at around 440 nm also existed in the materials. Moreover, the two typical bands of octahedral Cr(III) at 445 and 595 nm were found in the spectra of the calcined Cr-MCM-48(x) where $0.05 \le x \le 0.1$, consistent with the wide angle XRD results shown in Fig. 1a. Hence, only Cr(VI) chromate was found in Cr-MCM-48 samples with low Cr loading, but the samples synthesized at higher Cr loading contained both Cr(VI) chromate and Cr(III) species.

As for Ce-MCM-48 samples, in general, the position of ligand-to-metal charge-transfer ($\mathrm{O}^{2-} \to \mathrm{Ce}^{4+}$) spectra depends on the ligand field symmetry surrounding the Ce center, and the electronic transitions from oxygen to a tetracoordinated Ce^{4+} require higher energy than a hexacoordinated one [15]. According to the spectra in Fig. 5, there was a weak broad absorption band at 200–300 nm and an intense band at around 350 nm, appearing for all Ce/Si ratios, and the increasing band intensities were found with an increase in the Ce content. Therefore, the absorption bands at those positions related to the presence of Ce^{4+} species with tetracoordination in the samples. Additionally, there was no absorption band at a higher wavelength



Fig. 8 SEM images of Ce-MCM-48 with the Ce/Si ratio, y, of a 0.01, b 0.03, c 0.05, d 0.07, and e 0.09



(405 nm) corresponding to the hexacoordinated Ce⁴⁺ of CeO₂, as described in Wangcheng's work [13]. It could be concluded that much a higher amount of the tetracoordinated Ce in Ce-MCM-48 was present in the MCM-48 framework than those reported elsewhere [13, 15].

3.5 TGA

Weight losses for all synthesized samples were observed in the TGA plots (Fig. 6a). All Cr-MCM-48 samples revealed typical weight loss patterns, as reported elsewhere [33, 34]. It could be divided into three stages: the first stage attributed to the loss of physisorbed water below 100 °C, the second one belonged to the removal of organic components at a temperature below 350 °C and the last one at 350–600 °C corresponded to the removal of carbon residues. Furthermore, the different features on the TGA curves of the Cr-MCM-48 and the pure MCM-48, might

indicate the interaction between the incorporated Cr component and the surfactant molecules [34]. Similar observation was also reported by Kawi et al. who synthesized MCM-48 supported Cr by introduction of chromium chloride during gel preparation of hydrothermal synthesis of MCM-48.

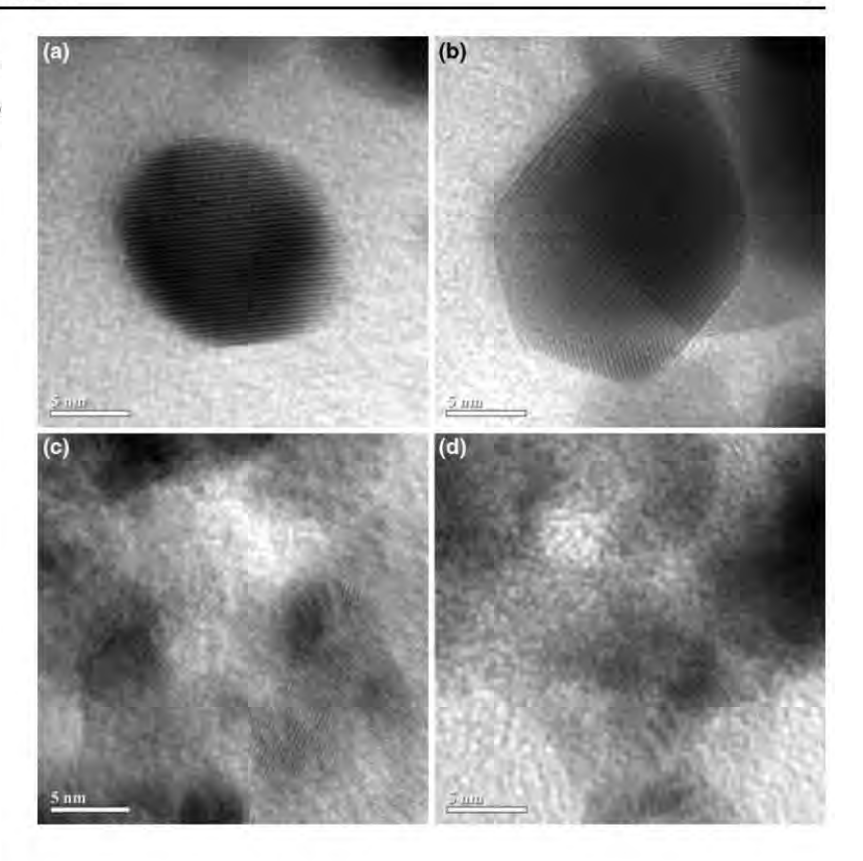
TGA curves of the synthesized Ce-MCM-48 in all Ce/Si ratios provided weight loss patterns similar to the pure MCM-48 as illustrated in Fig. 6b. The weight loss steps occurred through the temperature range, as described above.

3.6 FE-SEM

When more chromium was loaded in the MCM-48 supported with a Cr content of 0.005 and 0.01 mol, it was the first time we were able to observe the morphology change of calcined samples from the truncated octahedron of



Fig. 9 TEM images of Cr-MCM-48 (0.005) with incident direction along a [100] and b [432]; and Cr-MCM-48-(0.01) with incident direction along c [100] and d projection of [100]



MCM-48 (see Fig. 7a) to the edge-truncated octahedron [35], implying that the chromium incorporated in MCM-48 affected the morphology of material, as shown in Fig. 7b, c. Our results were consistent with the study of Jha et al. [23], who obtained differences in the morphology of samples after incorporating various metals into MCM-41. The M-MCM-41 (M = Ti, V, Cr) showed spongy, flowerlike, and agglomerated structures, respectively. These might be attributed to the presence of foreign ions in the synthesis gel, changing the surfactant-silicate interactions affected by the nature of metal source used [23]. These results are also in good agreement with those obtained by Parvulescu et al. [36]. They noticed that the morphological structure of MCM-41 surface could be modified by various metal ions. Furthermore, the enlargement of our samples (see Fig. 7d) revealed the primary particles of around 20 nm agglomerating to bigger edge-truncated octahedral particles in Fig. 7a, b. Similar observation was found in the calcined Ce-MCM-48 samples with all Ce/Si ratios, but the parent truncated octahedral MCM-48 still remained, as shown in Fig. 8.

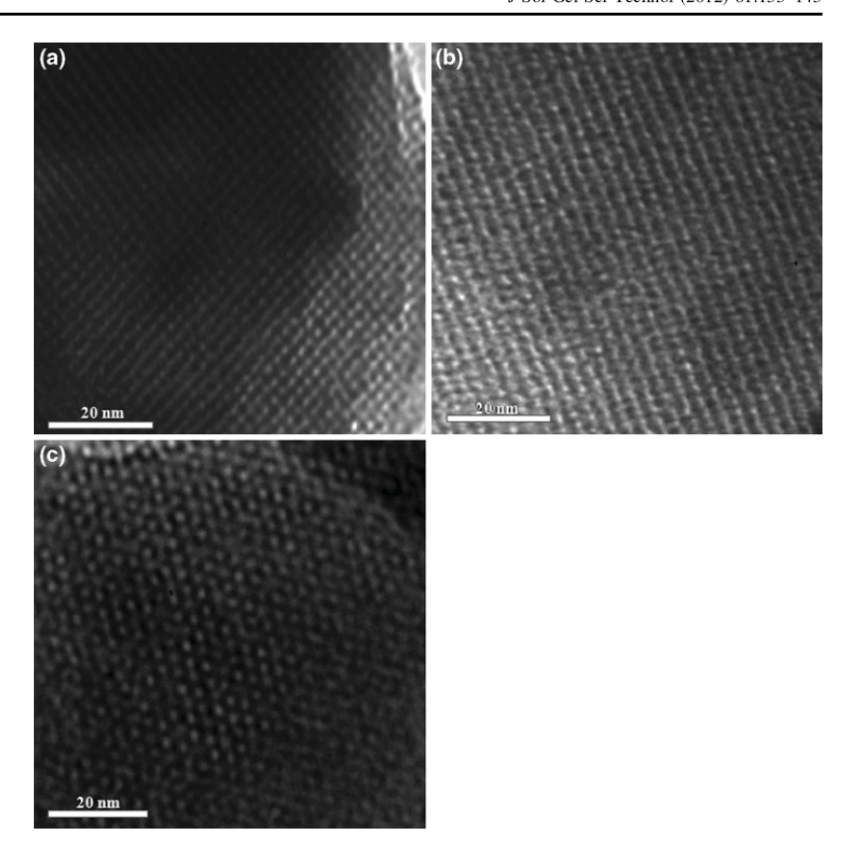
3.7 TEM

TEM images of the calcined Cr-MCM-48-(0.005) with the incident direction along [100] and [432] (Fig. 9a, b) were similar to the study of Alfredsson and Anderson [37], demonstrating that the pore structure along this direction was a uniform channel system. From Fig. 9c, d, TEM images of the calcined Cr-MCM-48-(0.01) with the incident along [100] and [100] projection not only exhibited a uniform pore structure, but also reflected the structure of the pore channel. All TEM images agreed well with the XRD results given in Fig. 1a.

Figure 10 illustrates the TEM images of Ce-MCM-48-(y), where y = 0.01, 0.05, 0.09 with the incident direction along [531], [100] and [111], respectively. They all indicated the la3d symmetry, as reported elsewhere [18, 38]. These results can confirm that the introduction of Ce does not damage the silica framework, and the pore structure is still maintained the cubic la3d symmetry even at a high Ce content. Besides, the long-range ordered structures were obtained, confirming the XRD patterns in Fig. 2a.



Fig. 10 TEM images with incident direction along a [531], b [100] and c [111] of Ce-MCM-48-(0.01, 0.05 and 0.09), respectively



4 Conclusions

In summary, the chromium- and cerium-incorporated MCM-48 were successfully synthesized by hydrothermal technique. They retained not only a long-range ordered structure of materials, but also their high specific surface area with a narrow pore size distribution after the incorporation of metal. The spectroscopic characterizations confirmed that Cr-MCM-48 contained Cr(VI) species at a low Cr content while both of the Cr(VI) and Cr(III) species existed in the rich Cr content. Ce-MCM-48 with all Ce contents showed the presence of Ce4+ tetracoordination in the framework in DRUV while the wide-angle XRD results indicated the existence of CeO2 crystallites in the extraframework at high Ce content. The morphology of metal-MCM-48 depended on the metal incorporated, in which the Cr-MCM-48 provided the edge-truncated octahedron morphology whereas the Ce-MCM-48 preserved the parent material shape. The hydrothermal stability for both metalincorporated MCM-48 materials relied on the amount of metal loading.

Acknowledgments This research is financially supported by the Thailand Research Fund and the Center for Petroleum, Petrochemicals, and Advanced Materials, Chulalongkorn University, Thailand. The authors would like to thank Mr. John M. Jackson for English proofreading.

References

- 1. Kresge CT, Leonowicz ME, Roth WJ, Vartuli JC, Beck JS (1992) Nature 359:710
- Beck JS, Vartuli JC, Roth WJ, Leonowicz ME, Kresge CT, Schmitt KD, Chu CTW, Olson DH, Sheppard EW, McCullen SB, Higgins JB, Schlenker JL (1992) J Am Chem Soc 114:10834
- Shao Y, Wang L, Zhang J, Anpo M (2008) Micropor Mesopor Mater 109:271–277
- Vinu A, Srinivasu P, Miyahara M, Ariga K (2006) J Phys Chem B 110:801
- 5. Corma A (1997) Chem Rev 97:2373
- 6. Sakthivel A, Selvam P (2002) J Catal 211:134-143
- 7. Samanta S, Mal NK, Bhaumik A (2005) J Mol Catal A Chem 236:7-11
- 8. Laha SC, Gläser R (2007) Micropor Mesopor Mater 99:159–166
- 9. Sakthivel A, Dapurkar SE, Selvam P (2001) Catal Lett 7:155-158
- 10. Liu L, Hi L, Zhang Y (2006) J Phys Chem B 110:15478-15485



- 11. Liu H, Wang Z, Hu H, Liang Y, Wang M (2009) J Solid State Chem 182:1726-1732
- 12. Prabhu A, Kumaresan L, Palanichamy M, Murugesan V (2010)
- Appl Catal A 374:11–17
 13. Wangcheng Z, Guanxhong L, Yanglong F, Yun G, Yanqin W, Yunsong W, Zhigang Z, Xiaohui L (2008) J Rare Earths 26:515-522
- 14. Wang L, Shao Y, Zhang J, Anpo M (2006) Chem Lett 35:70-71
- 15. Shao Y, Wang L, Zhang J, Anpo M (2005) J Phys Chem B 109:20835-20841
- 16. Dai Q, Chen G, Wang X, Lu G (2007) Stud Surf Sci Catal 165:81-84
- 17. Kadgaonkar MD, Laha SC, Pandey RK, Kumar P, Mirajkar SP, Kumar R (2004) Catal Today 97:225-231
- 18. Longloilert R, Chaisuwan T, Luengnaruemitchai A, Wongkasemjit S (2011) J Sol Gel Sci Technol 58:427-435
- 19. Phiriyawirut P, Magaraphan R, Jamieson AM, Wongkasemjit S (2003) Micropor Mesopor Mater 64(1-3):83-93
- 20. Ksapabutra B, Gulari E, Wongkasemjit S (2004) Mater Chem Phys 88:34-42
- 21. Jun S, Kim JM, Ryoo R, Ahn YS, Han MH (2000) Micropor Mesopor Mater 41:119-127
- 22. Wang L, Wang L, Zhang J (2009) J Mater Sci 44:6512-6518
- 23. Jha RK, Shylesh S, Bhoware SS, Singh AP (2006) Micropor Mesopor Mater 95:154-163

- 24. Shen S, Guo L (2000) Cat Today 129:414-420
- 25. Kim WJ, Yoo JC, Hayhurst DT (2000) Micropor Mesopor Mater 39:177
- 26. Kaneda M, Tsubakiyama T, Carlsson A, Sakamoto Y, Ohsuna T, Terasaki O (2002) J Phys Chem B 106:1256-1266
- 27. Khalil KMS (2007) J Colloid Interface Sci 315:562-568
- 28. Xia Y, Mokaya R (2003) J Phys Chem B 107:6954
- 29. Xia Y, Mokaya R (2004) Micropor Mesopor Mater 68:1
- 30. Cheng C, He H, Zhou W, Klinowski J, Goncalves J, Gladden L (1996) J Phys Chem 100:390
- 31. Luan Z, He H, Zhou W, Cheng C, Klinowski J (1995) J Chem Soc Faraday Trans 9:2955
- 32. Arnold ABJ, Niederer JPM, Niessen TEW, Hölderich WF (1999) Micropor Mesopor Mater 28:353
- Subrahmanyam C, Louis B, Rainone F, Viswanathan B, Renken A, Varadarajan TK (2003) Appl Catal A 241:205-215
- 34. Kawi S, Te M (1998) Catal Today 44:101-109
- 35. Breen TL, Tien J, Oliver SRJ, Hadzic T, Whitesides GM (1999) Science 284:950
- 36. Parvulescu V. Anastasescu C. Su BL (2003) J Mol Catal A Chem 1:3919
- 37. Alfredsson V, Anderson WM (1996) Chem Mater 8:1141-1146
- 38. Ohsuna T, Sakamoto Y, Terasaki O, Kuroda K (2011) Solid State Sci 13:736-744



Materials Letters 94 (2013) 65-68



Contents lists available at SciVerse ScienceDirect

Materials Letters

journal homepage: www.elsevier.com/locate/matlet



Synthesis and characterization of Fe-Ce-MCM-48 from silatrane precursor via sol-gel process

Hussaya Maneesuwan, Rujirat Longloilert, Thanyalak Chaisuwan, Sujitra Wongkasemjit*

The Petroleum and Petrochemical Collège and Center of Excellence on Petrochemical and Materials Technology, Chulalongkorn University, Bangkok 10330. Thailand

ARTICLE INFO

Article history: Received 4 September 2012 Accepted 28 November 2012 Available online 12 December 2012

Keywords; Bimetallic mesoporous molecular sieves Fe-Ce-MCM-48 Silatrane Sol-gel process

ABSTRACT

A series of Fe (0.01 mol) and Ce (0.01 to 0.09 mol) incorporated into MCM-48 framework was successfully synthesized by sol-gel method using cetyltrimethylammonium bromide (CTAB) as a structural directing agent; and silatrane, FeCl₃, and cenium glycolate as silica, iron, and cerium sources, respectively. X-ray diffraction (XRD) patterns showed well-defined order cubic mesoporous structures while N₂ adsorption/desorption measurements indicated that the synthesized bimetallic materials had a BET surface area of up to 1225 m²/g, large mesopores (3.1 nm), mean pore volume, and diameters of 0.83 cm²/g and 2.89 nm, respectively. X-ray fluorescence (XRF) revealed the total metal content of the final product. UV-visible absorption spectra confirmed that both iron (Fe³⁺) and centum (Ce⁴⁺) species highly dispersed in the framework. Scanning electron microscopy (SEM) showed the truncated octahedron morphology of Fe-Ce-MCM-48.

@ 2012 Elsevier B.V. All rights reserved,

1. Introduction

The mesoporous materials discovered by Mobil group are known as the M41S family [1]. These materials can overcome the limitations of microporous materials unable to allow large reactants to penetrate inside the pores. The main members of the M41S family are hexagonal MCM-41, cubic MCM-48, and unstable lamellar MCM-50 mesostructures. Among them, MCM-48 is the most attractive material, owing to its three-dimensional, interconnected channels, providing more advantages-including fast diffusion and resistance to pore blocking of coming moleculesover the one-dimensional pores of MCM-41. Moreover, due to its long-range order, large surface area, and narrow pore size distribution, MCM-48 has been used as an adsorbent, catalyst, and catalyst support, sensor, as well as an inorganic template for the synthesis of advanced nanostructure [2-5]. However, the pure silica MCM-48 lacks catalytic active sites, and thus, many researchers have attempted to incorporate heteroatoms (such as Fe, Ce, Cr, V, Ti, etc. [6-8]) into the mesoporous framework to enhance its redox properties. MCM-48, supporting two or more metal atoms, is very attractive since one metal can modify the structural and redox properties of the other. Consequently, bimetallic catalysts usually improve catalytic activity, selectivity, and stability of the monometallic catalysts. Many reports have shown that Fe-containing materials have a high activity in phenol hydroxylation [6,9] and cerium enhances hydrothermal stability [7,10]. Generally, in

Fig. 1. XRD patterns of MCM-48, Fe-MCM-48, Ce-MCM-48 and Fe-Ce-MCM-48.

0167-577X/\$- see front matter © 2012 Elsevier B.V. All rights reserved. http://dx.doi.org/10.1016/j.matlet.2012.11.139

<sup>(211)
(220)
(420) (332)
(420) (332)

0.01</sup>Fe-MCM-48
0.03Ce-MCM-48
0.09Ce-MCM-48
0.09Ce-MCM-48
0.01Fe0.03Ce-MCM-48
0.01Fe0.03Ce-MCM-48
0.01Fe0.03Ce-MCM-48
0.01Fe0.03Ce-MCM-48
0.01Fe0.03Ce-MCM-48
0.01Fe0.03Ce-MCM-48
0.01Fe0.03Ce-MCM-48

^{*}Corresponding author. Tel.: +66 2 218 4133; fax: +66 2 215 4459. E-moß address: dsujitra@chula.ac.th (S. Wongkasemjit).

catalytic reactions, the catalyst is exposed to high temperatures or boiling water; therefore, the loss of hydrothermal stability could be a serious barrier for application. Simultaneous incorporation of these two metals on to MCM-48 might enhance both its phenol hydroxylation and hydrothermal properties. In this study, Fe-Ce-MCM-48 loading different iron and cerium contents was hydrothermally synthesized via sol-gel method and characterized using XRD, XRF, N2 adsorption/desorption, DRUV, and SEM.

2. Experimental

Materials: Fumed silica (99.8%, SiO2), cerium (IV) hydroxide (Ce(OH)4), and iron (III) chloride hexahydrate (FeCl3 · 6H2O) from Sigma-Aldrich, USA: hexadecyltrimethyl ammonium bromide (CTAB) from Fluka, Denmark; triethylenetetramine (TETA) from Facai, Thailand; ethylene glycol (EG) from J.T. Baker, USA;

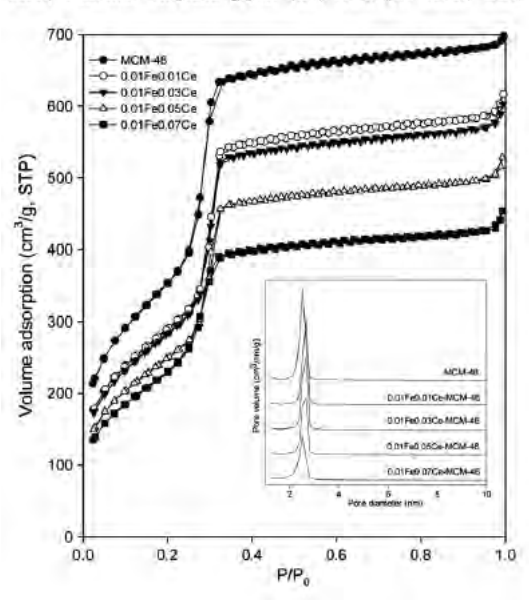


Fig. 2. N₂ adsorption/desorption isotherms of MCM-48 and Fe-Ce-MCM-48.

triethanolamine (TEA) from QREC, Asia; and acetronitrile and sodium hydroxide (NaOH) from Labscan, Asia, were used without purification.

Synthesis of xFe-yCe-MCM-48: Bimetallic MCM-48 materials were synthesized using Wongkasemjit's method [11]. A desired amount of FeCl₃ 6H₂O was dissolved in water. The solution was stirred continuously while adding 2 M NaOH. The mixture was then slightly heated at 50 °C while adding CTAB, followed by dissolving silatrane precursor, which was synthesized according to the method described elsewhere [12]. A required amount of cerium glycolate, prepared according to the method in Ref. [13], was added and stirred for 1 h. The molar ratio composition of the gel was 1.0SiO2:0.3CTAB:0.5NaOH:62.0H2O:xFe:yCe, where $0.01 \le x$, $y \le 0.09$. The mixture was autoclaved for 16 h in a

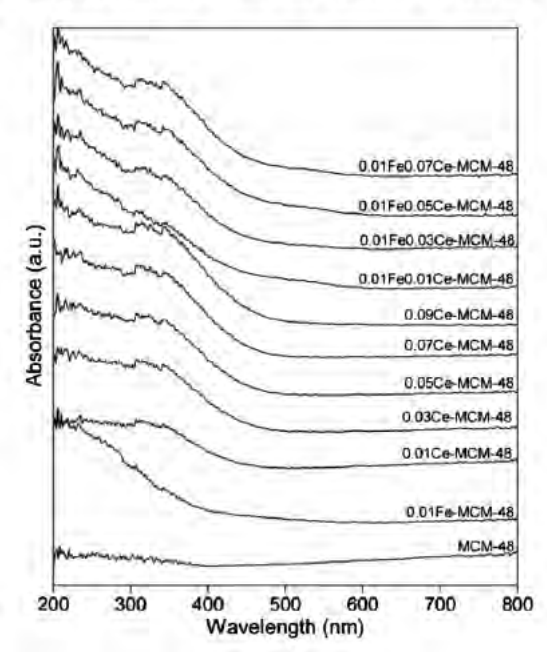


Fig. 3. DRUV-vis spectra of MCM-48, Fe-MCM-48, Ce-MCM-48 and Fe-Ce-MCM-48.

Textural properties of MCM-48 and metal modified MCM-48.

Sample	Fe/Si*(mole ratio)	Ce/Si*	(mole ratio)	BET surface	pore volume (cm ² /g)	pore	a ₀ (nm)	$d_{233} ({\rm nm})$	wall thickness ⁵ (nm
	Gel	Product	Gel	Product	area (m²/g)	(cm·)g)	diameter (nm)			
MCM-48	0	0	Ü	0	1673	1.07	2.56	8.57	3.50	1,46
0.01Fe-MCM-48	0.01	0.004	D	D.	1295	0.98	3.04	8.65	3.53	1.28
0.01 Ce-MCM-48	0	0	0.01	0.004	1469	0.91	2.47	8.57	3.50	1.54
0.03Ce-MCM-48	0	0	0.03	0.010	1318	0.82	2.49	8.45	3.45	1:49
0.05Ce-MCM-48	0	0	0.05	0.018	1213	0.76	2.52	8.40	3.43	1.46
0.07Ce-MCM-48	0	0	0.07	0.028	1128	0.76	2.68	8.72	3.56	1,50
0.09Ce-MCM-48	0	0	0.09	0.030	1131	0.74	2.63	8.52	3.48	1.44
0.01 Fe-0.01Ce-MCM-48	0.01	0.005	0.01	0.005	1214	0.93	3.07	8.87	3.62	1.33
0.01Fe-0.03Ce-MCM-48	0.01	0.005	0.03	0.014	1225	0.91	2.97	8.77	3.58	1.35
0.01Fe-0.05Ce-MCM-48	0.01	0.004	0.05	0.020	1080	0.80	2.95	8.74	3.57	1.35
0.01 Fe-0.07Ce-MCM-48	0.01	0.005	0.07	0.033	1070	0.68	2.55	8.72	3.56	1.55

Wall thickness = q₀/3.0919 - pore diameter/2.
 Data were obtained from XRF.

Teflon-lined stainless steel vessel and treated at 140 °C. The resultant solid product was filtered and washed with distilled water. After drying, the sample was calcined at 550 °C for 6 h in air at a heating rate of 0.5 °C/min. Pure MCM-48, Fe-MCM-48, and Ce-MCM-48 were also synthesized, using the same method as the bimetallic MCM-48, for comparison.

Characterization: XRD patterns were recorded on a Rigaku X-ray diffractometer with CuK α radiation over the range of 2θ = 2–6°. XRF was carried out using a PANalytical AXIOS PW 4400. The N₂ adsorption/desorption was determined by a Quantasorb JR instrument using the Brunauer–Emmett–Teller (BET) method. Diffuse reflectance UV–visible (DRUV) spectra were measured on a Shimadzu UV–2550. SEM micrographs were obtained using a Hitachi S–4800.

3. Results and discussion

XRD: The XRD patterns of the calcined samples shown in Fig. 1 indicate that Ce-MCM-48 with a Ce/Si molar ratio from 0.01 to 0.09 developed patterns consistent with our previously reported MCM-48 [11] and JCPDS no. 00-051-1592 in 2θ range of $2-6^\circ$, being indexed to the [211], [220], [420], and [332] reflections of the la3d cubic phase of MCM-48. As the content of heteroatoms increased, all the peaks obviously shifted to lower angles, implying the dilation of material structure. The radii of Ce^{4+} (Paulling radius=64 pm) are larger than that of Si^{4+} (Paulling radius=42 pm). There should be an enlargement in the unit cell parameter as the bimetal cations are incorporated, resulting in a larger M-0 bond distance. This result is confirmed by the increase of the d spacing of bimetallic

materials [14-15]. Mono- and bimetallic MCM-48 containing Fe/Si of more than 0.01 M ratios were not successfully achieved, probably due to an imbalance of charge matching [16]. Thus, high Fe/Si ratios could not be synthesized while bimetallic samples of xFe-yCe-MCM-48 with x=0.01 and $0.01 \le y \le 0.07$ provided a cubic morphology of MCM-48. According to the study of Zhao et al. [17] on the formation of cubic phase using $g = V/a_0l$, where g is the local effective surfactant-packing parameter, V is the volume of hydrophobic tail, q_0 is the effective headgroup area of the cationic ammonium, and I is the kinetic length of the hydrophobic tail of the surfactant, the cubic phase can be easily formed if g is large. The presence of the anionic species of FeCl₃ and Ce(C2H4O2)2 metal precursors increases the local effective surfactant-packing parameter (g) value, causing a phase change from hexagonal to cubic. Moreover, Mahoney [16] also found that the unequal distribution of charge density in the electric double layer resulted in a curvature of surface in which the cubic structure prefers a high curvature radius with high g. A comparison between those two anions, C2H4O2 and Cl , reveals C₂H₄O₂²⁻ to be more effective in reducing the thickness of the double electric layer because of its higher valence state [17]. Therefore, $C_2H_4O_2^2$ provides a better assembly between the ammonium cations and the inorganic silicate anions. The XRD results clearly showed that the cubic structure of bimetallic products was successfully obtained at various amounts of Ce with a 0.01 Fe/Si molar ratio.

 N_2 adsorption/desorption isotherms: The N_2 adsorption/desorption isotherms and pore size distribution curves of the products are shown in Fig. 2. All of the samples showed a steep increase in the volume of the adsorbed nitrogen at $P/P_0 = 0.20 - 0.35$, exhibiting the type IV isotherm, which confirms the mesoporous

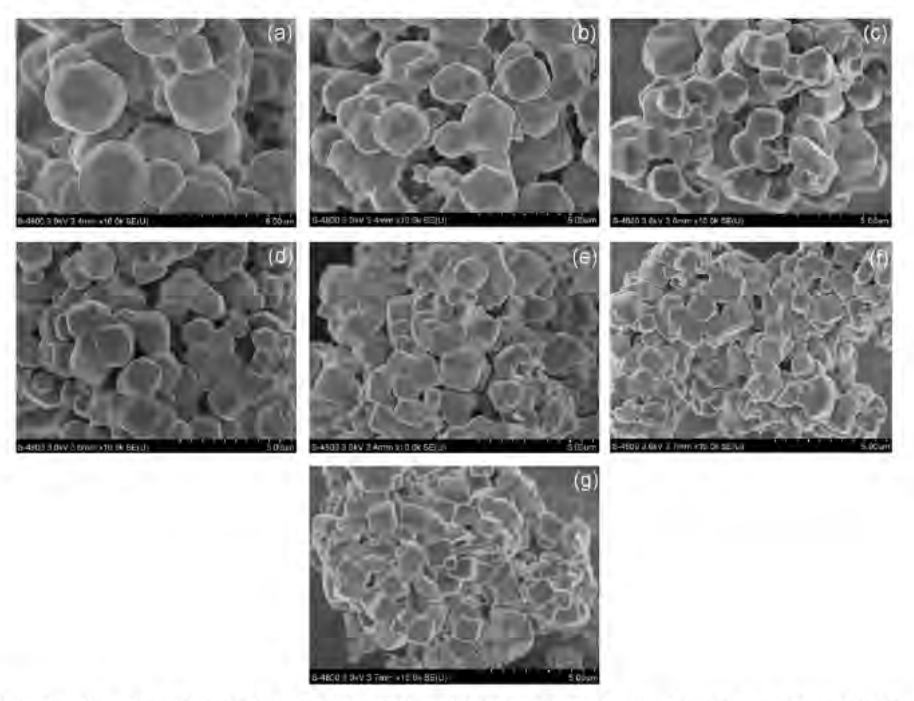


Fig. 4. FE-SEM images of (a) MCM-48, (b) 0.01Ce-MCM-48, (c) 0.01Fe-MCM-48, (d) 0.01Fe0.01Ce-MCM-48, (e) 0.01Fe0.03Ce-MCM-48, (f) 0.01Fe0.05Ce-MCM-48, and (g) 0.01Fe0.07Ce-MCM-48,

structure with a narrow pore size distribution, having an average pore size \sim 2-3 nm. The structural parameters of various samples are summarized in Table 1. Compared with pure MCM-48, the incorporation of the heteroatom resulted in higher pore diameter and unit cell (a0). BET surface area decreased with an increase in the amount of incorporated metal. This result could be explained by some destruction of metallic MCM-48 pore structure, which is in agreement with the XRD's results [18]. However, a high BET surface area of more than 1000 m²/g was obtained for all samples.

XRF spectroscopy: The XRF results (Table 1) confirmed the total amounts of Fe and Ce introduced into MCM-48. However, the actual amount of the metal was less than the added amount, due to the solubility of Fe and Ce sources in the medium.

DRUV-vis spectroscopy: DRUV-vis spectra of the synthesized samples are presented in Fig. 3. The absorption band is absent for MCM-48, while Fe-MCM-48 showed a strong absorption at 200 nm, attributed to the charge-transfer transitions involving isolated framework ${\rm Fe^{3+}}$ in ${\rm FeO_4}$ tetrahedral coordination [10]. In addition, there is no absorption band at 500-600 nm, referring to octahedral coordination in extra framework [9]. The result suggests that iron indeed exists inside the MCM-48 framework. For Ce-MCM-48, they exhibited a weak broad band at 200-300 nm and an intense band at 350 nm. These bands corresponded to Ce4+ tetrahedral coordination. No extra framework band at 405 nm was observed [19]. As the cerium content increased, the band at 350 nm also increased. Fe-Ce-MCM-48 exhibited iron and cerium bands at 200 and 350 nm, respectively. Both iron and cerium were very well incorporated into the MCM-48 framework.

FE-SEM: SEM images of the samples are shown in Fig. 4 Ce-MCM-48 morphology was quite the same as pure MCM-48 because the anionic $C_2H_4O_2^{2-}$ facilitates the formation of the cubic structure. However, Cl- in FeCl3 does not seem to support the cubic formation, thus causing more distortion from MCM-48 in the Fe-MCM-48 morphology. Bimetallic Fe-Ce-MCM-48 showed much more distortion since there are two metal atoms and high counter ions in the system. Moreover, as the metal contents in bimetallic materials increased, crystal size trended downward (Fig. 4d-g). As described by Vekilov and Kashchiev, at a high metal ratio, there are more ions in the solution able to form many nuclei, resulting in tiny crystal growth [20-21].

4. Conclusions

Fe-Ce-MCM-48 mesoporous structures were successfully synthesized using silatrane as a silica source. High iron content in MCM-48 could not be achieved while various amounts of Ce in MCM-48 were well incorporated. Highly dispersed Fe and Ce in the bimetallic framework at 0.01Fe/Si and various cerium contents (Ce/Si=0.01-0.07) was observed and all synthesized samples provided a high surface area and narrow pore size distribution.

Acknowledgments

This research is financially supported by the Thailand Research Fund, Ratchadapisake Sompote Endowment Fund, Part of the "Strengthen CU's Researcher's Project", and the Center of Excellence on Petrochemical and Materials Technology, Chulalongkorn University, Thailand. The authors would like to thank Mr. John M. Jackson for English proofreading.

Appendix A. Supporting information

Supplementary data associated with this article can be found in the online version at http://dx.doi.org/10.1016/j.matlet.2012. 11.139.

References

- [1] Kresge CT, Leonowicz ME, Roth WJ, Vartuli JC, Beck JS. Nature 1992;359:
- 710–2.
 [2] Taguchi A, Schüth F. Microporous Mesoporous Mater 2005;77:1–45.

- Loger NZ, Kaučič V. Acta Chim Slov 2006;53:117–35.
 Lysenko ND, Shvets AV, Il'in VG. Theor Exp Chem 2008;44:3.
 Jiang T, Wu D, Song J, Zhou X, Zhao Q, Ji M, et al. Powder Technol 2011;207: 422–7.
- [7] Selvaraj M, Park DW, Ha CS. Microporous Mesoporous Mater 2011;138: 94-101
- 94-101. [8] Gomes HT, Selvam P, Dapurkar SE, Figueiredo JL, Faria JL. Microporous Mesoporous Mater 2005;86:287-94. [9] Liu H, Lu C, Gao Y, Wang J. Nanotechnology 2006;17:997-1003. [10] Shao Y, Wang L, Zhang J. Anpo M. J Phys Chem B 2005;109:20835-41. [11] Longloilert R, Chaisuwan T, Luengnaruemitchai A, Wongkasemjit S. J Sol-Gel Sci Technol 2011;58:427-23

- [11] Longloilert R, Chaisuwan T, Luengnaruemitchai A, Wongkasemjit S. J Sol-Gel Sci Technol 2011;58:427–35.
 [12] Charoenpinjikarn W, Suwankruharn M, Kesapabutr B, Wongkasemjit S, Jamieson AM. Eur Polym J 2001;37:1441–8.
 [13] Ksapabutr B, Gulari E, Wongkasemjit S, Mater Chem Phys 2004;83:34–42.
 [14] Zhang Y, Gao F, Wan H, Wu C, Kong Y, Wu X, et al. Microporous Mesoporous Mater 2008;113:393–401.
 [15] Rath D, Parida kM. Ind Eng Chem Res 2011;50:2839–49.
 [16] Mahoney LM. Photocatalysis studies using mesoporous modified V-MCM-48 Stober synthesis. PhD thesis. Kansas State University; 2010.
 [17] Zhao W, Kong L, Luo Y, Li Q. Microporous Mesoporous Mater 2007;100: 111-7.

- [18] Ii D. Ren T. Yan L. Suo I. Mater Lett 2003:57:4474-7.
- [19] Longloilert R, Chai suwan T, Luengnaruemitchai A, Wongkasemjit S. J Sol-Gel Sci Technol 2012;61:133–43.
 [20] Vekilov PG. Cryst Growth Des 2010;10:12.
 [21] Kashchiev D, Van Rosmalen GM. Cryst Res Technol 2003;38:7–8.

225

Chonnikarn Deeprasertkul, Rujirat Longloilert, Thanyalak Chaisuwan,

Sujitra Wongkasemjit*

The Petroleum and Petrochemical College and Center of Excellence fo Petrochemical and

Materials Technology, Chulalongkorn University, Bangkok, Thailand

ABSTRACT

Ceria or cerium oxide, with high surface area and ordered structure, was prepared by

the nanocasting method using MCM-48 porous material as a hard template. Optimal

conditions were investigated to obtain ordered mesoporous ceria having high surface areas.

A high surface area of 224.7 m²/g and ordered structure of synthesized cerium oxide was

obtained with 50% weight ceria using 30 min stirring time at 100 °C evaporation

temperature of solvent. The mesoporous ceria was characterized using an X-ray

diffractometer (XRD), X-ray fluorescence spectrometer (XRF), N2 adsorption/desorption,

Transmission electron microscopy (TEM), Scanning electron microscopy (SEM), and

Temperature-programmed reduction (TPR). The TPR results provided only surface reduction

temperatures at 400°-600 °C.

Keywords: Mesoporous ceria; MCM-48 template; Nanocasting process; Silatrane

*Corresponding author.

Tel.: +66 2 218 4133; fax: +66 2 215 4459.

E-mail address: dsujitra@chula.ac.th (Sujitra Wongkasemjit).

1. INTRODUCTION

Cerium oxide or ceria (CeO₂) has also been widely used for many applications, such

as oxygen storage capacity [1] and environmental catalysis [2] but the most important

application of ceria is as a three-way catalysis promoter in catalytic converter, for the elimination of toxic auto-exhaust gases [3, 4-6]. Ceria has two characteristics [4] appropriate for use in three-way catalysts: (1) an oxidation state between Ce³⁺ and Ce⁴⁺, CeO₂/Ce₂O₃, under oxidizing and reducing conditions and (2) oxygen storage and release properties.

The catalytic performance of cerium oxide can be increased by its structural properties, such as surface area and crystal shape. Ceria with mesoporous structure and high surface areas has been synthesized by nanocasting method with various templates, both soft and hard [7,8]. The hard templates have shown many advantages over the soft ones, especially for producing highly crystalline walls, predictability and controllability [4, 7]. Moreover, the hard templates can provide well-ordered structure of frameworks, leading to high surface areas of replica.

In this study, the ordered mesoporous ceria materials were synthesized via nanocasting process using MCM-48 directly synthesized from home-made silatrane as a hard template. Optimal conditions of the nanocasting method were investigated to obtain ordered mesoporous ceria having high surface areas. Physical and reduction properties were characterized using various techniques.

2. Experimental

2.1 Synthesis of ordered mesoporous ceria

The MCM-48, used as a silica hard template and synthesized following Wongkasemjit's method [9], and inorganic cerium nitrate (50, 60, 70, and 80% weight of ceria) were dissolved in 5 ml of ethanol. After stirring (30 min, 1, 2, and 4h), the ethanol in the mixture was removed by evaporation in an oven (50°, 100 °C) or at ambient temperature. The process was repeated to get the two and three filling cycles of ceria. The obtained powder was heated in a ceramic crucible at 550 °C for 6 h to decompose the nitrate species. The silica hard template was removed by using 2M NaOH at 50 °C three times, and the mixture was centrifuged to obtain the product. The product was washed by deionized water

and centrifuged until the washing was neutral and dried at 100 °C. The products were characterized by XRD. The morphology of the products was characterized using SEM and TEM. Specific surface area, pore volume, and average pore size were determined using the Brunauer–Emmett–Teller (BET) method on a Quantasorb JR instrument. The element contents in products were analyzed by XRF. The reducibility of products was analyzed by TPR.

3. RESULTS AND DISCUSSION

3.1 Nanocasting Process

3.1.1 Effect of Cerium Oxide Percentage by Weight

The XRD pattern (Fig. 1(a)) of MCM-48 showed reflection peaks at {211}, {220}, {420}, and {332} corresponding to the *Ia3d* cubic structure, and consistent with our previous work [9]. The ordered mesoporous (MSP) ceria at 50 – 70% weight of cerium oxide (Fig. 1(b)), which was the negative replica of the MCM-48 template, showed the same characteristic diffraction peaks at {211} and {220} as the silica template, whereas the 80% weight showed only one peak at {211}. These results suggested that the ceria replicas still retained some order from their template. The XRD pattern of the 50% weight of ceria showed higher intensity and sharper peaks than those of 60, 70, and 80% weight of ceria, respectively. This might be due to agglomeration of ceria in the pore channel of MCM-48 from the higher ceria loading during the casting process as described by Liotta et al. [10]. Moreover, the intensity of the ordered mesoporous ceria exhibited lower intensity than the MCM-48, indicating less order of the replica than the template. The XRD pattern of 50% weight showed the sharpest diffraction peak and highest intensity, meaning that its replica was more crystalline and more ordered than the remains, and led to a high surface area (234.3 m²/g). The best ceria percentage to obtain a high surface area with maintaining MCM-48 structure was 50%.

3.1.2 Effect of Stirring Time of Mixture

The obtained XRD patterns of all ordered mesoporous ceria, shown in Fig.1(c), exhibited diffraction peaks at {211} and {220}, as shown for MCM-48. The intensity of the peak at {211} decreased with an increase in stirring time, due to the larger amounts of the precursors that went inside the pore and agglomerated, resulting in the less ordered structure at 4 h stirring time [10, 11]. These results indicate that the ordered mesoporous ceria at 30 min stirring time had the most ordered structure. Specific surface area results also decreased with an increase in the stirring time. A high surface area (246.6 m²/g) was obtained at 30 min stirring time. Thus, the obtained ceria at the longer stirring time became less ordered, resulting in a lower surface area. Thus, the appropriate stirring time was 30 min.

3.1.3 Effect of Evaporated Temperature of Solvent

The effect of the evaporated temperature of solvent was studied because the precursor inside the pore void was expected to migrate and impregnate inside the pore during the evaporation of solvent [12]. The XRD patterns of the ordered mesoporous ceria are shown in Fig.1 (d), also giving the diffraction peaks at {211} and {220} although the sample obtained at ambient temperature showed less ordered than the others having nearly the same intensity. It can be concluded that the structure of the retained MCM-48 and the studied range of the temperature had no influence on the migration of the precursor inside the pore. The highest surface area (254 m²/g) was obtained from the sample evaporated at 100 °C. Such a result is probably due to the fact that the evaporation time at 100 °C was the shortest (around 1 hour) while the evaporation time at ambient was the longest (2 days). At the longer evaporation time, the precursor had more opportunity to migrate inside the pore at the ambient temperature, causing the pore blocking and the distortion of the mesoporous structure, as indicated in the less-ordered XRD pattern [13]. The suitable evaporation temperature in this study, then, was at 100 °C since it took the shortest time to evaporate the solvent out from the template while retaining the structure of the template and showing the highest surface area.

3.1.4 Effect of Filling Cycle

In the nanocasting process, the precursor could not completely fill the vacancies of the template at the first filling cycle due to the volume contraction rate [7]. The XRD results (Fig.1 (e)) also exhibited the diffraction peaks at {211} and {220}, referring to the MCM-48 structure, meaning that the structure of the template was still retained although the filling cycle was increased. The XRD peaks obtained from three filling cycles (Fig.1 (e)) exhibited the sharpest diffraction peaks at {211} and {220} when compared to the others. The sharpest peak was achieved at the three filling cycles, suggesting that it better duplicated the structure of the template than the others. In other words, it has a more ordered structure. This result confirmed that a repeated filling cycle can effectively increase the filling degree, as described by Sophie *et al.* [14].

The N_2 adsorption-desorption isotherms of the MCM-48 and ordered mesoporous ceria are shown in Fig. 2. The ordered mesoporous ceria were analyzed and it was found that the classification of the synthesized ceria was a type IV isotherm with H3 hysteresis loop, IUPAC classification, corresponding to mesoporous materials with slit-like pores. The isotherms show the first step up at P/Po = 0.5-0.7, corresponding to the capillary condensation and the other step at P/Po = 0.9-1.0, reflecting the interparticle porosity [15].

The structural parameters of various samples are summarized in Table 1. With the increased filling cycle, BET specific surface area and the pore volume decreased, meaning that ceria infiltrated the template pore [15]. The pore size of the ordered mesoporous ceria was in a range of 4.5–4.8 nm which was larger than the wall thickness of MCM-48 (1.53 nm). This could indicate that the fillings of the pores overlapped in some region of the template [16]. As can be seen from Table 1, the highest surface area of the ordered mesoporous ceria obtained was 224.7 m²/g at one filling cycle. The other ceria products were still larger than the ceria powder (directly calcined ceria from the precursor at 550°C for 6 h). The XRF results (Table 1) confirmed small amount of Si remained in the ordered mesoporous ceria after removal of the template.

SEM images of ceria and ordered mesoporous ceria were shown in Fig. 3. The ordered mesoporous ceria possessed spherical morphology, comprised of small, round crystalline structures of ceria. Interestingly, additional filling cycles resulted in a denser spherical morphology of the ordered mesoporous ceria (Fig. 3 (b)-(d)). The SEM results can be well related to the surface area results that the denser spherical morphology gave the lower surface area.

To confirm the order of the mesoporous ceria structure, TEM was used to analyze. The mesoporous ceria (Fig. 3 (e), (f)) was well ordered after removal of the silica template.

3.2. Temperature Programmed Reduction (TPR)

TPR profiles of the ceria powder and the ordered mesoporous ceria are shown in Fig. 4. Two groups of the reduction peaks were observed. The first peak at low temperature from 350° to 650 °C is related to the reduction of the surface-capping oxygen of CeO₂ whereas the high temperature peak at 700°–850 °C resulted from the reduction of the bulk-phase lattice oxygen [3, 5]. The highest intensity of the low-temperature peak (Fig.4 (a)) was observed on the ordered mesoporous ceria obtained at one filling cycle. Areas under the peak corresponded to the total gas consumption, implying that the ordered mesoporous ceria obtained from one filling cycle and having the highest surface area consumed the highest H₂. This is its advantage for use as a catalyst in three-way catalyst.

The redox equation of ceria is shown below [17]. The Ce³⁺/Ce⁴⁺ redox cycle provides not only unique redox properties, but also the ability to store and release oxygen via conversion between the Ce³⁺ and Ce⁴⁺ oxidation states [18], making it suitable to convert toxic auto-exhaust gases to less harmful gases [19].

$$2 \text{ CeO}_2 + \text{H}_2$$
 \longrightarrow $\text{Ce}_2\text{O}_3 + \text{H}_2\text{O}$

4. CONCLUSIONS

The ordered mesoporous ceria were successfully synthesized using mesoporous MCM-48 silica, as hard template via nanocasting method. The optimum conditions achieved were by using 50% weight of ceria, 30 min stirring time, 100 °C evaporation temperature, and one filling cycle. The XRD and TEM results confirmed that the ordered mesoporous ceria retained ordering from MCM-48 while the XRF results confirmed the removal of silica template from the ordered mesoporous ceria. In comparison of the ordered mesoporous ceria with commercial ceria powder; the ordered mesoporous ceria exhibited a much larger surface area and also showed a larger area under the TPR peak, referred to the strong reduction of the surface-capping oxygen.

ACKNOWLEDGEMENTS

The work is supported by the Thailand Research Fund, the Ratchadapisake Sompote Endowment Fund, and the Center of Excellence for Petrochemical and Materials Technology, Chulalongkorn University, Thailand. The authors are also thankful to Professor Ram Seshadri for kindly sponsoring a Ph.D. student to experience different research techniques at the Materials Department, University of California, Santa Barbara, USA, and Mr. John M. Jackson for English proof-reading.

REFERENCES

- [1]. P. Ji, J. Zhang, F. Chen, M. Anpo, J.Phys.Chem 112 (2008) 17809-17813.
- [2]. X. Liang, J. Xiao, B. Chen, Y. Li, Inorg. Chem.49 (2010) 8188-8190.
- [3]. G. Rango Rao, B. G. Mishra, Bulletin of the Catalysis Society of India 2 (2003) 122-134.
- [4]. E. Rossinyol, J. Arbiol, F. Peiro, A. Cornet, J.R. Morante, B. Tian, T. Bo, D. Zhao, Sens. Actuators, B 109 (2005) 57-63.
- [5]. H. Zhu, Z. Qin, W. Shan, W. Shen, J. Wang, J. Catal. 225 (2004) 267–277.
- [6]. A. Trovarelli, Science and Engineering, 38:4, 439-520.

- [7]. A. Lu, D. Zhao, Y. Wan, Nanocasting, RSC Nanoscience & Nanotechnology No.11, UK, 2010.
- [8]. H. Zhang, S.C. Wang, D. Xue, Q. Chen, Z.C.Li, Journal of Physics (2009) 152.
- [9]. R. Longloilert, T. Chaisuwan, A. Luengnaruemitchai, S. Wongkasemjit, J Sol-Gel Sci Technol 58 (2011) 427-435.
- [10]. L.F. Liotta, G. Di Carlo, F. Puleo, G. Pantaleo, G. Deganello, Stud. Surf. Sci. Catal. 175 (2010) 401-404.
- [11]. L.F. Liotta, G. Di Carlo, F. Puleo, G. Marci, G. Deganello, Stud. Surf. Sci. Catal. 175 (2010) 417-420.
- [12]. W. Yue, W. Zhou, Progress in Natural Science 18 (2008) 1329-1338.
- [13]. T. Horikawa, D.D. Do, D. Nicholson, Adv. Colloid Interface Sci.169 (2011) 40-58.
- [14]. S. Lepoutre, J. Smatt, C. Laberty, H. Amenitsch, D. Grosso, M. Linden, Microporous and Mesoporous Mater. 123 (2009) 185–192.
- [15]. W. Shen, X. Dong, Y. Zhu, H. Chen, J. Shi, Microporous and Mesoporous Mater. 85 (2005) 157-162.
- [16]. F. Ying, S. Wang, C.T. Au, S.Y. Lai, Microporous and Mesoporous Mater. 142 (2011) 308-315.
- [17]. E. Rogemond, R. Frety, V. Perrichon, M. Primet, S. Salasc, M. Chevrler, F. Mathis, J. Catal. 169 (1997) 120-131.
- [18]. P. Ji, J. Zhang, F. Chen, M. Anpo, M. J. Phys. Chem. C 112 (2008) 17809-17813.
- Y. Zhang, S. Andersson, M. Muhammed, Appl. Catal., B: Environmental 6 (1995) 325-337.

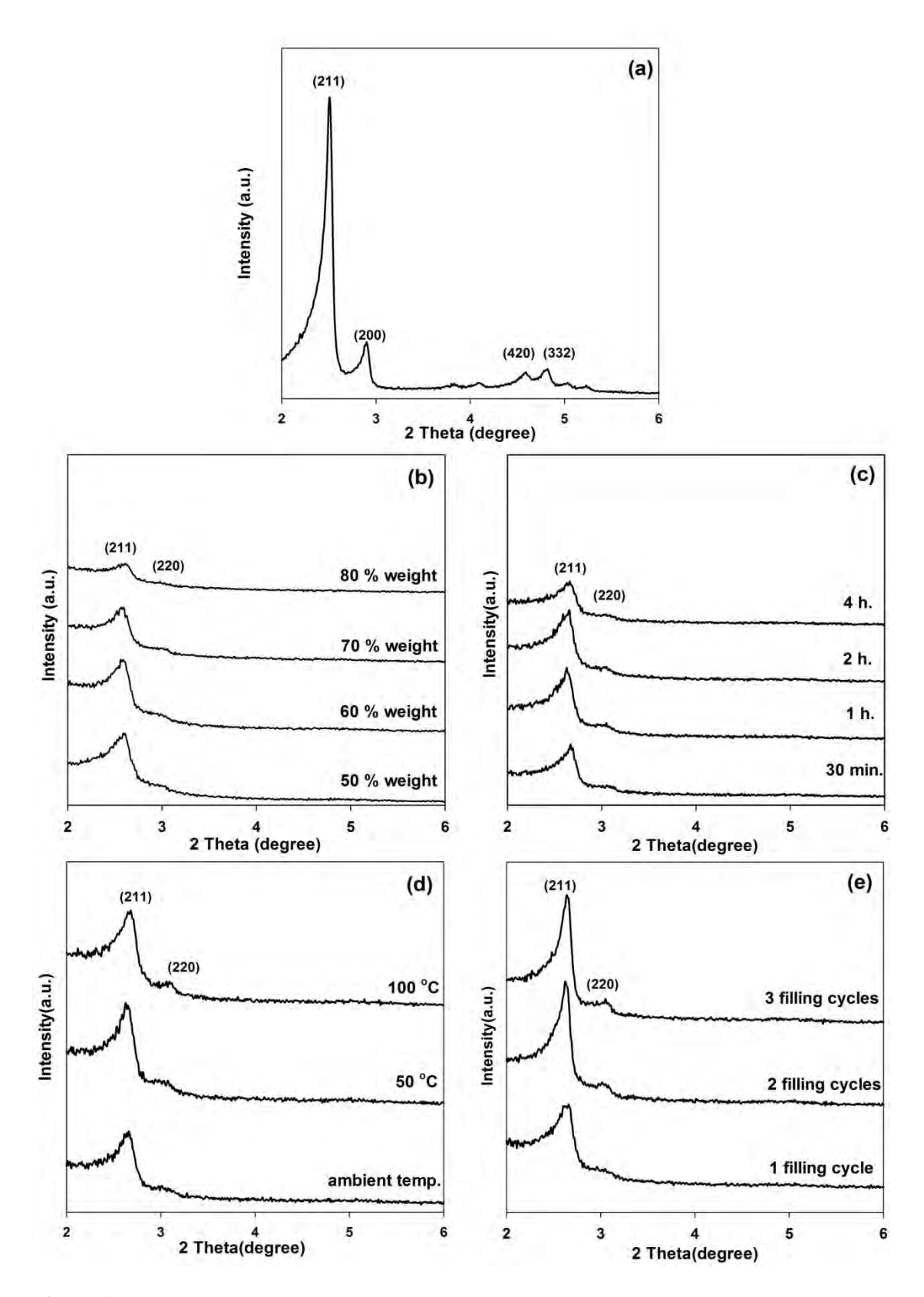


Figure 1 XRD patterns of (a) MCM-48 and the ordered mesoporous ceria resulted from various (b) ceria percentages by weight, (c) stirring times, (d) evaporation temperatures of solvent, and (e) filling cycles.

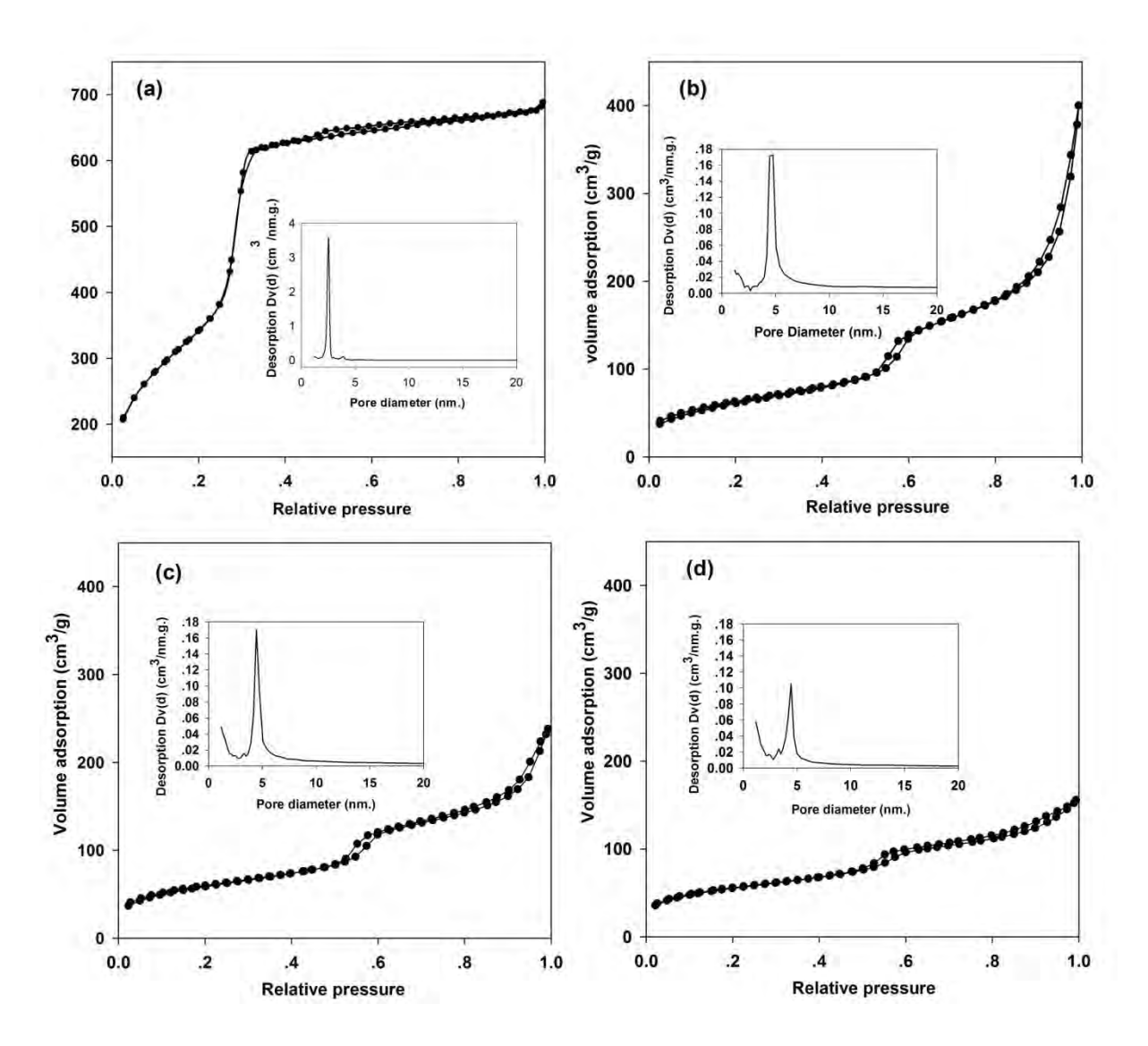


Figure 2 N_2 adsorption-desorption isotherms and pore size distribution (inset) of (a) MCM-48 and the ordered mesoporous ceria resulted from (b) one, (c) two, and (d) three filling cycles.

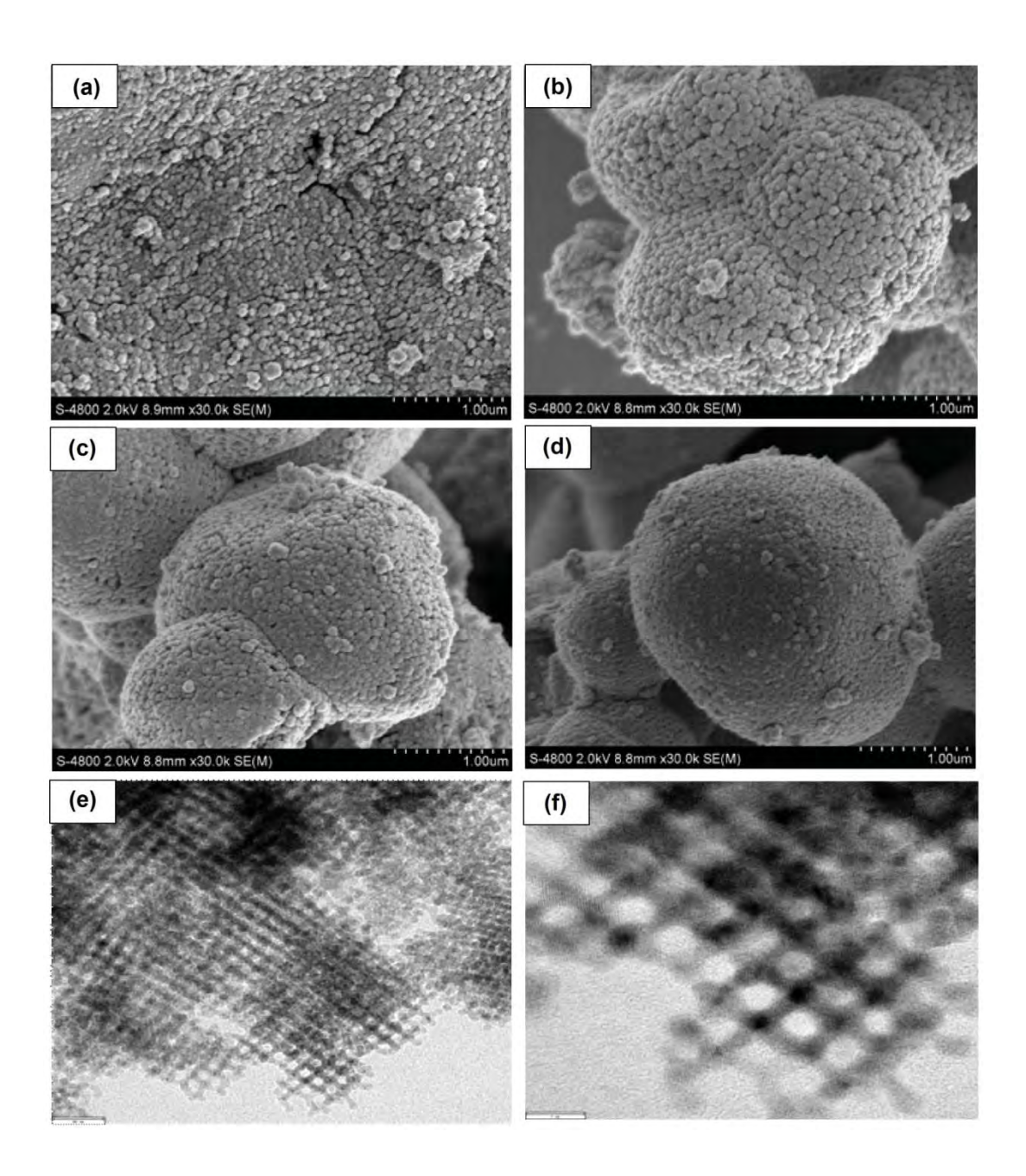


Figure 3 SEM images of (a) ceria, and ordered mesoporous ceria resulted from (b) one, (c) two and (d) three filling cycles, and (e) and (f) TEM images of the synthesized ceria.

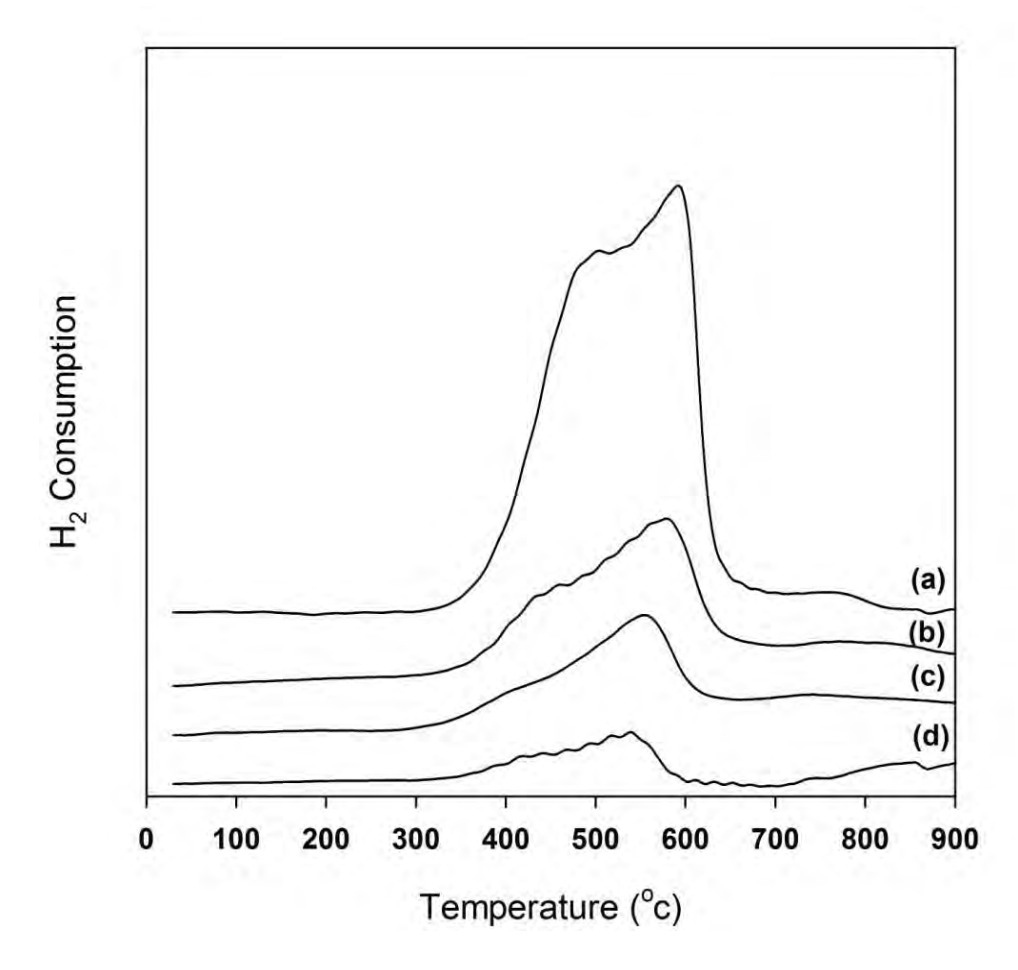


Figure 4 TPR profiles of the synthesized ceria resulted from (a) one, (b) two, and (c) three filling cycles (d) ceria powder.

Table 1 BET and XRF analyses of MCM-48, ceria powder and ordered mesoporous ceria at different filling cycles.

Sample	Element o	Element contents* (%)	(%	BET surface area	Pore volume	Pore size	$a_0^{\rm a}$ (nm)	d_{211} (nm)	Pore volume Pore size a_0^a (nm) d_{211} (nm) Wall thickness ^b
				(m^2/g)	(cm^3/g)	(mu)			(mm)
	Ce	0	Si						
MCM-48		1	1	1614	1.1	2.5	8.60	3.51	1.53
Ceria powder	ı	1	1	77.1	1	1	1	1	1
Ordered MSP ceria (1 filling cycle)	54.526	43.541	1.933	224.7	9.0	4.8	1	1	1
Ordered MSP ceria (2 filling cycles)	58.791	38.764	2.445	207.9	0.4	4.5	1	1	1
Ordered MSP ceria (3 filling cycles)	53.415	44.395	2.190	192.0	0.2	4.5	ı	ı	1

^a $a_0 = d_{211}(6)^{1/2}$.

^b wall thickness = $a_0/3.0919$ – pore diameter/2.

^{*} Data were obtained from XRF.

Important role of anionic counterion on Ce-MCM-48 synthesis using silatrane

precursor via sol-gel process

Hussaya Maneesuwan, Thanyalak Chaisuwan, and Sujitra Wongkasemjit*

The Petroleum and Petrochemical College and Center of Excellence on Petrochemical and

Materials Technology, Chulalongkorn University, Bangkok 10330, Thailand

*Corresponding author: Tel.: +66 2 218 4133: fax: +66 2 215 4459.

E-mail address: dsujitra@chula.ac.th (S. Wongkasemjit)

Abstract

Cerium incorporated MCM-48 mesoporous materials were synthesized via sol-gel

process using silatrane as a silica source and various cerium precursors containing different

anionic counterions, viz. glycolate (C₂H₄O₂²⁻), hydroxide (HO⁻), fluoride (F⁻), sulfate (SO₄²⁻),

and nitrate (NO₃) ions. The effect of the anionic counter ion on the synthesis was

systematically studied. The obtained products were characterized by x-ray diffraction

(XRD), N₂ physisorption, diffuse reflectance spectroscopy (DRUV-vis), x-ray fluorescence

(XRF), scanning electron microscopy (SEM), and transmission electron microscopy (TEM).

It was found that the amounts of cerium glycolate and cerium hydroxide had no effect on the

cubic phase of MCM-48 while the other cerium salts caused the cubic phase transformation

to the hexagonal phase as increasing the content of the cerium salt since those counterions

increased the silica condensation rate in the order of: $F < SO_4^2 < NO_3^2$.

Keywords: Ce-MCM-48; Mesoporous materials; Sol-Gel process; Silatrane; Counterions.

1. Introduction

The discovery of M41S family started the revolution in the mesoporous inorganic materials due to the attractive properties such as high surface area, ordered pore structure and narrow pore size distribution [1]. Among this family, the cubic MCM-48 material is the most interesting material because the interconnected pore channels and bi-gyroidal structure [2-3]. However, the cubic structure, the intermediate phase between the hexagonal phase of MCM-41 and the lamella phase of MCM-50, is formed in a narrow range of the synthesis condition. Previously, our research group successfully synthesized MCM-48 using less CTAB amount and home-made silatrane as a silica source [4]. The home-made silatrane is more effective due to its high moisture stability, resulting in slower hydrolysis rate [4-5]. Thus, the same synthesis method for MCM-48 was also adapted for preparation of monometallic [6] and bimetallic [7] MCM-48 at the ambient temperature. In fact, there are many parameters affecting the structure of mesoporous silicas, such as geometry of surfactant, co-surfactant, concentration of surfactant, counterions, and charging density matching [8]. Srinivasu et al. [9] reported that counterions were the important key for cubic Fm3m mesoporous aluminosilicates (AlKIT-5) formation in term of anionic binding strength. Chao et al. [10] focused on the counterion effect on the formation of SBA-15 mesoporous silicas. They found that the high affinity of SO₄²⁻ induced P123 rod-like micelles structure better than Cl⁻ and NO₃. Various counter anions provided different values of the surface packing parameter, g, leading to different formations of mesostructures [11]. Lin et al. [12] investigated that anions directly influenced on the binding interaction between surfactant and silicates. Fluoride anion binds tighter than chloride, sulfate, and nitrate anions. Wang et al. [13] proposed that the promoter sulfate anion improved the structure stability due to its high hydration energy. Nevertheless, the over-promoter obstructed the interaction between silicate anions and surfactant cations which leads to less order of MCM-48 formation. Zhao et al. [14] also studied factors influencing on the synthesis of Fe-MCM-48, and found that sulfate

anion was more favorable than nitrate and chloride anions for cubic structure formation. Mahoney et al. [15] observed that the interaction strengths between the anions and the surfactants, between $Cr(H_2O)_6^{3+}$ and the silicate species, the hydration energy, ionic radii, and charge density of anions are all important for the Cr-MCM-48 synthesis. The salt effect of cerium ion incorporated MCM-48 materials has been studied. Wang et al. [16] successfully synthesized Ce-MCM-48 with hydrothermal stability by the addition of sulfate anion and increasing the crystallization temperature to dehydrate hydrated silicates and surfactant and to accelerate the interaction between surfactant and silicate species. The presence of fluoride anion also enhanced the hydrothermal stability of Ce-MCM-48 to improve the degree of polymerization of silicates [17]. Therefore, in this work, we focused on how cerium counterions influenced on the cubic phase formation of Ce-MCM-48 by studying various cerium precursors containing different counterions, viz. glycolate, hydroxide, sulfate, fluoride, and nitrate anions. The amount of the cerium incorporated onto mesoporous silicates was also investigated.

2. Materials and method

2.1. Materials

Fumed silica (99.8%, SiO₂) from Sigma-Aldich, hexadecyltrimethyl ammonium bromide (CTAB) from Fluka, triethylenetetramine (TETA) from Facai, ethylene glycol (EG) from J.T. Baker, triethanolamine (TEA) from QREC, acetronitrile and sodium hydroxide (NaOH) from Labscan were used without purification. Cerium (IV) hydroxide (Ce(OH)₄), cerium (IV) sulfate (Ce(SO₄)₂), ammonium cerium (IV) nitrate ((NH₄)₂Ce(NO₃)₆), and cerium (IV) fluoride (CeF₄) from Aldrich were chosen as cerium precursors.

2.2. Preparation of xCe-MCM-48; $0.01 \le x \le 0.09$

The synthetic method of Wongkasemjit was applied for the synthesis of Ce-MCM-48 [18]. The molar ratio composition of gel product was 1.0SiO₂:0.3CTAB:0.5NaOH:

62.0H₂O:xCe, where $0.01 \le x \le 0.09$. Cerium precursors used in this work included cerium glycolate (Ce(C₂H₄O₂)₂); prepared according to ref [19], Ce(OH)₄, Ce(SO₄)₂, (NH₄)₂Ce(NO₃)₆, and CeF₄. The required amount of cerium precursor was dissolved in distilled water, followed by adding 2 M NaOH and CTAB, respectively. The mixture was continuously stirred and slightly heated at 50 °C. Silatrane, synthesized following elsewhere [20], was added into the mixture and aged at room temperature for 1 h. The resulting product was transferred into teflon-lined stainless steel vessel and autoclaved at 140 °C for 16 h. The product was recovered by filtration, washing with distilled water, and drying overnight at ambient temperature. The organic template was removed by calcination at 550 °C for 6 h at a heating rate of 0.5 °C/min. Pure MCM-48 was also synthesized with the same procedure for comparison.

2.3. Characterization

XRD patterns were obtained on a Rigaku X-ray diffractometer using CuK α radiation over the range of $2\theta = 2$ –6°. N_2 adsorption/desorption isotherms were measured using a Quantasorb JR instrument. The specific surface area was calculated using the Brunauer–Emmett–Teller (BET) method. The pore size was obtained using the Barrett-Joyner-Halenda (BJH) equation. DRUV-vis spectra were recorded from 200 to 800 nm on a Shimadzu UV-2550. XRF was used to determine the actual cerium loading in the final product using a PANalytical AXIOS PW 4400. FE-SEM micrographs were recorded on a Hitachi S-4800. TEM images were obtained using a JEOL JEM-2010 electron microscope.

3. Results and discussion

3.1. XRD

The XRD patterns of all calcined samples synthesized using various counter anions $(C_2H_4O_2^{2-}, OH^-, SO_4^{2-}, F^-, and NO_3^-)$ are given in Fig. 1. Undoubtedly, at dilute solution (0.01Ce/Si), all counterions showed *Ia3d* MCM-48 cubic structure having four diffraction

peaks of $\{211\}$, $\{220\}$, $\{420\}$, and $\{332\}$ planes. This is consistent to the work studied by Chao et al. [21] that low concentration condition would retard the self-assembling rates of surfactant and silica species to extend the equilibrium-assembly time. Thus, the effect of anionic counterions was not obvious at dilute synthetic condition. In general, mesoporous preparation was successful using sol-gel technique, consisting of hydrolysis and condensation reactions in the presence of acid or basic catalyst [22]. In this study, NaOH was used as catalyst to accelerate the hydrolysis reaction. According to the result in Fig. 1c-e, the presence of anionic counterions influenced the silica condensation rate which increased as follows: NO_3 -> SO_4 ²-> F.

For the NO₃ system, as increasing anion content beyond 0.05 Ce/Si (Fig. 1e), the silica condensation rate was too fast [23] to arrange itself, giving the equilibrium structure difficult to form mesoporous structure. In addition, nitrate ions was bound with water molecules because of its low hydration energy (-71.6 kcal/mol) [24], causing nitrate ions more reactive in the solution. The silica condensation rate was also affected by SO₄²-. A proper amount of SO₄²⁻ induces the dehydration reaction of anionic silicates and cationic surfactants and facilitates the formation of well-ordered MCM-48. High contents of SO₄²ions in the system would obstruct the electronic interaction between CTAB and silicates, resulting in a change of surface curvature and transformation to hexagonal phase [13], as shown in Fig. 1c. When the amount of SO₄²- increased to 0.09 Ce/Si, the hexagonal phase was collapsed to wormhole structure, a worse order in meso-structure formation, because more anions obstructed the silicate oligomers to competitively adsorb on the micellar surface [12]. Therefore, the polymerization of the silicates was less effective at higher anion concentration [12]. Contrarily, F counterions increased the silica condensation [25-26], see Fig. 1d, giving 2D-hexagonal p6mm structure, when the concentration was above 0.01Ce/Si without collapsing. The other word, the silica condensation rate was not as fast as NO₃ and SO₄²-, providing enough assembly time to form mesostructure. Our result was in agreement

with those obtained by Lin et al. [12] who also reported that F was the most effective ion to form hexagonal phase. However, the excess F also obstructed the interaction of surfactants and silicates [25].

Interestingly, not only C₂H₄O₂², but also OH anionic counterions performed very well the bicontinuous cubic *Ia3d* mesostructure, as shown in Fig. 1a-b. Generally, OH from NaOH was used to catalyze the hydrolysis reaction in the basis condition. By using Ce(OH)₄ as a cerium precursor, OH from this precursor was also promoted the silica hydrolysis as well. In the presence of C₂H₄O₂²⁻ generated from cerium glycolate, the ordered cubic mesostructure was also obtained. This result could be explained in term of the surfactant packing parameter, $g = V/a_0 l$ [27], where V is the total volume of the surfactant tail, a_0 is the effective area of the surfactant head group, and l is the length of the surfactant tail. The hydrophobic part of C₂H₄O₂² would assemble with the hydrophobic region of micelles and increase the surfactant tail volume, resulting in a large g and thus easy cubic phase formation [28]. Hartmann et al. [29] successfully synthesized Al-MCM-48 using Al isopropoxide as an aluminium source because the hydrophobic part of isopropoxide anions aggregated with the hydrophobic region of surfactants and coincidently performed the same function as C₂H₄O₂²⁻. In addition, the hindrance C₂H₄O₂²⁻ could interrupt the interaction between the surfactants and silica species at high concentration, as a result, the presence of C₂H₄O₂²-exhibited broader peaks than those obtained from the OH system. These results could be implied that the formation of mesostructure is dependent on the interaction between the surfactants and silica species, the silica condensation rate, hydration energy, charge density, and the equilibrium of reaction [15, 21]. Among these anionic counterions studied C₂H₄O₂²⁻ and OH were the most suitable ones to form the cubic Ce-MCM-48 phase for the whole range of 0.01-0.09 Ce/Si

3.2. N₂ adsorption/desorption

Figure 2 shows the isotherms and the pore size distribution (insets) of the cubic MCM-48 and Ce-MCM-48 samples using C₂H₄O₂²⁻ and OH⁻ as anionic counterions. The characteristics of the type IV mesoporous structure were obtained by a steep increase in the volume of adsorbed nitrogen at the region of $P/P_0 = 0.20-0.35$. Figure 3a performed the isotherms of Ce-MCM-48 using SO_4^{2-} counterion. All isotherms also demonstrated the type IV mesostructure. As the amount of SO_4^{2-} increased, the adsorption isotherm curves were less steep and exhibited a H3 hysteresis loop at P/P_0 over 0.80 due to the partial breakdown of the framework, generating the voids between the particles [30]. For the F system, similar observation to the SO_4^{2-} system was also observed, except no occurrence of the H3 hysteresis loop, see Fig. 3b. At 0.03 Ce/Si, SO_4^{2-} and F showed a low steep of the isotherm and broad peak of the pore size distribution since the cubic phase was transforming to less order of the hexagonal phase. When the contents of SO_4^{2-} and F were increased to 0.05 Ce/Si, the isotherm and the pore size distribution became more steep and narrow due to more order and uniform pore of hexagonal phase. The type IV mesophase also performed in NO₃ system, but the adsorption isotherm curve was lower steep as NO₃ increased because of the less order of the mesostructure. Moreover, these isotherms contained a H3 hysteresis loop at P/P_{θ} over 0.80 for 0.03–0.09 Ce/Si due to the interparticle voids [30]. This loop was bigger as the amorphous phase dominated. In addition, all isotherm curves slightly shifted toward higher relative pressures with the increases of anions and cerium incorporation, suggesting some disorder in the pore structure [31]. The structural properties of the calcined sample are listed in Tables 1–3. All Ce-MCM-48 samples prepared from various cerium precursors provided high surface area over 1000 m²/g. A decrease of surface area was observed from the samples with a lower order of mesophase using higher cerium precursor content. However, there was no significant change in pore volume, pore diameter, and wall thickness.

3.3. DRUV

The DRUV spectra of MCM-48 and Ce-MCM-48 are presented in Fig. 4. The absorption band was absent for MCM-48 while Ce-MCM-48 exhibited a weak broad band around 200–300 nm and a more intense band at 320 nm due to the charge transfer of ligand to metal (O²-→Ce⁴+) in different environments of Ce center [32]. It could be inferred that the absorption at 320 nm occurred from the presence of the tetra-coordinated Ce⁴+ species in the framework, and no extra-framework of the hexa-coordinated Ce⁴+ species was observed at 405 nm [32-33]. Expectedly, all samples showed that the band intensity increased with the cerium content. It can be concluded that the tetra-coordinated Ce⁴+ species was highly dispersed into the MCM-48 framework.

3.4. XRF

The actual amount of all cerium incorporated MCM-48 is given in Tables 1–3. All final products had lower cerium content than the synthesis gel. It was suggested that during the washing process, some of cerium ions were eliminated due to the existence of soluble cerium hydroxide, consistent to the work studied by Mahoney and coworker [15].

3.5. SEM

The morphology of the calcined samples is shown in Fig. 5. The truncated octahedral shape was obtained for MCM-48 and Ce-MCM-48 using C₂H₄O₂²⁻ and OH counterions. For the F', SO₄²⁻ and NO₃ systems, the morphology was more distorted from pure MCM-48 since these anions affect to the fast condensation rate of silica, causing the {100} surface to grow faster than the {111} surface [34]. The presence of NO₃ provided the fastest condensation, as discussed in the XRD results, therefore the growth ratio of the {100} over {111} surface was the highest, exhibiting the cubic shape of the morphology (Fig. 5f) instead of the truncated octahedral shape because the {111} surface was hardly seen. The F and SO₄²⁻ systems showed bigger areas of the {111} surface (Fig. 5d-e) due to a slower condensation rate, thus the more truncated octahedral shape was observed.

3.6. TEM

Figure 6 shows the TEM image of Ce-MCM-48 using $C_2H_4O_2^{2-}$ as an anionic precursor. The image clearly indicates not only the projection along [432] direction, but also the well-ordered crystalline [32]. The TEM result also informs that the introduction of Ce does not destroy the silica framework.

4. Conclusions

The presence of OH and C₂H₄O₂²⁻ from cerium salts allowed the cubic phase to form while the others, F̄, SO₄²⁻ and NO₃̄, could not maintain the MCM-48 structure at the concentrated solution. The factor that influences the phase formation was dependent of the amounts of the surfactants and the silica species, the silica condensation rate, hydration energy, charge density, and the equilibrium of the reaction. The obtained cubic phase products also gave a high surface area over 1000 m²/g with narrow pore size distribution and a high Ce dispersion into the MCM-48 framework.

Acknowledgements

This research is financially supported by the Thailand Research Fund through the Royal Golden Jubilee Scholarship (Grant No. PHD/0013/2554), the Ratchadapisake Sompote Endowment Fund, and the Center of Excellence for Petrochemical and Materials Technology, Chulalongkorn University, Thailand. The authors are also thankful to Mr. John M. Jackson for English proof-reading.

References

- [1]. C.T. Kresge, M.E. Leonowicz, W.J. Roth, J.C. Vartuli, J.S. Beck, Nature 359 (1992) 710-712.
- [2]. N.Z. Logar, V. Kaučič, Acta. Chim. Slov. 53 (2006) 117-135.

- [3]. M.O. Coppens, Structuring Catalyst Nanoporosity,in: A. Cybulski, J. A. Moulijn, Structured Catalysts and Reactors, CRC press, 2005, pp. 779-805.
- [4]. R. Longloilert, T. Chaisuwan, A. Luengnaruemitchai, S. Wongkasemjit, J. Sol-Gel Sci. Technol. 58 (2011) 427-435.
- [5]. W. Charoenpinijkarn, M. Suwankruhasn, B. Kesapabutr, S. Wongkasemjit, A. M. Jamieson, Eur. Polym. J. 37 (2001) 1441-1448.
- [6]. R. Longloilert, T. Chaisuwan, A. Luengnaruemitchai, S. Wongkasemjit, J. Sol-Gel Sci. Technol. 61 (2012) 133-143.
- [7]. H. Maneesuwan, R. Longloilert, T. Chaisuwan, S. Wongkasemjit, Mater. Lett. 94 (2013) 65-68.
- [8]. C. Gao, Formation mechanism of anionic-surfactant-templated mesoporous silica (AMS), PhD thesis, Stockholm University, 2009.
- [9]. P. Srinivasu, S. Alam, V.V. Balasubramanian, S. Velmathi, D.P. Sawant, W. Böhlmann et al., Adv. Funct. Mater. 18 (2008) 640-651.
- [10]. M.C. Chao, C.H. Chang, H.P. Lin, C.Y. Tang, C.Y. Lin, J. Mater. Sci 44 (2009) 6453-6462.
- [11]. S. Che, H. Li, S. Lim, Y. Sakamoto, O. Terasaki, T. Tatsumi, Chem. Mater. 17 (2005) 4103-4113.
- [12]. H.P. Lin, C.P. Kao, C.Y. Mou, Microporous Mesoporous Mater. 48 (2001) 135-141.
- [13]. L. Wang, Y. Shao, J. Zhang, M. Anpo, Microporous Mesoporous Mater. 95 (2006) 17-25.
- [14]. W. Zhao, L. Kong, Y. Luo, Q. Li, Microporous Mesoporous Mater. 100 (2007) 111-117.
- [15]. L. Mahoney, C.M. Wu, H.S. Kibombo, E. Thiruppathi, J. Baltrusaitis, S. Rasalingam et al., Microporous Mesoporous Mater. 170 (2013) 211-225.
- [16]. L. Wang, Y. Shao, J. Zhang, M. Anpo, Chem. Lett. 35 (2006) 3.

- [17]. Y. Shao, L. Wang, J. Zhang, M. Anpo, J. Phys. Chem. B 109 (2005) 20835-20841.
- [18]. R. Longloilert, T. Chaisuwan, A. Luengnaruemitchai, S. Wongkasemjit, J. Sol-Gel Sci. Technol. 58 (2011) 427-435.
- [19]. B. Ksapabutr, E. Gulari, S. Wongkasemjit, Mater. Chem. Phys. 83 (2004) 34-42.
- [20]. W. Charoenpinijkarn, M. Suwankruharn, B. Kesapabutr, S. Wongkasemjit, A. M. Jamieson, Eur. Polym. J. 37 (2001) 1441-1448.
- [21]. M.C. Chao, C.H. Chang, H.P. Lin, C.Y. Tang, C.Y. Lin, J. Mater. Sci. 44 (2009), 6453-6462.
- [22]. L.L. Hench, J.K. West, Chem. Rev. 90 (1990) 33-72.
- [23]. P. Srinivasu, S. Alam, V.V. Balasubramanian, S. Velmathi, D.P. Sawant, W. Böhlmann et al., Adv. Funct. Mater. 18 (2008) 640-651.
- [24]. L.A. Richards, A.I. Schäfer, B.S. Richards, B. Corry, small 8 (2012) 1701-1709.
- [25]. L. Wang, Y. Shao, J. Zhang, M. Anpo, Res. Chem. Intermed. 34 (2008) 267-286.
- [26]. A.E.C. Palmqvist, Curr. Opin. Colloid Interface Sci. 8 (2003) 145-155.
- [27]. J.N. Israelachvili, D.J. Mitchell, B.W. Ninham, J. Chem. Soc., Faraday Trans. 72 (1976) 1525.
- [28]. L.M. Mahoney, Photocatalysis studies using mesoporous modified V-MCM-48 Stober synthesis, PhD thesis, Kansas State University, (2010).
- [29]. M. Hartmann, C. Bischof, Stud. Surf. Sci. Catal. 117 (1998) 249.
- [30]. T. Vrålstad, G. Øye, M. Rønning, W.R. Glomm, M. Stöker, J. Sjöblom, Microporous Mesoporous Mater. 80 (2005) 291-300.
- [31]. S.H. Park, B.H. Kim, M. Selvaraj, T.G. Lee, J. Ind. Eng. Chem. 13 (2007) 637-643.
- [32]. Z. Wangcheng, L. Gaunzhong, G. Yanglong, G. Yun, W. Yunsong, J. Rare Earth 26 (2008) 59-65.
- [33]. H. Yue, H. Zhao, L. Liu, S. Wang, Q. Ruan, T. Wang, Front. Chem. Eng. China 2 (2008) 135-139.

[34]. O.I. Lebedev, G.V. Tendeloo, O. Collart, P. Cool, E.F. Vansant, Solid State Sci. 6 (2004) 489-498.

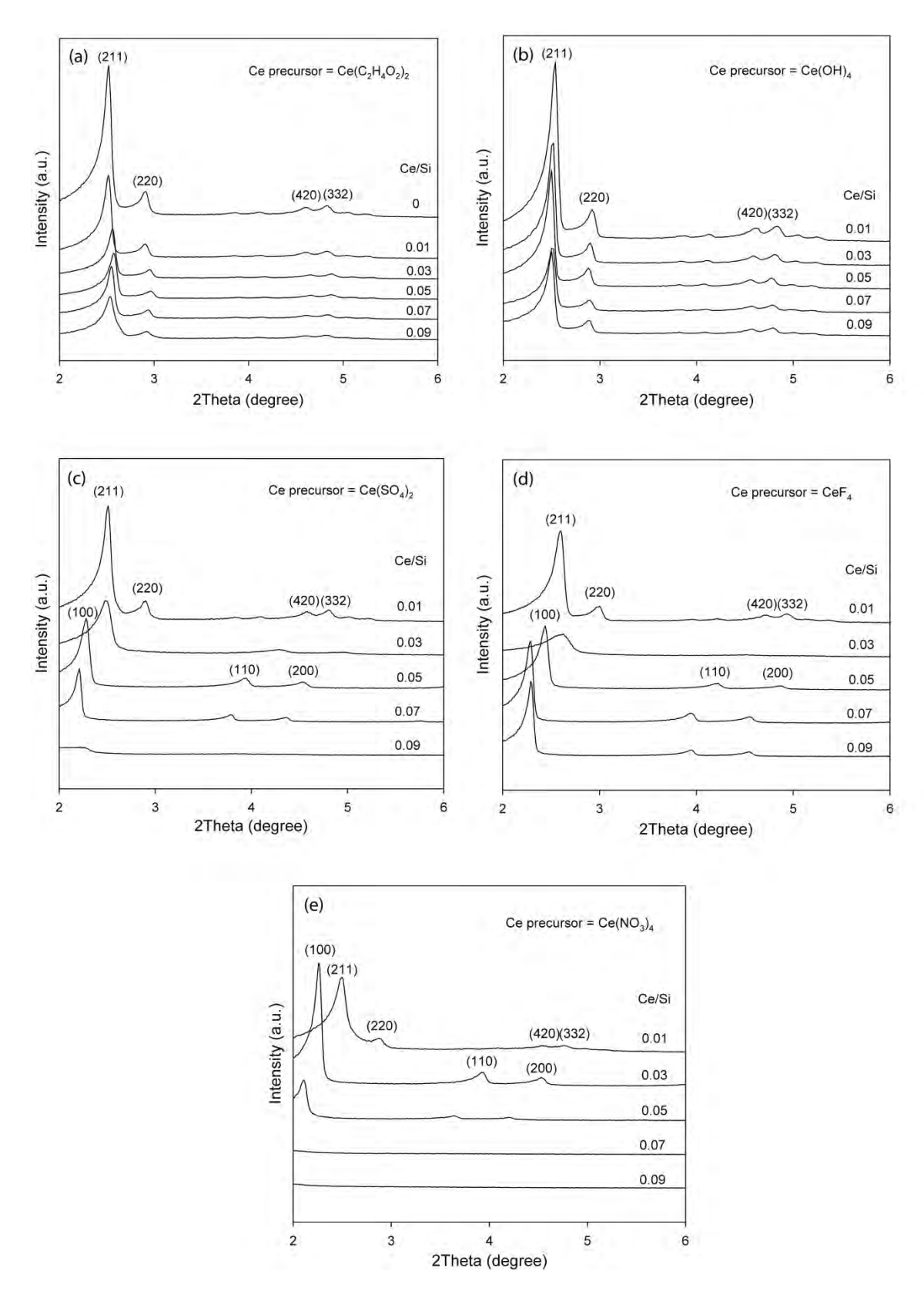


Fig. 1. XRD patterns of Ce-MCM-48 obtained from various cerium precursors: (a) $Ce(C_2H_4O_2)_2$; (b) $Ce(OH)_4$; (c) $Ce(SO_4)_2$; (d) CeF_4 and (e) $Ce(NO_3)_4$

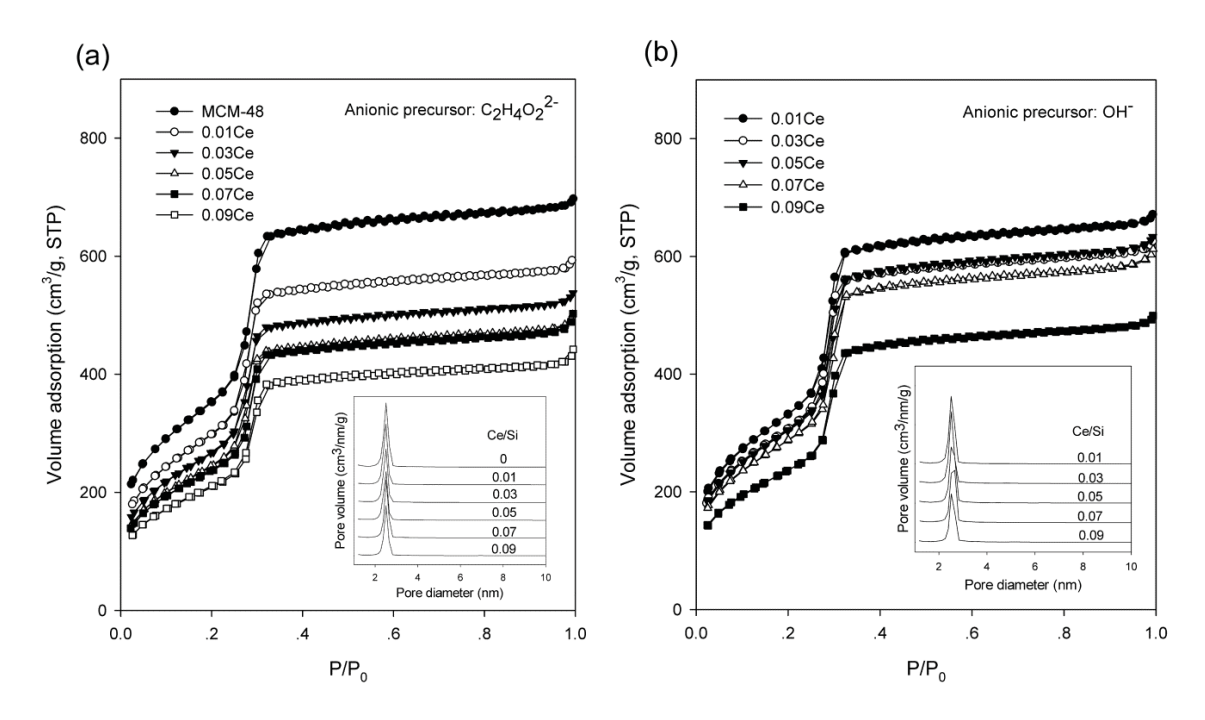


Fig. 2. Nitrogen adsorption-desorption isotherms of Ce-MCM-48 obtained from various concentrations of cerium precursor using: (a) $C_2H_4O_2^{\ 2-}$ and (b) OH^- counterions.

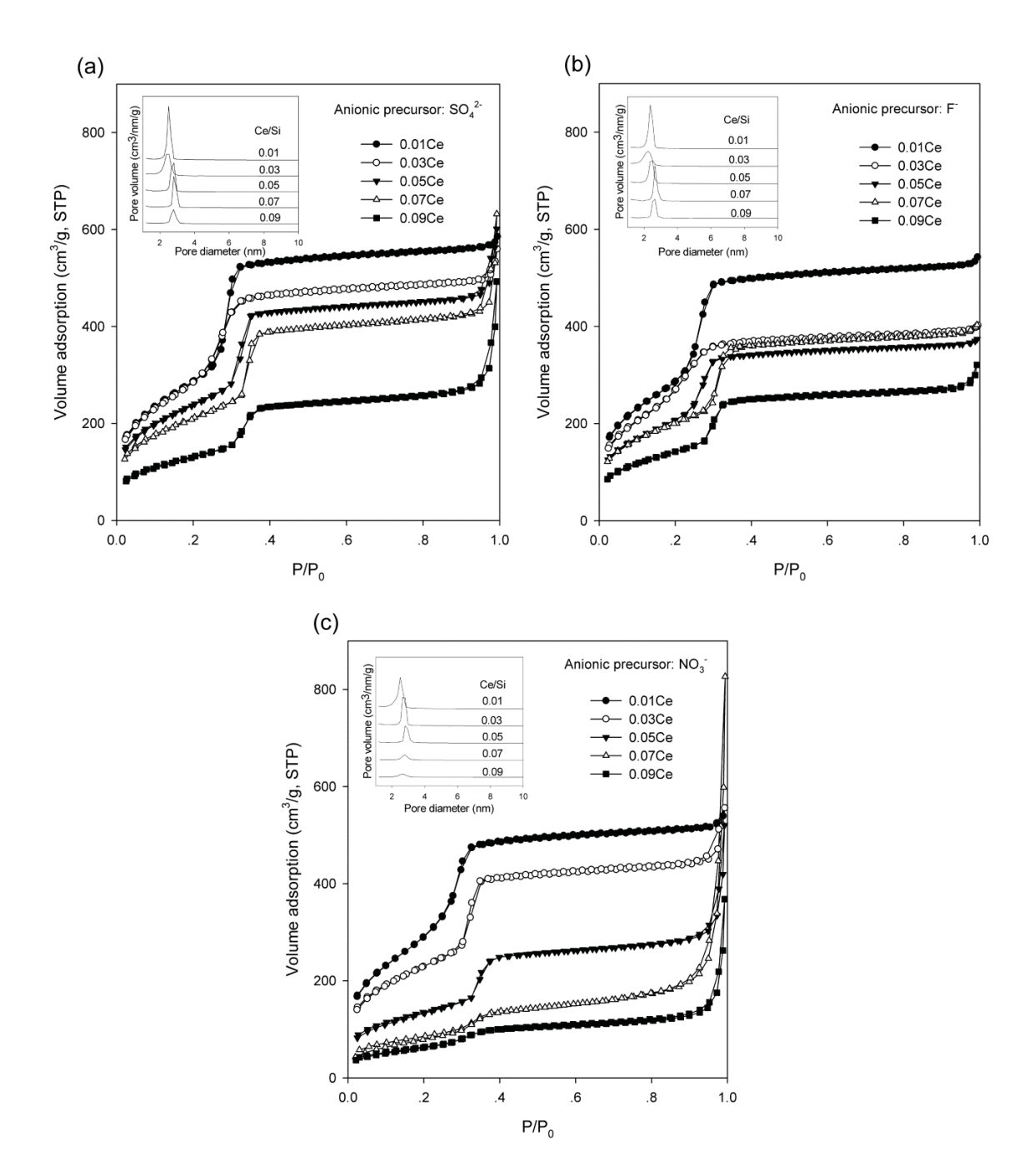


Fig. 3. Nitrogen adsorption-desorption isotherms of Ce-MCM-48 obtained from various concentrations of cerium precursor using: (a) SO_4^{2-} ; (b) F and (c) NO_3^{-1} counterions.

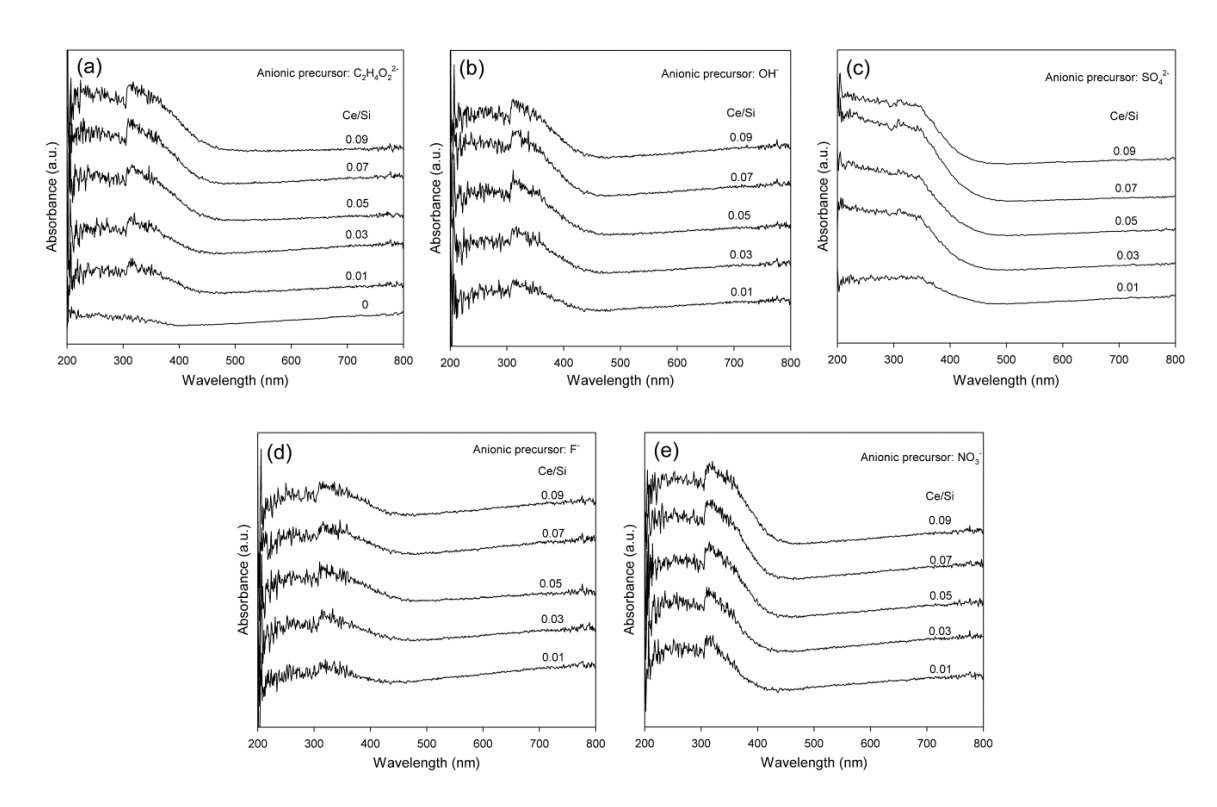


Fig. 4. DRUV-vis spectra of Ce-MCM-48 obtained from various concentrations of cerium precursor using: (a) $C_2H_4O_2^{2-}$; (b) OH^- ; (c) SO_4^{2-} ; (d) F^- and NO_3^- counterions

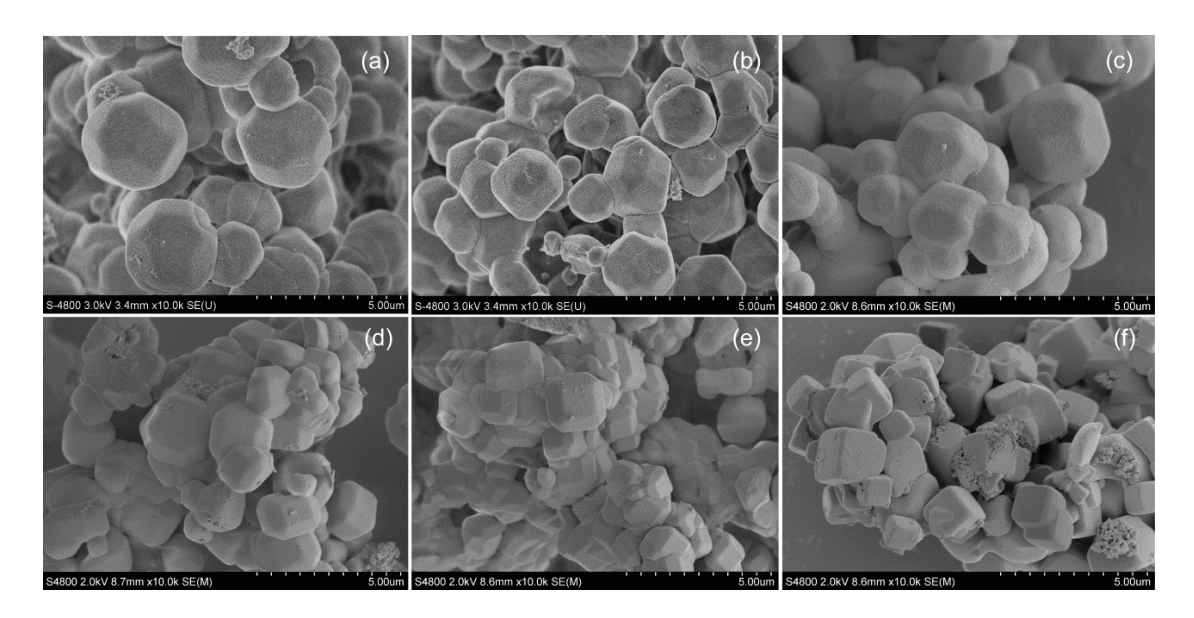


Fig. 5. FE-SEM images of (a) MCM-48 and 0.01Ce-MCM-48 obtained from cerium precursors containing: (b) $C_2H_4O_2^{\ 2^-}$; (c) OH^- ; (d) $SO_4^{\ 2^-}$; (e) F^- and (f) NO_3^-

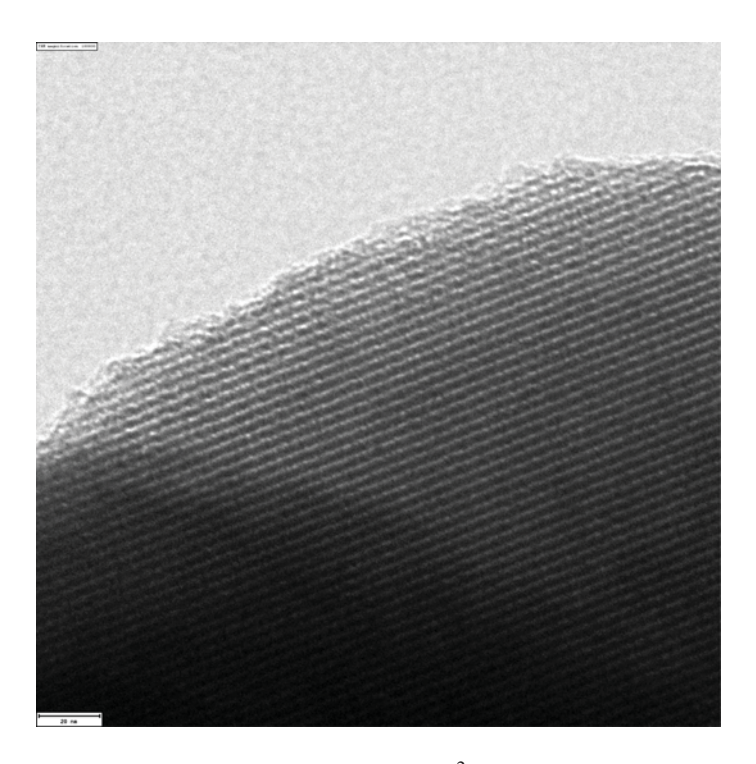


Fig. 6. TEM image of 0.01CeMCM-48 using $C_2H_4O_2^{\ 2^-}$ as an anionic precursor along the (432) direction.

Table 1 Textural properties of MCM-48 and Ce-MCM-48 using Ce(C₂H₄O₂)₂ and Ce(OH)₄ as Ce precursors.

Ce precursor	C	Ce/Si*	Phase	BET	pore	pore	a_0^{-a}	d ₂₁₁	wall
	om)	(mole ratio)	formation	surface area	volume	diameter			thickness ^b
	Gel	Product		(m^2/g)	(cm^2/g)	(mm)	(mm)	(mu)	(mu)
1	0	0	MCM-48	1673	1.07	2.56	8.57	3.50	1.46
$\mathrm{Ce}(\mathrm{C}_2\mathrm{H}_4\mathrm{O}_2)_2$	0.01	0.004	MCM-48	1469	0.91	2.47	8.57	3.50	1.54
	0.03	0.010	MCM-48	1318	0.82	2.49	8.45	3.45	1.49
	0.05	0.018	MCM-48	1213	0.76	2.52	8.40	3.43	1.46
	0.07	0.028	MCM-48	1128	0.76	2.68	8.48	3.46	1.50
	0.09	0.030	MCM-48	1131	0.74	2.63	8.52	3.48	1.44
$Ce(OH)_4$	0.01	0.003	MCM-48	1535	1.03	2.68	8.52	3.48	1.42
	0.03	0.010	MCM-48	1458	96.0	2.63	8.62	3.52	1.47
	0.05	0.018	MCM-48	1364	0.97	2.85	8.67	3.54	1.38
	0.07	0.030	MCM-48	1271	0.93	2.93	8.65	3.53	1.33
	0.09	0.039	MCM-48	1077	0.76	2.83	8.67	3.54	1.39

 a $a_0 = d_{211}(6)^{1/2}$, b Wall thickness = $a_0/3.0919$ – pore diameter/2, * Data were obtained from XRF.

Table 2 Textural properties of MCM-48 and Ce-MCM-48 using Ce(SO4)₂ and CeF₄ as Ce precursors.

Ce precursor	Ce	Ce/Si*	Phase	BET	pore	pore	a_0^{-a}	d ₂₁₁	wall
	(mol	(mole ratio)	formation	surface area	volume	diameter			thickness ^b
I	Gel	Product		(m^2/g)	(cm^2/g)	(mu)	(mm)	(mu)	(mm)
	0.01	0.004	MCM-48	1357	0.88	2.62	8.62	3.52	1.48
	0.03	0.017	MCM-41	1312	0.83	2.52		,	1
	0.05	0.021	MCM-41	879	0.87	3.96		ı	ı
	0.07	0.032	MCM-41	765	0.82	4.29	1	ı	1
	60.0	0.046	Wormhole	484	0.62	5.11	1	ı	ı
	0.01	0.003	MCM-48	1463	0.83	2.26	8.33	3.40	1.56
	0.03	0.009	MCM-41	1331	0.62	2.24		ı	ı
	0.05	0.014	MCM-41	1070	0.57	2.51		ı	1
	0.07	0.017	MCM-41	1018	0.62	2.65	1	ı	ı
	60.0	0.019	MCM-41	719	0.46	2.65		ı	

 a $a_0 = d_{211}(6)^{1/2}$, b Wall thickness = $a_0/3.0919$ – pore diameter/2, * Data were obtained from XRF.

Table 3 Textural properties of MCM-48 and Ce-MCM-48 using Ce(NO₃)₄ as Ce precursors.

Ce precursor		Ce/Si*	Phase	BET	pore	pore	\mathbf{a}_0^{a}	d ₂₁₁	wall
	om)	(mole ratio)	formation	surface area	volume	diameter			thickness ^b
	Gel	Product		(m^2/g)	(cm^2/g)	(mu)	(mu)	(mm) (mm)	(mm)
Ce(NO ₃) ₄	0.01	900.0	MCM-48	1320	0.83	2.53	8.65	8.65 3.53	1.53
	0.03	0.013	MCM-41	1166	08.0	2.66	1	1	ı
	0.05	0.026	MCM-41	653	0.65	2.80	1	1	1
	0.07	0.038	Amorphous	384	0.93	2.81	1	ı	ı
	0.00	0.051	Amorphous	288	0.41	2.67	1	1	ı

 $^{^{}a}$ $a_{0} = d_{211}(6)^{1/2}$, b Wall thickness $= a_{0}/3.0919 - pore$ diameter/2, * Data were obtained from XRF.

Synthesis of fe-ti-mcm-48 from silatrane precursor via sol-gel process

and its hydrothermal stability

HussayaManeesuwan, ThanyalakChaisuwan, SujitraWongkasemjit*

The Petroleum and Petrochemical College and Center of Excellence for Petrochemical and

Materials Technology, Chulalongkorn University, Bangkok 10330, Thailand

*Corresponding author: Tel.: +66 2 218 4133: fax: +66 2 215 4459.

E-mail address: dsujitra@chula.ac.th (S. Wongkasemjit)

Abstract

A series of bimetallic Fe-Ti-MCM-48 materials were successfully

synthesized via sol-gel method using cetyltrimethylammonium bromide (CTAB) as a

template, silatrane, iron (III) chloride and titanium (IV) isopropoxide as silica, iron

and titanium sources, respectively. The samples were characterized by X-ray

diffraction (XRD), N₂ physisorption, diffuse reflectance UV-vis spectra (DRUV), X-

ray fluorescence (XRF), transmission electron microscopy (TEM) and scanning

electron microscope (SEM). The results indicated that high specific surface area was

obtained. As increase metal content, the mesoporous order and surface area

decreased. The synthesized Fe-Ti-MCM-48 with 0.01Fe/Si and 0.01Ti/Si ratio still

retained a cubic structure after hydrothermal treatment at 100 °C for 72 h.

Keywords: Fe-Ti-MCM-48, Bimetallic materials, Mesoporous materials, Silatrane,

Sol-gel process, Hydrothermal stability.

Introduction

The cubic MCM-48, a main member in M41S family discovered by Mobil group [1], performs three-dimensional pore channel that can avoid pore blocking and provide faster reactants diffusion than one-dimensional pore system of MCM-41 [2-4]. Due to tunable pore diameter, well-defined structure, and large surface area, MCM-48 has been used in many applications, such as catalyst, catalyst support, adsorbent, sensor, and template, for the synthesis of advanced nanostructures [5-9]. However, pure silica porous material is inert for catalytic applications because of its lack of active sites. In order to create the active sites, the metal ions such as Fe, Ce, Cr, V and Ti have been used to modify the MCM-48 silica framework [10-12]. Among the metals, iron containing mesoporous silica gave a good catalytic performance for the selective oxidation processes, such as Friedel-Crafts [13], styrene epoxidation [14], Fischer-Tropsch [15], and phenol hydroxylation [16-17]. Titanium substituted mesoporous silicates also have excellent ability in photocatalytic activity [18-19], styrene epoxidation [14], toluene oxidation [20], and phenol hydroxylation [21]. However, in this case the structure of Ti-MCM-41 collapsed under mild conditions for phenol hydroxylation with H₂O₂ [21]. Xiao et al. [22] found that an ordered mesoporous titanasilicate retained the structure after treatments in boiling water for 120 h. Chen et al. [23] studied on Ti-substituted MCM-41 with various treatments and reported that the structural stability can be improved by Ti incorporation. Galacho et al. [24] also demonstrated that Ti-MCM-41 maintained the structure after 12 h in boiling water and the hydrothermal stability of titanium substituted samples increased as increase titanium content. The incorporation multi-components of metal atoms can modify silica surface that might

create new properties and improve catalytic activity, selectivity, acidity, hydrophobicity, and stability of the single-component catalysts [25-27]. Wang et al. [27] studied the liquid-phase epoxidation of styrene, and found that bimetallic Zr-Ti-MCM-41 had high catalytic activity and selectivity over single metal Zr-MCM-41 or Ti-MCM-41. MCM-41 incorporated with copper and titanium was first synthesized by Kong et al. [28] who indicated that Cu-Ti-MCM-41 had relatively high thermal stability. Wang et al. [29] found that Ti-containing Cr-modified MCM-48 photocatalysts had the photocatalytic performance for decomposition of H₂S under visible light with 92% efficiency for H₂S removal. The reduction of NO with NH₃ using Fe-Mo-SBA-15 as a catalyst performed higher catalytic activity than monometallic modified SBA-15 [30]. Bimetallic V-Fe-SBA-15 [31] and Ce-Fe-SBA-15 [32] were used for hydroxylation of phenol. An appropriate metals mol ratio (V/Fe and Ce/Fe) in SBA-15 would enhance the catalytic performance [31-32]. Popova et al. [33] reported that titanium- and iron- modified MCM-41 achieved higher catalytic activity, compared to monosubstituted material for toluene oxidation. Fe-Ti incorporated-SBA-15 and MCM-41 were synthesized for hydroxylation of styrene with H₂O₂ [26] and the conversion of styrene was controlled by metal content. Iron and titanium have the ability to catalyze in the same reactions of phenol hydroxylation [16-17, 21] and styrene epoxidation [14], incorporation these two metal atoms into mesoporous silica might thus enhance the catalytic activity over the monometallic material. Up till now, there are few published reports on bimetallic MCM-48 due to its difficulty to prepare [29].

In this work, Fe-Ti-MCM-48 with different Fe/Si and Ti/Si mol ratios was synthesized under hydrothermal condition via sol-gel process. The hydrothermal

stability was also studied to determine the destruction of catalyst structure that might decrease the catalytic ability.

Materials and methods

Materials

Fumed silica (99.8%, SiO₂) and iron (III) chloride hexahydrate (FeCl₃·6H₂O) from Sigma-Aldich, titanium (IV) isopropoxide (Ti(OCH(CH₃)₂) ₄) from Acros Organics, hexadecyltrimethyl ammonium bromide (CTAB) from Fluka, ethylene glycol (EG) from J.T. Baker, triethanolamine (TEA) from QREC, acetronitrile and sodium hydroxide (NaOH) from Labscan were used without purification.

Preparation of Bimetallic materials

xFe-yTi-MCM-48 were synthesized, following Wongkasemjit's method [34]. The molar ratio composition of the obtained gel was 1.0SiO₂:0.3CTAB: 0.5NaOH:62.0H₂O:xFe:yTi, where $0.01 \le x$, $y \le 0.09$. Firstly, FeCl₃·6H₂O was dissolved in distilled water, followed by adding 2 M NaOH and CTAB. The mixture was continuously stirred and slightly heated at 50 °C. The desired amount of silatrane, prepared according to the method reported in the literature [35], was added into the solution. Then the required amount of Ti(OCH(CH₃)₂)₄ was added dropwise into the mixture and stirred for 1 h. The resulting mixture was transferred into a teflon-lined stainless steel vessel and autoclaved at 140 °C for 16 h. The powder product was washed and filtered with distilled water. After drying, the organic template was removed by calcination at 550 °C for 6 h with a heating rate of 0.5 °C/min. Pure MCM-48, Fe-MCM-48 and Ti-MCM-48 were prepared using the same procedure.

Characterization

The powder X-ray diffraction (XRD) patterns were recorded on a Rigaku X-ray diffractometer with CuK α radiation over the range of $2\theta = 2$ -6°. N_2 adsorption and desorption isotherms were measured using by a Quantasorb JR instrument using the Brunauer–Emmett–Teller (BET) method. The diffuse reflectance UV-visible (DRUV-vis) analysis of samples was carried out by a Shimadzu UV-2550. X-ray fluorescence (XRF) was observed on a PANalytical AXIOS PW 4400. The morphology was determined by using field emission- scanning electron microscope (FE-SEM) with a Hitachi S-4800 model. Transmission electron microscopy (TEM) was investigated the microstructure using a JEOL JEM-2010.

Hydrothermal stability test

Following the method by Jiang et al. [36], 0.1 g of calcined sample was added into a teflon-lined stainless steel vessel containing 50 ml distilled water and treated at 100 °C for different times (12, 24, 36, 48, and 72 h). The sample was recovered by filtration and dried overnight at ambient temperature. The treatment product was characterized by XRD.

Results and discussion

XRD

Figure 1 shows the XRD patterns of MCM-48, Fe-MCM-48, Ti-MCM-48 and Fe-Ti-MCM-48. All samples exhibited the intense {211} peak and weak {220}, {420}, and {332} peaks which suggest the *Ia3d* cubic phase of MCM-48 mesoporous materials [34]. Comparing with pure MCM-48, XRD patterns of metal incorporated MCM-48 slightly shifted to higher angle with a decrease in the peak strength, implying that the different sizes of metal, the radii of Fe³⁺ (Paulling radius = 64 pm) and Ti⁴⁺ (Paulling radius = 60 pm) were larger than Si⁴⁺ (Paulling radius =

42 pm), causing the geometric distortion from the ideal tetrahedral coordination [37]. The synthesis of Fe-MCM-48 with Fe/Si ratio beyond 0.01 was not successful due to the imbalance of charge matching, as explained in elsewhere [38]. Therefore, bimetallic xFe-yTi-MCM-48 only when x = 0.01 and $0.01 \le y \le 0.09$ was obtained the cubic structure. On the other hand, Ti-MCM-48 was successfully synthesized using Ti(OCH(CH₃)₂)₄ as titanium precursor that generated isopropoxide anion. According to the surfactant-packing parameter (g); $g = V/a_0 l$ where V is the volume of the hydrocarbon chain of surfactant monomer, a_0 is the effective head group area of the cationic ammonium and l is the apparent length of the hydrophobic tail of the surfactant, the hydrophobic part of isopropoxide anion combined with the hydrocarbon region of the surfactant to result in an increase in V [39]. Thus, following the surfactant-packing parameter equation, a large g value was also obtained as well. Besides, Mahoney et al. [40] suggested that the cubic formation was favorable of high curvature surface and large g because of the imbalance of charge distribution. Between titanium and iron precursors, isoproproxide anion was more effective precursor than chloride anion to form MCM-48. In addition, it was also found that the peak shifted to lower angle as the content of titanium increased for Ti-MCM-48. The reason was explained by Gao et al. [31] that more titanium incorporated and large size of titanium would enlarge the structure [31]. The XRD pattern clearly exhibited that bimetallic Fe-Ti-MCM-48 can be prepared at various Ti contents with 0.01 Fe/Si. The change in the relative intensities and the obvious shift to higher angle of the bimetallic products suggested that TiO2 nanocrystal was present on the internal pore wall of MCM-48 [41]. The wide angle XRD pattern of Fe-Ti-MCM-48 is shown in Fig. 2. The broad peak at 23° referred to the amorphous SiO_2 . Two peaks at 2θ values of 28° and 42° were also observed, corresponding toTiO₂ anatase {101} and {004} crystal planes, respectively [42-43]. In addition, the peak at 28° increased as the titanium content increased, but this peak was obscurely seen due to overlapping with the amorphous silica peak. Thus, the broad characteristic peaks of anatase phase can be implied that the trace amount of titanium nanocrystal was formed.

N_2 adsorption-desorption

The isotherms and the pore size distribution of MCM-48 and Fe-Ti-MCM-48 samples are shown in Fig. 3. All adsorption isotherms were type IV, typical of mesoporous materials that exhibit the sharp capillary condensation steps at relative pressure of $0.20 \le p/p_0 \le 0.35$. As a result, the capillary condensation of bimetallic MCM-48 became less steep when the amount of Ti increased, indicating a broader pore size distribution. Thus, as more Ti incorporated into the structure, the structure was less ordered, as can be seen from the XRD patterns in Fig. 1. The structure parameters of the samples are given in Table 1. The average pore sizes of the obtained samples were 2–3 nm. Also, the uniform narrow pore size distribution was demonstrated. Fe-MCM-48 performed large pore volume and slim wall thickness similar to those reported by Das and co-workers [44]. All Ti-MCM-48 samples had higher wall thickness than siliceous MCM-48 due to the incorporation of Ti into MCM-48 framework. The specific surface area of Ti-MCM-48 and Fe-Ti-MCM-48 decreased as the metal content increased since there was some destruction of the metallic MCM-48 in agreement with the XRD results [45]. Nevertheless, all samples resulted in high surface area.

DRUV

The DRUV spectra (Fig. 4a-b) were analyzed to characterize the coordination circumstance of metal ion coordination. There was no absorption band observed for

MCM-48. For Fe-MCM-48 (Fig. 4a), a broad band between 200 and 350 nm centered at 220 nm, was assigned to the charge transfer transitions involving isolated Fe³⁺ in tetrahedral geometry [46]. Ti-MCM-48 in Fig. 4a also showed one intense peak at 210 nm which referred to the ligand metal charge transfer between O²⁻ and Ti⁴⁺ in tetrahedral framework coordination [47], and the intensity increased as increasing the amount of Ti content. The Fe-Ti-MCM-48 samples exhibited a broad absorption at 200–300 nm, as shown in Fig. 4b, which attributed to the charge transfer transitions between tetrahedral oxygen ligand and the central Ti⁴⁺ and Fe³⁺ that overlapped at the same wavelength position. However, the presence of the band at around 500 nm demonstrated some M-O-M clusters existence of isolated Ti sites [26], corresponding to nanocrystalline TiO₂, which is in good agreement with XRD wide angle.

XRF

The XRF results indicated the actual amounts of Fe and Ti introduced into MCM-48. The metal contents in the final product had lower amount than those in the gel, as shown in Table 1, due to the solubility of Fe and Ti precursors in the medium.

SEM

Figure 5 shows the SEM micrographs of pure MCM-48, Fe-MCM-48, Ti-MCM-48, and Fe-Ti-MCM-48. The truncated octahedral shape of MCM-48 was shown in Fig. 5a. Fe-MCM-48 and Ti-MCM-48 morphologies shown in Fig. 5b-c had some distortion from the pure MCM-48 due to the larger size of Fe and Ti, as discussed above. Because of the existence of both Fe and Ti, bimetallic Fe-Ti-MCM-48 exhibited even more distortion in the structure. Moreover, the bimetallic crystal size decreased as the amount of Ti increased since the more ions generated many nuclei and resulted in more small growing crystal [48-49].

TEM

The structural order of 0.01Fe0.01TiMCM-48 observed by TEM indicated the projection along (100) direction [34], see Fig. 6a-b, showing the highly ordered cubic structure with uniform mesopores. Fortunately, the introduction of Fe and Ti atoms did not destruct the mesoporous structure.

1. Hydrothermal stability

Figure 7 presents the XRD patterns of 0.01Fe0.01Ti-MCM-48 sample after hydrothermal treatment at 100 °C for 0, 12, 24, 36, 48, and 72. It was shown that 0.01Fe0.01Ti-MCM-48 has the characteristic peaks of {211} and {220} after 12 h treatment, but the diffraction peaks of {420} and {322} were not seen due to the distortion of the structure from the incorporation of Fe and Ti, making the sample less order. However, the diffraction peaks of {211} and {220} retained for 48 h treatment while the {211} peak still maintained after 72 h treatment. For 0.01Fe (0.03-0.07)Ti-MCM-48 and (0.03-0.09)Ti-MCM-48, the characteristic peaks disappeared after 12 h treatment (not shown) because the more amounts of the metal incorporated resulted in the more distortion, leading to easier destruction. The XRD patterns of pure MCM-48 and 0.01Fe-MCM-48 collapsed after 48 h treatment whereas the peak of 0.01Ti-MCM-48 disappeared after 24 h treatment. In addition, they lost the diffraction {220} peak after the 12 h treatment. It revealed that the Fe-O-Si bonds and Ti-O-Si bonds have low resistance for water attack [46]. For MCM-48, the water molecule caused the hydrolysis of Si-O-Si bonds, resulting in the poor silica wall which led to the collapse of the silicate structure [50]. Of all synthesized bimetallic MCM-48, the most hydrothermal stable one is 0.01Fe0.01Ti-MCM-48. It could be suggested that the existence of extraframework titanium shielded the siloxane bonds (Si-O-Si) and obstructed the interaction with water molecules which enhanced the stability in boiling water [24]. Nevertheless, Fe-Ti-MCM-48 with 0.01Fe/Si and 0.03-0.07 Ti/Si showed the deterioration stability. There are two possible reasons supporting this situation. The first one is from both high amount of tinatium and two different types of metal atoms incorporated in the structure, resulting in the distortion and easier destruction. The other reason is from the extraframework of titania blocking the pore of MCM-48, causing the partially wall breakage and a decrease in surface area [29].

Conclusions

A series of iron and titanium incorporated MCM-48 mesoporous materials with high surface area were successfully synthesized from silatrane via sol-gel method. High iron content is unfavorable for the Fe-MCM-48 formation while Ti-MCM-48 resulted in the cubic structure. The introduction of iron and titanium ions led to a decrease of Fe-Ti-MCM-48 surface area generated the extraframework. The resulting 0.01Fe0.01Ti-MCM-48 mesoporous molecular sieve has highly hydrothermal stability suitable for many applications.

References

- [1] C.T. Kresge, M.E. Leonowicz, W.J. Roth, J.C. Vartuli, J.S. Beck, Nature 359 (1992) 710-712.
- [2] A. Taguchi, F. Schüth, Microporous Mesoporous Mater. 77 (2005) 1-45.
- [3] N.Z. Logar, V. Kaučič, Acta. Chim. Slov. 53 (2006) 117-135.
- [4] V. Meynen, P. Cool, E.F. Vansant, Microporous Mesoporous Mater.125 (2009) 170-223.

- [5] P. Xue, G.Z. Lu, Y.L. Guo, Y.S. Wang, Y. Guo, J. Mol. Catal. B: Enzym. 30 (2004) 75-81.
- [6] I.B. Isabel, M. África, L.D. Antonio, P.P. Joaquin, V.R. Maria, Eur. J. Pharm. Sci. 26 (2005) 365-373.
- [7] L.Huang, Q.L. Huang, H.N. Xiao, M. Eic, Microporous Mesoporous Mater. 111 (2008) 404-410.
- [8] M. Kruk, M. Jaroniec, R. Ryoo, S.H. Joo, J. Phys. Chem. B 104 (2000) 7960-7968.
- [9] C. Huo, H. Zhang, H. Zhang, B. Yang, P. Zhang, Y. Wang, Inorg. Chem. 45 (2006) 4735-4742.
- [10] W. Zhao, Y. Luo, P. Deng, Q. Li, Catal. Lett. 73 (2001) 2-4.
- [11] M. Selvaraj, D.W. Park, C.S. Ha, Microporous Mesoporous Mater. 138 (2011) 94–101.
- [12] H.T. Gomes, P. Selvam, S.E. Dapurkar, J.L. Figueiredo, J.L. Faria, Microporous Mesoporous Mater. 86 (2005) 287–294.
- [13] M.S. Hamdy, G. Mul, J.C. Jansen, A. Ebaid, Z. Shan, A. R. Overweg, Th. Maschmeyer, Catal. Today 100 (2005) 255-260.
- [14] W. Tanglumlert, T. Imae, T.J. White, S. Wongkasemjit, Catal. Commun. 10 (2009) 1070-1073.
- [15] L.A. Cano, M. V. Cagnoli, J.F. Bengoa, A.M. Alvarez, S.G. Marchetti, J. Catal. 278 (2011) 310-320.
- [16] H. Liu, G. Lu, Y. Guo, Y. Guo, J. Wang, Nanotechnology 17 (2006) 997-1003.
- [17] F. Adam, J. Andas, I.Ab. Rahman, Chem. Eng. J. 165 (2010) 658-667.
- [18] R. Peng, D. Zhao, N.M. Dimitrijevic, T. Rajh, R. T. Koodali, J. Phys. Chem. C 116 (2012) 1605-1613.

- [19] T. Liou, B. Lai, Appl. Catal. B 115-116 (2012) 138-148.
- [20] M. Popova, Á. Szegedi, P. Németh, N. Kostova, T. Tsoncheva, Catal. Commun. 10 (2008) 304-308.
- [21] C.H. Rhee, J.S. Lee, Catal. Lett. 40 (1996) 261-264.
- [22] F.-S. Xiao, Y. Han, Y. Yu, X. Meng, M. Yang, S. Wu, J. Am. Chem. Soc. 6 (2002) 124.
- [23] L.Y. Chen, S. Jaenicke, G.K. Chuah, Microporous Mater. 12 (1997) 323-330.
- [24] C. Galacho, M.M.L.R. Carrott, P.J.M. Carrott, I.P.P. Cansado, Adv. Mat. Res. 107 (2010) 63-70.
- [25] D. Rath, K.M. Parida, Ind. Eng. Chem. Res. 50 (2011) 2839-2849.
- [26] Y. Wu, Y. Zhang, J. Cheng, Z. Li, H. Wang, Q. Sun, B. Han, Y. Kong, Microporous Mesoporous Mater. 162 (2012) 51-59.
- [27] Y. Wang, Y. Guo, G. Wang, Y. Liu, F. Wang, J. Sol-Gel Technol. 57 (2011) 185-192.
- [28] Y. Kong, S. Jiang, J. Wang, S. Wang, Q. Yan, Y. Lu, Microporous Mesoporous Mater. 86 (2005) 191-197.
- [29] Z. Wang, X. Ci, H. Dai, L. Yin, H. Shi, Appl. Surf. Sci. 258 (2012) 8258-8263.
- [30] H. Zhang, C. Tang, C. Sun, L. Qi, F. Guo, L. Dong, Y. Chen, Microporous Mesoporous Mater. 151 (2012) 44-55.
- [31] F. Gao, Y. Zhang, C. Wang, C. Wu, Y. Kong, B. Zhao, L. Dong, Y. Chen, J. Nanosci. Nanotechnol. 7 (2007) 4508-4514.
- [32] Y. Zhang, F. Gao, H. Wan, C. Wu, Y. Kong, X. Wu, B. Zhao, L. Dong, Y. Chen, Microporous Mesoporous Mater. 113 (2008) 393-401.
- [33] M. Popova, A. Szegedi, Z. Cherkezova-Zheleva, I. Mitov, N. Kostova, T. Tsoncheva, J. Hazard. Mater. 168 (2009) 226-232.

- [34] R. Longloilert, T. Chaisuwan, A. Luengnaruemitchai, S. Wongkasemjit, J. Sol-Gel Sci. Technol. 58 (2011) 427-435.
- [35] W. Charoenpinijkarn, M. Suwankruharn, B. Kesapabutr, S. Wongkasemjit, A.M. Jamieson, Eur. Polym. J. 37 (2001) 1441-1448.
- [36] T. Jiang, D. Wu, J. Song, X. Zhou, Q. Zhao, M. Ji, H. Yin, Powder technol. 207 (2011) 422-427.
- [37] S. Wang, Y. Shi, X. Ma, Microporous Mesoporous Mater. 156 (2012) 22-28.
- [38] H. Maneesuwan, R. Longloilert, T. Chaisuwan, S. Wongkasemjit, Mater. Lett. 94 (2013) 65-68.
- [39] W. Zhao, L. Kong, Y. Luo, Q. Li, Microporous Mesoporous Mater. 100 (2007) 111-117.
- [40] L.M. Mahoney, Photocatalysis studies using mesporous modified V-MCM-48 Stober Synthesis, PhD thesis, Kansas State University, 2010
- [41] G.D. Mihai, V. Meynen, M. Mertens, N. Bilba, P. Cool, E.F. Vansant, J. Mater. Sci. 45 (2010) 5786-5794.
- [42] J. Jao, Q. Xu, L. Li, J. Colloid Interface Sci. 316 (2007) 596-603.
- [43] A. Jaroenworaluck, N. Pijarn, N. Kosachan, R. Stevens, Chem. Eng. J. 181-182 (2012) 45-55.
- [44] S.K. Das, M.K. Bhunia, A. Bhaumik, Open Catal. J. 5 (2012) 56-65.
- [45] D. Ji, T. Ren, L. Yan, J. Suo, Mater. Lett. 57 (2003) 4474-4477.
- [46] Y. Shao, L. Wang, J. Zhang, M. Anpo, J. Phys. Chem. B 109 (2005) 20835-20841.
- [47] D. Zhao, S. Budhi, A. Rodriguez, R.T. Koodali, Int. J. Hydrogen Energy 35 (2010) 5276-5283.
- [48] P.G. Vekilov, Cryst. Growth Des. 10 (2010) 12.

[49] D. Kashchiev, G.M. Van Rosmalen, Cryst. Res. Technol. 38 (2003) 7-8.

[50] K.A. Koyano, T. Tatsumi, Y. Tanaka, S. Nakata, J. Phys. Chem. B 101 (1997) 436.

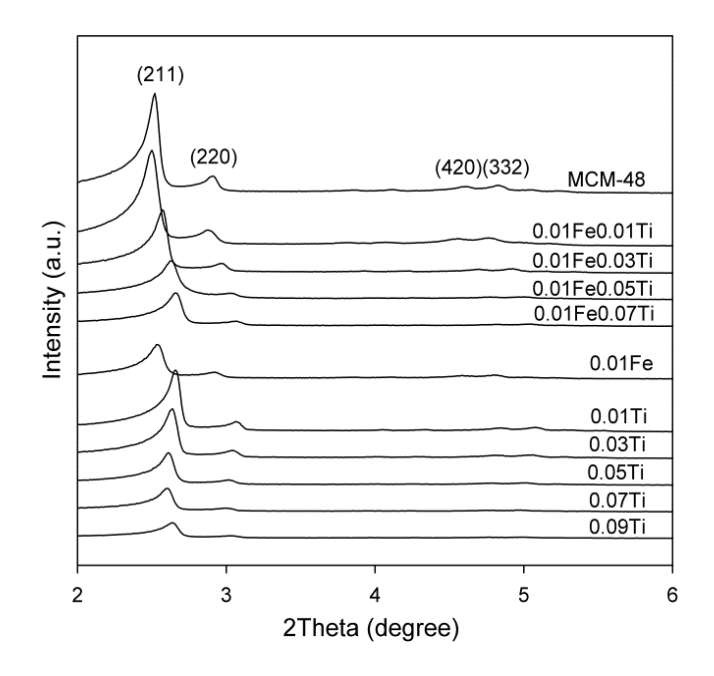


Figure 1 Small angle XRD patterns of MCM-48, Fe-MCM-48, Ti-MCM-48, and Fe-Ti-MCM-48

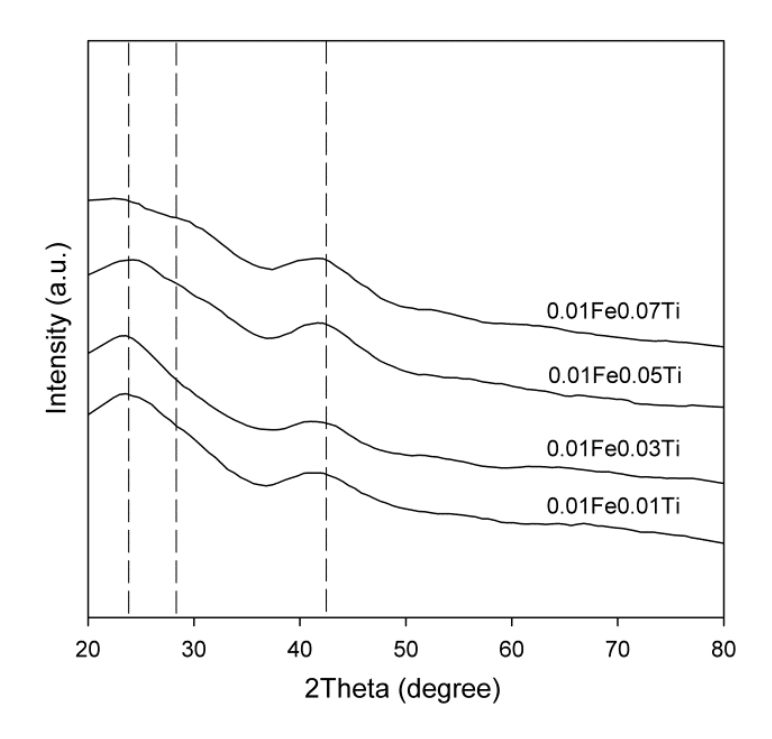


Figure 2 Wide angle XRD patterns of 0.01Fe0.01Ti-MCM-48, 0.01Fe0.03Ti-MCM-48, 0.01Fe0.05Ti-MCM-48 and 0.01Fe0.07Ti-MCM-48

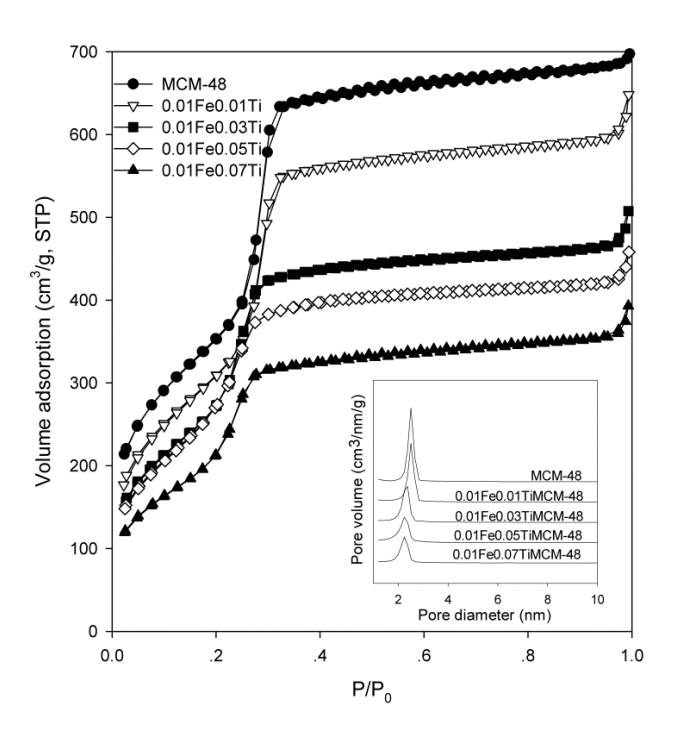


Figure 3 Nitrogen adsorption-desorption isotherms of MCM-48 and Fe-Ti-MCM-48

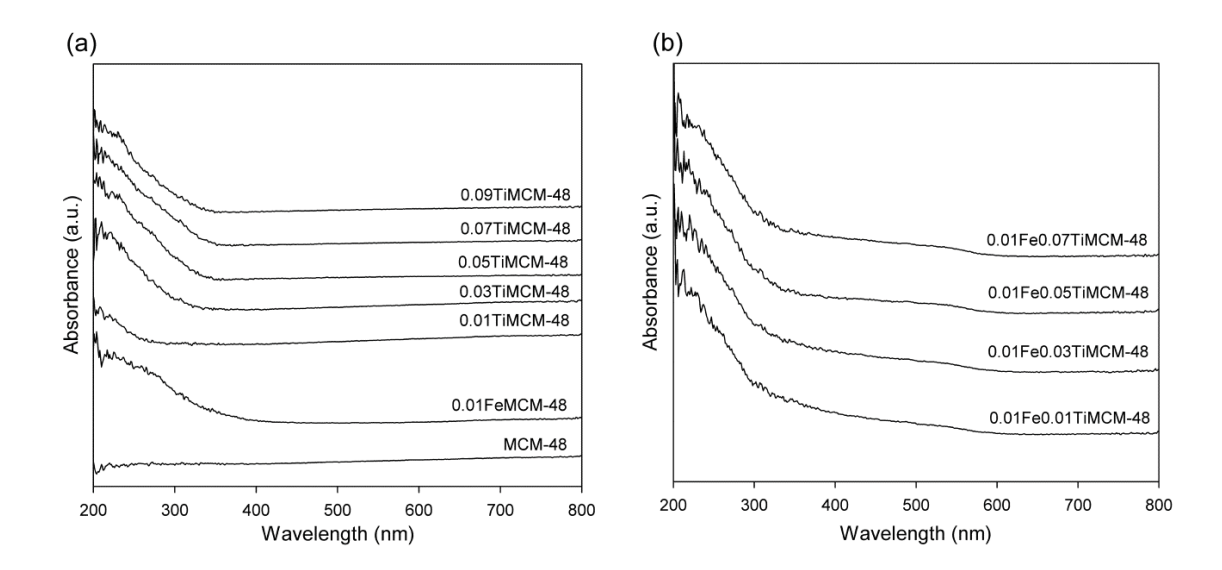


Figure 4 DRUV-vis spectra of samples: (a) MCM-48, Fe-MCM-48 and Ti-MCM-48; (b) Fe-Ti-MCM-48

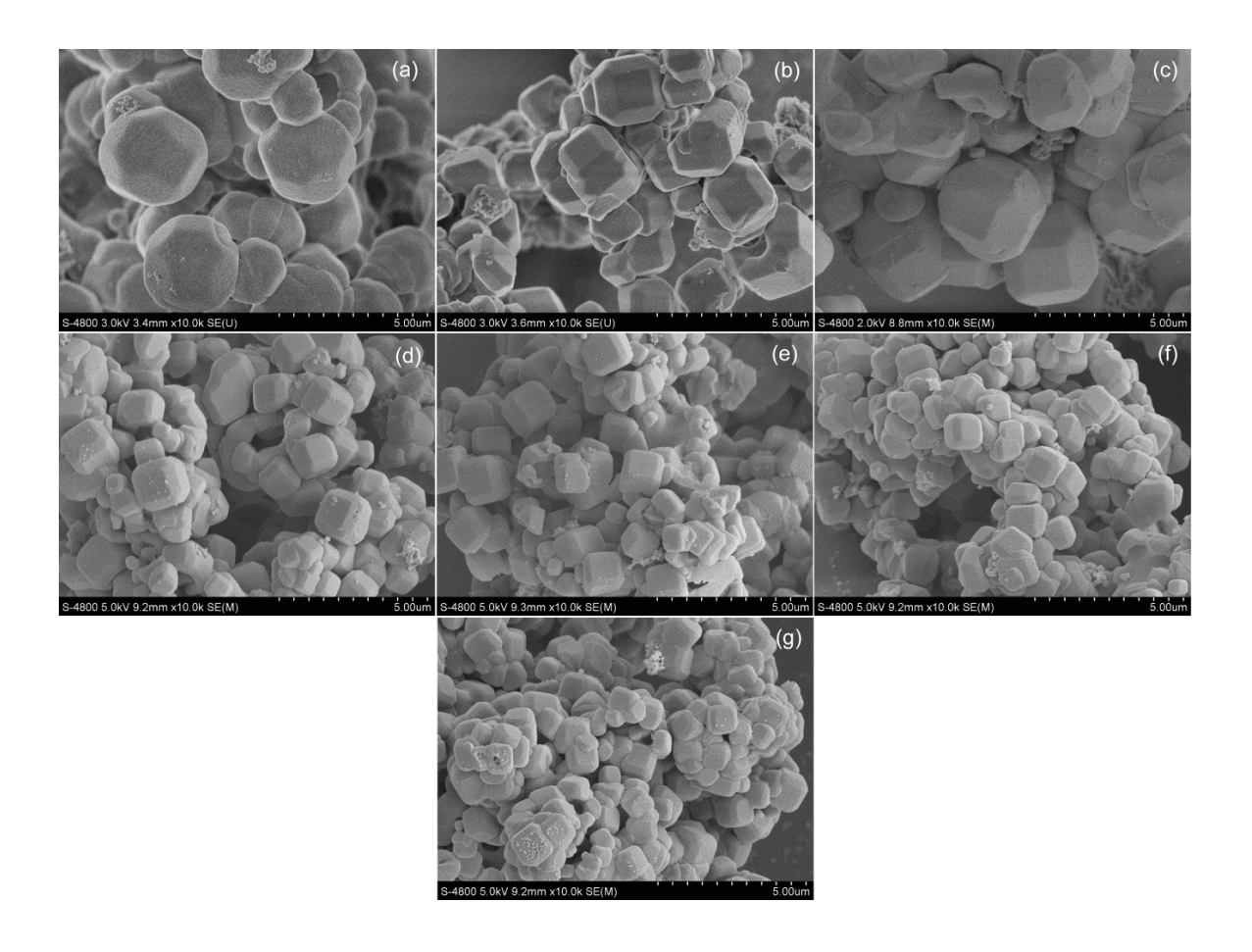


Figure 5 FE-SEM images of samples: (a) MCM-48; (b) 0.01Fe-MCM-48; (c) 0.01Ti-MCM-48; (d) 0.01Fe0.01Ti-MCM-48; (e) 0.01Fe0.03Ti-MCM-48; (f) 0.01Fe0.05Ti-MCM-48, and (g) 0.01Fe0.07Ti-MCM-48

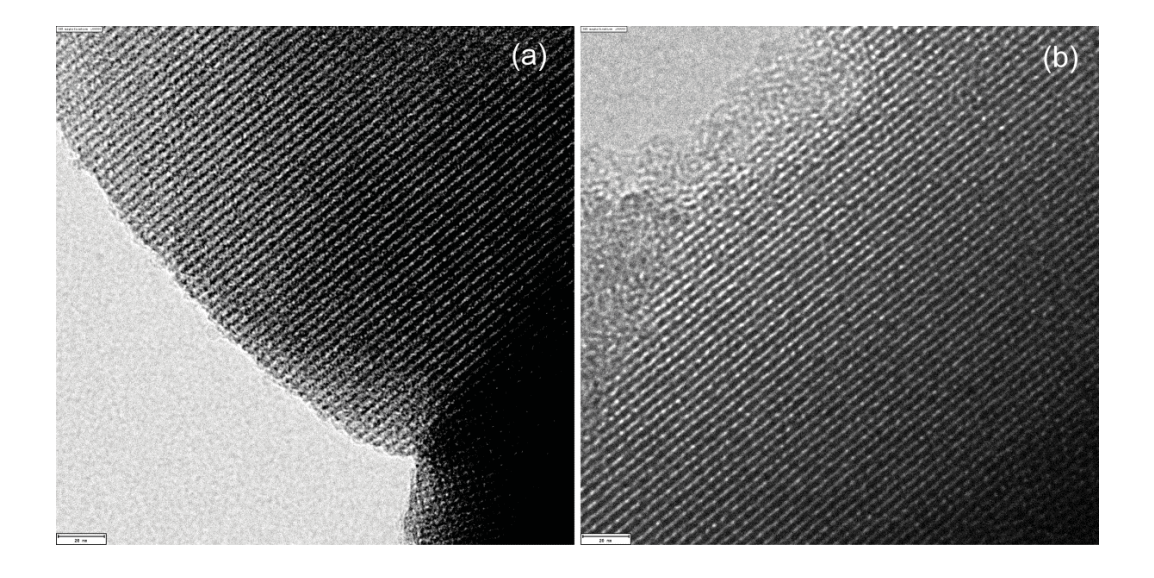


Figure 6 TEM images of 0.01Fe0.01TiMCM-48 along the (100) direction

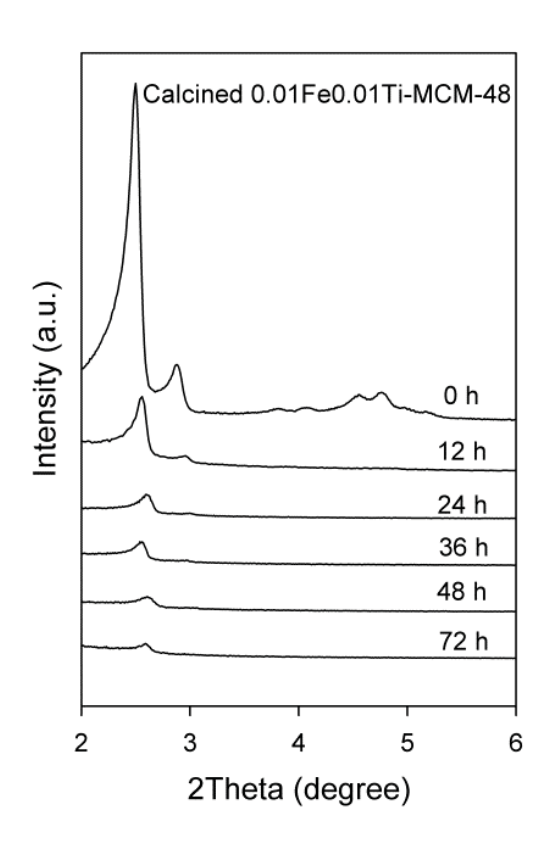


Figure 7 XRD patterns of 0.01Fe0.01Ti-MCM-48 after hydrothermal treatment at 100 °C for different times (0, 12, 24, 36, 48 and 72 h)

Table 1 Textural properties of MCM-48 and metal modified MCM-48.

Sample	Fe (mol	Fe/Si* (mole ratio)	Ti. (mole	Ti/Si* (mole ratio)	BET surfaçe area	pore	pore diameter	a 0 ^a	d_{211}	wall thickness ^b
	Gel	Product	Gel	Product	(m^2/g)	(cm ² /g)	(mu)	(mm)	(mu)	(mu)
MCM-48	0	0	0	0	1673	1.07	2.56	8.57	3.50	1.46
0.01Fe-MCM-48	0.01	0.004	0	0	1295	0.98	3.04	8.65	3.53	1.28
0.01Ti-MCM-48	0	0	0.01	0.003	1549	0.84	2.18	8.13	3.32	1.61
0.03Ti-MCM-48	0	0	0.03	0.015	1201	0.64	2.12	8.18	3.34	1.63
0.05Ti-MCM-48	0	0	0.05	0.020	1239	0.63	2.02	8.28	3.38	1.65
0.07Ti-MCM-48	0	0	0.07	0.031	1227	99.0	2.14	8.33	3.40	1.65
0.09Ti-MCM-48	0	0	0.09	0.034	876	0.55	2.27	8.23	3.36	1.58
0.01Fe-0.01Ti-MCM-48	0.01	0.005	0.01	0.007	1460	96.0	2.64	8.65	3.53	1.48
0.01Fe-0.03Ti-MCM-48	0.01	90000	0.03	0.020	1362	0.72	2.21	8.40	3.43	1.61
0.01Fe-0.05Ti-MCM-48	0.01	0.007	0.05	0.028	1269	89.0	2.14	8.23	3.36	1.59
0.01Fe-0.07Ti-MCM-48	0.01	0.006	0.07	0.035	1049	0.58	2.21	8.13	3.32	1.52

 $\frac{a}{a_0} = d_{211}(6)^{1/2}$, $\frac{b}{a_0}$ Wall thickness = $\frac{a_0}{3.0919}$ – pore diameter/2, * Data were obtained from XRF.

APPENDICES INTERNATIONAL PRESENTATIONS

POLYCHAR 19 – World Forum on Advanced Materials March 20-24, 2011, Kathmandu, Nepal

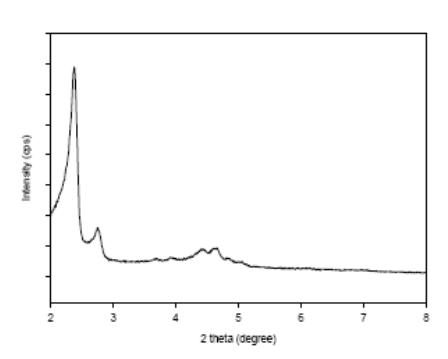
NOVEL SILICA SOURCE FOR SYNTHESIS OF MCM-48 VIA SOL-GEL PROCESS

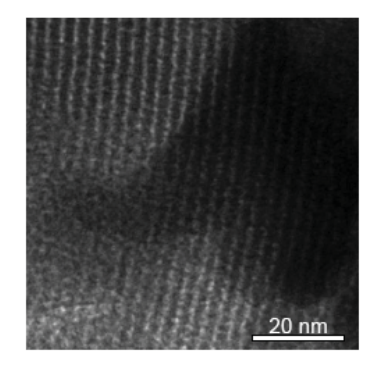
Rujirat Longloilert, Thanyalak Chaisuwan, Apanee Luengnaruemitchai, and Sujitra Wongkasemjit* The Petroleum and Petrochemical College, and the Center for Petroleum, Petrochemicals, and Advanced Materials, Chulalongkorn University, Bangkok 10330, Thailand

E-mail: I.rujirat@gmail.com,pigatung@hotmail.com

Keywords: MCM-48, silatrane, truncated octahedral shape

High-quality cubic MCM-48 was successfully synthesized using a new silica source known as silatrane and cetyltrimethylammonium bromide (CTAB) as the structure-directing agent via sol-gel process. The effects of synthesis parameters, such as crystallization temperature, crystallization time, surfactant concentration, quantity of NaOH and silica source on the product structure were investigated. The synthesized samples were characterized using X-ray diffractometer (XRD), N2 adsorption-desorption isotherms, and electron microscopy. The optimized conditions for this product was to crystallize the samples at 140°C for 16 h with CTAB/SiO2 ratio of 0.3 and NaOH/ SiO2 ratio of 0.5. The XRD result exhibited a well-resolved pattern, corresponding to the la3d space group of MCM-48. The BET surface area of this product was as high as 1300 m²/g with a narrow pore size distribution of 2.86 nm. The scanning electron microscopic (SEM) images also showed the truncated octahedral shape and well-ordered pore system of MCM-48 particles.





References

¹ Monnier, A.; Schüth, F.; Huo, Q.; Kumar, D.; Margolese, D.; Maxwell, R.S.; Stucky, M.; Krishnamurty, G.D.; Petroff, P.; Firouzi, A.; Janicke, M., *Science* **1993**, 261,1299-1303.

² Díaz, I.; Pérez-Pariente, J.; Terasaki, O., J. Mater. Chem. 2004, 14, 48-53.

Submission preference	: oral		poster	₹	or any	
POLY		 R 19 – V		 Forum <i>c</i>	on Advance	 d Materials

March 20-24, 2011, Kathmandu, Nepal

MCM-48-Polybenzoxazine mixed matrix membranes for CO₂/CH₄ separation

Nuttheewan Kittisarunlerd, Thanyalak Chaisuwan, Apanee Luengnaruemitr, and Sujitra Wongkasemjit*

The Petroleum and Petrochemical College and National Center of Excellence for Petroleum, Petrochemicals and Advanced Materials, Chulalongkorn University, Phayathai Road, Soi Chula 12, Patumwan, Bangkok 10330 Thailand.

INTRODUCTION

The existence of carbon dioxide in natural gas decreases the heat value of natural gas remarkably. Furthermore, in a moist environment, it may produce carbonic acid, which corrodes not only the equipment, but also the pipes in the transportation. Therefore, removal of carbon dioxide from natural gas is an important topic. Membrane is one of the attractive techniques for gas separation. In this study, mesoporous MCM-48 synthesized from silatrane via sol–gel process was added to polybenzoxazine (PBZ) to fabricate mixed matrix membranes (MMMs) for improving performance of the $\mathrm{CO}_2/\mathrm{CH}_4$ gas separation.

EXPERIMENTAL

Synthesis of MCM-48: CTAB was dissolved in a solution containing water and 2 M NaOH. The mixtures were vigorously stirred with slightly heating to dissolve surfactant. Silatrane precursor was then added, followed by stirring for 1 h. The mixture was transferred to a Teflon-lined stainless steel autoclave and heated at 140 °C for 16 h. The resulting solid product was collected by filtration and dried overnight at ambient conditions. The surfactant was removed by calcination at 550 °C for 6 h to obtain mesoporous MCM-48.

Preparation of Polybenzoxazine Membranes: The benzoxazine precursor was synthesized mixing bisphenol–A (BPA, $C_{15}H_{16}O_2$), formaldehyde (CH $_2O$), and 1,6–hexadiamine (hda, $C_6H_{16}N_2$) in 1,4–dioxane as solvent. The mixture was heated and stirred continuously until viscous liquid was obtained and cast onto a glass plate wrapped with aluminum foil. The thickness of the membrane was approximately 300 μ m. The membrane was dried at room temperature in air for one day. Finally, the membrane was placed in an air-circulating oven at 110 °C for 24 h.

Preparation of Mixed Matrix Membranes (MMMs): Various contents of MCM-48 were dispersed in 1,4–dioxane and stirred for 3 h. before sonicating for 15 min to improve the dispersion of particles in the solution. Then, approximately 15 %(w/w) of the total amount of polybenzoxazine was added into the MCM-48 solution. The mixture was stirred to enhance its homogeneity. After the remaining polybenzoxazine was added, the final mixture was further stirred continuously for 2 day before the casting.

Gas Permeation Measurements: The single–component gas permeation (CH₄ and CO₂) experiments of all membranes were carried out at 25 °C in sequences using a gas permeation testing unit in which the membrane was placed on a metal plate. The area of the membrane in contact with the gas was 44.2 cm². The pressure difference across the membrane was maintained at 25 psi.

RESULTS AND DISCUSSION

Figure 1 shows ¹H-NMR spectrum of polybenzoxazine precursors to confirm the synthesis process.

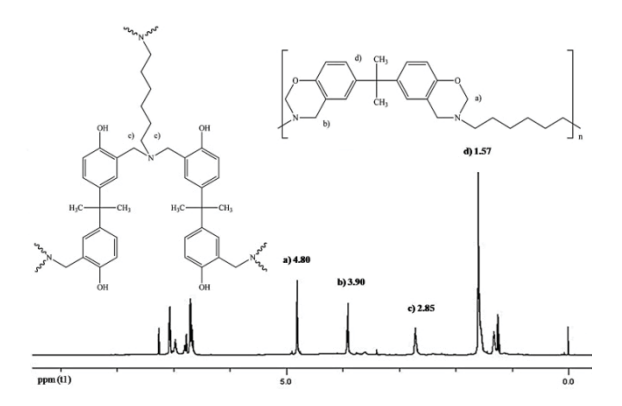


Figure 1 ¹H-NMR spectrum of polybenzoxazine precursors

Figure 2 shows SEM micrograph for a cross-section morphology of polybenzoxazine membrane filled with 10 wt.% of MCM-48 loading.

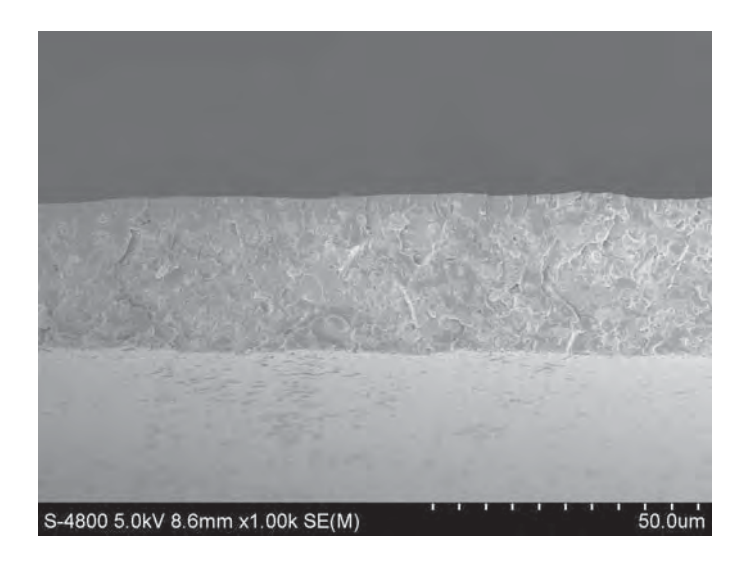


Figure 2 SEM micrograph of a cross-section of MMM with 10 wt.% of MCM-48 loading

ACKNOWLEDGEMENTS

- The Center for Petroleum, Petrochemicals and Advanced Materials (PPAM), Chulalongkorn University, Thailand.
 - Thailand Research Fund.

REFERENCES

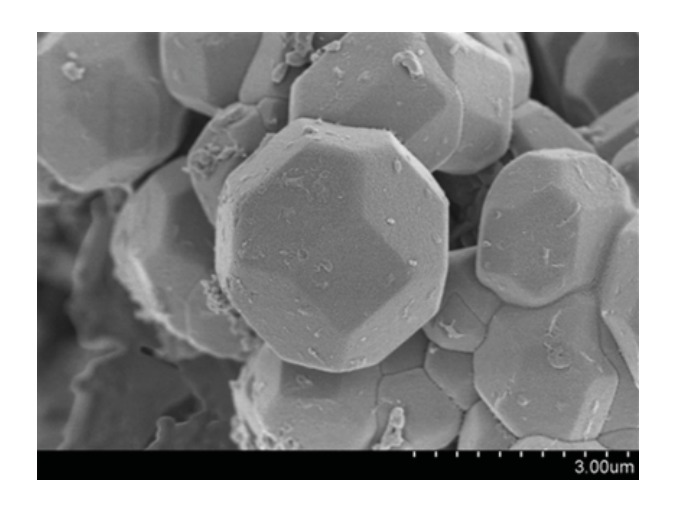
- 1. Allen, D.; Ishida, H.J. Appl. Polym. Sci. 2006, 101, 2798-2809.
- 2. Kim, S.; Marand, E.; Ida, J; Guliants, V. Chem. Mater. 2006, 18, 1149-1155.
- 3. Longloilert, R.; Chaisuwan, T.; Luengnaruemitchai, A.; Wongkasemjit, S. *J. Sol-Gel Sci Technol.* **2011**, *58*, 427–435.
- 4. Takeichi, T.; Kano, T.; Agag, T. Polymer. 2005, 46, 12172–12180.
- 5. Zhang, Y.;Balkus Jr., K.;Musselman, I.; Ferraris, J.J. Membr. Sci. 2008, 325, 28–39.

Synthesis and characterization of Ce-MCM-48 from silatrane via sol-gel process

Rujirat Longloilert^a, Thanyalak Chaisuwan^{a,b},

Apanee Luengnaruemitchai a,b, Sujitra Wongkasemjit a,b

Cerium incorporated into MCM-48 framework are hydrothermally synthesized via sol-gel process without any additives and characterized by X-ray diffraction, N_2 adsorption/desorption, Scanning electron microscopy (SEM), Transmission electron microscopy (TEM), Diffuse reflectance UV-vis spectroscopy, and Thermogravimetric analysis. Results indicate that the materials possess a long-range ordered structure, high specific surface area, and narrow pore size distribution. SEM images illustrate the truncated octahedron morphology which preserves the shape of the MCM-48 parent material. TEM images show the pore network of la3d symmetry after loading metal. Spectroscopic data confirm the existence of metals in the framework and extra-framework. The hydrothermal stability of MCM-48 is enhanced by carefully incorporating metal into the parent material.



SEM image of Ce-MCM-48 with the 0.01Ce/Si ratio

^{a)}The Petroleum and Petrochemical College, Chulalongkorn University

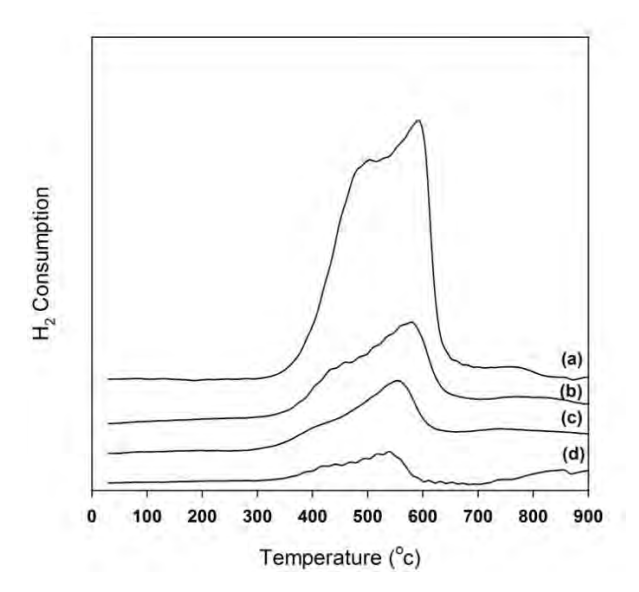
b) Center of Excellence on Petrochemical and Materials Technology

Synthesis of Ordered Mesoporous Ceria Using MCM-48 as Template

Chonnikarn Deeprasertkul^a, Sujitra Wongkasemjit^{a,b,*}, Thanyalak Chaisuwan^{a,b}

^{a)}The Petroleum and Petrochemical College, Chulalongkorn University

The catalytic performance of a catalyst can be increased by their structural properties, such as surface area, their crystal shape. In this study, ceria or cerium oxide with high surface area and ordered structure is prepared by nanocasting method using MCM-48 porous material, as a template. Optimal conditions of the nanocasting method are investigated to obtain ordered mesoporous ceria having high surface areas. The high surface area of 224.7 m²/g and the ordered structure of the synthesized cerium oxide are obtained at 50% weight of ceria using 30 min stirring time at 100 °C evaporated temperature. The resulting ordered mesoporous ceria is characterized using X-ray diffractometer (XRD), X-ray fluorescence spectrometer (XRF), N₂ adsorption/desorption, Transmission electron microscopy (TEM), Scanning electron microscopy (SEM), and Temperature programmed reduction (TPR).



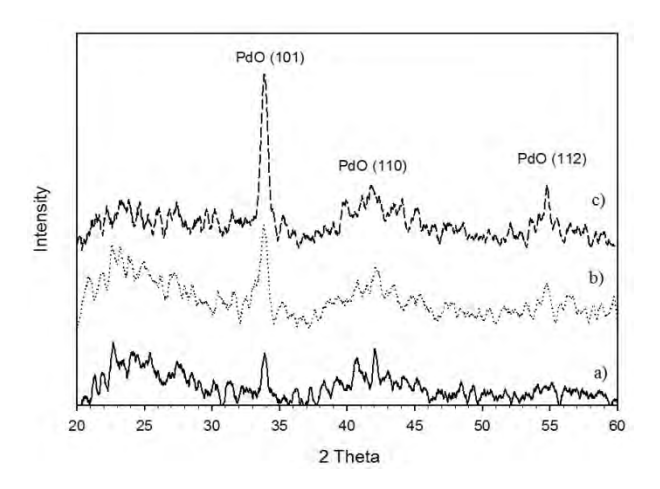
TPR profiles of ordered mesoporous ceria having different surface areas,(a)224.7 $\,\mathrm{m^2/g}$, (b)207.9 $\,\mathrm{m^2/g}$, (c)192.0 $\,\mathrm{m^2/g}$, (d) 77.1 $\,\mathrm{m^2/g}$ of ceria powder obtained without using nanocasting method.

b) Center of Excellence on Petrochemical and Materials Technology

Catalytic Activity of Pd Loaded on MCM-48

<u>Kanhatai Budmuang</u>^a, Sujitra Wongkasemjit^{a,b,*}, Apanee Luengnaruemitchai^{a,b}, and Thanyalak Chaisuwan^{a,b}

MCM-48, mesoporous material in M41S family, has attracted considerable interest owing to its periodic framework of regular mesopores, large surface area, good thermal stability, and 3-dimensional pore structure. All these properties are potentially advantageous for catalytic applications. In this work, palladium is used as a metal promoter loaded on the synthesized MCM-48 catalyst support synthesized from silatrane for Suzuki reaction to produce biphenyls via microwave technique. Pd-MCM-48 is synthesized via impregnation approach. The synthesized catalyst is characterized by X-ray diffraction (XRD), X-ray fluorescence (XRF), Temperature- programmed reduction method (TPR) and Transmission electron microscopy (TEM). The effects of Pd contents and reaction time are studied at 120 °C temperature and the product is characterized by gas chromatography-mass spectrometry (GC-MS). The result shows that 5%Pd-MCM-48 with 20 min reaction time gives the best result of ~41% yields.



Wide-angle XRD patterns of a) 1, b) 3, and c) 5%Pd-MCM-48

^a The Petroleum and Petrochemical College, Chulalongkorn University, Bangkok, Thailand ^bCenter of Excellence for Petrochemical and Materials Technology, Bangkok, Thailand

POLYCHAR 21 World Forum on Advanced Materials, 11-15 March 2013 Gwangju, Republic of KOREA

SYNTHESIS AND CHARACTERIZATION OF METAL-MCM-48 (M = TI, CR, AND CE) VIA HYDROTHERMAL TREATMENT AND SOL-GEL TECHNIQUE

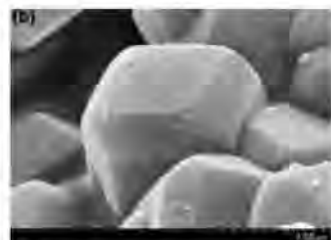
Sujitra Wongkasemjit^{*}, Rujirat Longloilert, Thanyalak Chaisuwan, Apanee Luengnaruemitchai

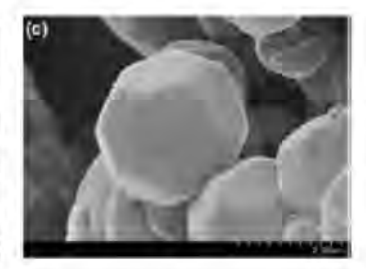
The Petroleum and Petrochemical College, and the Center for Petroleum, Petrochemicals, and Advanced Materials, Chulalongkorn University, Bangkok 10330, Thailand e-mail: dsujitra@chula.ac.th

Abstract

Silatrane prepared from fumed silica and triethanolamine (TEA) is used as a precursor for synthesis of MCM-48 and metal-MCM-48 (M = Ti, Cr, and Ce) via hydrothermal treatment and sol-gel technique using a cationic surfactant, derived from dodecyltrimethyl ammonium bromide, CTAB, as a dilute template. The products are characterized by X-ray diffraction (XRD), N₂ adsorption/desorption, scanning electron microscopy (SEM), Transmission electron microscopy (TEM), diffuse reflectance UV-vis spectroscopy (DR-UV), and thermogravimetric analysis (TGA). Results indicate that the materials possess a long-range ordered structure, high specific surface area, and narrow pore size distribution. SEM images illustrate the edge-truncated octahedron morphology of Ti- and Cr-MCM-48 while Ce-MCM-48 preserves the truncated octahedron of the MCM-48 parent material. TEM images show the pore network of *la3d* symmetry after loading metals. Spectroscopic data confirm the existence of metals in the framework and extraframework. At low Cr content, Cr-MCM-48 contains only Cr(VI) species while rich Cr content loading results in both the Cr(VI) and Cr(III) species.







FE-SEM images of a) Ti-, b) Cr-, and c) Ce-MCM-48

Acknowledgements: This research is financially supported by the Thailand Research Fund-Ratchadapisake Sompote Fund, and the Center of Excellence on Petrochemicals and Materials Technology, Chulalongkorn University, Thailand.